UNIVERSITY OF IOANNINA
SCHOOL OF SCIENCES
PHYSICS DEPARTMENT

Fractal States and Quantum Chaos in Disordered Graphene

Ioannis Kleftogiannis

A thesis submitted for the degree of Doctor of Philosophy

Ioannina, June 2011

ΠΡΑΚΤΙΚΟ
ΔΗΜΟΣΙΑΣ ΠΑΡΟΥΣΙΑΣΗΣ, ΕΞΕΤΑΣΗΣ ΚΑΙ ΑΞΙΟΛΟΓΗΣΗΣ ΔΙΔΑΚΤΟΡΙΚΗΣ ΔΙΑΤΡΙΒΗΣ

Σήμερα **16-06-11,** ημέρα Τετάρτη και ώρα **11.00,** στην αίθουσα **συνεδριάσεων του Τμήματος Φυσικής**, σύμφωνα με τον Οδηγό Μεταπτυχιακών Σπουδών του Πανεπιστημίου Ιωαννίνων, πραγματοποιείται η δημόσια παρουσίαση, εξέταση και αξιολόγηση της διδακτορικής διατριβής του υποψήφιου διδάκτορα **κ. Ιωάννη Κλεφτόγιαννη.**

Την επταμελή εξεταστική επιτροπή, που συγκροτήθηκε με απόφαση της Γενικής Συνέλευσης του Τμήματος Φυσικής (συν. 390/30-05-11), αποτελούν οι:

1) Καθ. Σπύρος Ευαγγέλου, (επιβλέπων, Τμήμ. Φυσικής Παν. Ιωαννίνων)
2) Καθ. Παναγιώτης Αργυράκης, (μέλος συμβ. επιτρ., Τμήμ. Φυσικής Παν. Θεσ/κης)
3) Λεκ. Δημήτρης Κατσάνος, (μέλος συμβ. Επιτρ., Τμήμ. Φυσικής Παν. Ιωαννίνων)
4) Καθ. Γεώργιος Ευαγγελάκης, (Τμήμ. Φυσικής Παν. Ιωαννίνων)
5) Αν. Καθ. Νίκος Παπανικολάου, (Τμήμ. Φυσικής Παν. Ιωαννίνων)
6) Επίκ. Καθ. Λευτέρης Λιδωρίκης, (Τμήμ. Υλικών Παν. Ιωαννίνων)
7) Επίκ. Καθ. Ευάγγελος Ευαγγέλου, (Τμήμ. Φυσικής Παν. Ιωαννίνων)

Παρόντα είναι και τα 7 μέλη της εξεταστικής επιτροπής. Το θέμα της διατριβής που εκπόνησε και παρουσίασε σήμερα ο κ. **Ιωάννης Κλεφτόγιαννης** είναι: «**Fractals and Quantum Chaos in Disordered Graphene**». Ο Πρόεδρος της εξεταστικής επιτροπής καθηγητής κ. **Σπύρος Ευαγγέλου** κάλεσε τον υποψήφιο να αναπτύξει το θέμα της διατριβής. Έγινε η παρουσίαση του θέματος από τον υποψήφιο. Στη συνέχεια, ο υποψήφιος απάντησε σε σχετικές ερωτήσεις από το ακροατήριο και αποκλειστικά από τα μέλη της επιτροπής. Η εξεταστική επιτροπή αποσύρθηκε με σκοπό να συσκεφτεί για την τελική αξιολόγηση του υποψηφίου και κρίσης της διατριβής.

Η συζήτηση διήρκεσε περίπου μισή ώρα. Η εξεταστική επιτροπή κατέληξε στα ακόλουθα συμπεράσματα:

1. <u>Διαπιστώνει</u>:

α) Η παρουσίαση και ανάπτυξη του θέματος της διδακτορικής του διατριβής ήταν αρίστη.

β) Η επιστημονική κατάρτιση του υποψήφιου είναι πλήρης.

γ) Η συγγραφή της διατριβής έγινε με τρόπο που δείχνει μεθοδικότητα και ενημέρωση του υποψήφιου πάνω στη βιβλιογραφία σχετική με το θέμα της διατριβής.

2. <u>Κρίνει</u>:

α) Η διατριβή είναι προϊόν μακρόχρονης προσπάθειας και καταλήγει σε σημαντικά αποτελέσματα τα οποία προάγουν την επιστήμη.

β) Η επάρκεια του υποψηφίου στο γνωστικό αντικείμενο της διατριβής είναι πλήρης.

Με βάση τα ανωτέρω, τα μέλη της Επιτροπής εγκρίνουν ομόφωνα τη διδακτορική διατριβή του κ. **Ιωάννη Κλεφτόγιαννη** και εισηγούνται ανεπιφύλακτα ομόφωνα την απονομή του τίτλου του διδάκτορα με βαθμό Άριστα.

Τα μέλη της εξεταστικής επιτροπής:

1) Καθ. Σπύρος Ευαγγέλου, (επιβλέπων, Τμήμ. Φυσικής Παν. Ιωαννίνων)
2) Καθ. Παναγιώτης Αργυράκης, (μέλος συμβ. επιτρ., Τμήμ. Φυσικής Παν. Θεσ/κης)
3) Λεκ. Δημήτρης Κατσάνος, (μέλος συμβ. Επιτρ., Τμήμ. Φυσικής Παν. Ιωαννίνων)
4) Καθ. Γεώργιος Ευαγγελάκης, (Τμήμ. Φυσικής Παν. Ιωαννίνων)
5) Αν. Καθ. Νίκος Παπανικολάου, (Τμήμ. Φυσικής Παν. Ιωαννίνων)
6) Επίκ. Καθ. Λευτέρης Λιδωρίκης, (Τμήμ. Υλικών Παν. Ιωαννίνων)
7) Επίκ. Καθ. Ευάγγελος Ευαγγέλου, (Τμήμ. Φυσικής Παν. Ιωαννίνων).

Ο Πρόεδρος της επιτροπής

Καθ. Σπύρος Ν. Ευαγγέλου.

Abstract

One of the most intriguing subject in modern physics is nanoscience, building the background for understanding the fundamental principles of nanoelectronics. Graphene since its fabrication in 2004 has become one of the main subjects of research in nanoscience. It is the first 2d metal ever made, it has extraordinary electronic properties and offers a vast field for applications and fundamental theoretical work. In this thesis we study the electronic properties of graphene in the presence of disorder, which is an inevitable factor in every mesoscopic system. We accomplish the study of related phenomena through well established methods of mesoscopic physics, like Fractals and Quantum Chaos. This allows us to study the interplay between the well-known electronic behavior of pure graphene, and the diffusive or localization phenomena introduced by the disorder.

Acknowledgements

I would like to take this opportunity to thank all the people who have been involved with my work during my time at Ioannina. Firstly, my supervisor Prof. Spiros Evangelou for providing his help and guidance, without him I wouldn't broad my knowledge in physics. Lecturer D.E.Katsanos for his help in programming and the discussions about various things during my PhD. Dr. Ilias Amanatidis for his collaboration and friendly attitude which provided useful discussions in Physics. Jean-Louis Pichard and his student Axel Freyn for their accommodation and guidance, which helped me earn valuable experience in Physics research. Most importantly I would like to thank my family for their continuing financial and psychological support all these years.

Table of Contents

Chapter 1

Introduction

Graphene, the first 2D metal ever made, is a single layer of carbon atoms densely packed in a honeycomb lattice structure. Graphene was fabricated for the first time in 2004 by the Manchester group of A. Geim and K. Novoselov [1, 2], via mechanical exfoliation of graphite. They were awarded the Nobel prize for Physics in 2010. Graphene has extraordinary properties never encountered in conventional materials before, such as, great flexibility and high electron mobility with electron velocities near the Fermi energy approaching the speed of light c, much higher than in any conventional semiconductor. It can be cut into long strips known as graphene nanoribbons [3] or confined structures known as graphene flakes [4] making it an excellent candidate for replacing silicon in future nanoelectronics. A lot of other techniques for fabricating graphene have also been developed, like epitaxial growth on silicon carbide [5], on metal substrates [6] or by cutting carbon nanotubes [7, 8].

The theoretical study of graphene, through well known quantum methods of solid state physics has revealed some extraordinary effects never encountered in conventional systems before. Its underlying honeycomb lattice structure leads to special

quantum interference effects inducing localization of wavefunctions at the edges of graphene called edge states[10][11]. Moreover, they contribute to energies near the Fermi level, being strongly dependent on the edge morphology. It is clear that the electronic properties of graphene are extremely sensitive to the choice of boundary conditions. The study of these topological effects and their role in the electronic properties of graphene is very important for its incorporation in nanoelectronics. The theoretical study has also revealed the relativistic nature of electrons close to the Fermi energy, opening an interdisciplinary field of relativistic solid state physics[1,11]. The relativistic nature of electrons for over half a century was known for graphite which consists of many layers of graphene stacked together[11]. At the Fermi level the electrons in graphene behave as free relativistic massless particles described by the Dirac equation. This is called the Dirac point. From this point of view graphene can be used as an effective model for studying quantum electrodynamics, with obvious advantages for relativistic quantum experiments like the small space dimensionality required.

Fractals and chaos on the other hand are well established phenomena in classical non-linear dynamical systems. Their existence in the quantum world has been studied extensively during the last decades, mainly in low-dimensional disordered systems known as mesoscopic systems. They lie between the microscopic and the macroscopic scale[12]. The nature of Quantum Chaos is not related to dynamical evolution, but with the statistical properties of the energy spectrum. The disordered quantum systems have been shown to obey the same universal laws as Quantum Chaos They are described by a mathematical theory of fully random matrices, which became known as Random Matrix Theory(RMT)[12,13,14].

On the other hand, signs of the fractal geometry have been shown to exist in

the quantum world, e.g. the electron wavefunctions of disordered two dimensional mesoscopic systems[15,16,17,18]. The fractal nature of wavefunctions close to the metal-insulator transition(MIT) is well known[19,20]. Exactly at the transition point they are characterized by non trivial critical scaling behavior, they are complex objects known as multifractals described by a whole spectrum of fractal dimensions. The wavefunctions below the (MIT) show a diffusive behavior, with the corresponding energy levels obeying the universal laws of RMT as in Quantum Chaos. For sufficiently large enough disorder, above the transition point, quantum destructive interference effects lead to Anderson localization[21].

Graphene is the first real 2D metal ever made, it offers a great opportunity for testing the well established phenomena of Quantum Chaos and Fractals, which were usually studied through the 2d-system known as two dimensional electron gas(2DEG)[22]. Moreover, the confined nature of the experimentally produced finite graphene systems like flakes, with strongly topology dependent electronic properties, pose important questions about their role in the nature of quantum chaos and fratal states. Quantum chaos near the Dirac point is also expected to address relativistic issues. It has been studied experimentally by Ponomarenko and his colleagues [23] obtaining a chaotic nature described by the Dirac equation. They are commonly known as Dirac billiards, proposed by Berry and Mondragon [24]. Theoretical calculations by L. Huang et. al. [25] in graphene billiards predict a different quantum chaotic behavior when compared to the experimentally obtained, while other theoretical calculations in weakly disordered graphene with periodic boundary conditions [26] have shown relativistic chaotic nature independent of the sample size. For strong disorder Anderson localization[21], always prevails.

In this thesis we study the fractal nature of wavefunctions and the chaotic behavior

of the energy levels in disordered graphene near the Dirac point. Firstly, we check the existence of fractal states at the Fermi level in the presence of disorder. The study is carried out in conjunction with the well-known behavior of other conventional disordered materials. Then we address the following question, how the unconventional topology of graphene affects this fractal nature for confined structures? Do edge states survive with disorder and how it can be combined with the fractal nature of the wavefunctions? We study also the role of edge states in the quantum chaotic behavior of graphene near the Dirac point, through the statistical properties of the energy levels.

In chapter two we give a brief introduction of graphene, analyzing in detail its unconventional electronic properties via a simple tight binding model introduced in the appendix. This model allows to derive its relativistic band structure and the topological electronic properties, like edge states.

In chapter three, after a brief introduction to fractals, we study in detail the fractal properties of the wavefunctions of disordered graphene, in conjunction with other systems like the square lattice and the chain. We also show important symmetry properties for disordered graphene such as chiral symmetry.

In chapter four, after a brief introduction to Quantum chaos, we compare the quantum chaotic nature of disordered graphene with a square lattice having on-diagonal short-range disorder.

In chapter five we present our conclusions. In the Appendix we discuss the tight binding model, for various types of lattices in order to determinate their electronic properties.

Bibliography

[1]Geim, A. K. and Novoselov, K. S, Nature Materials 6,183-191 (2007)

[2]K.S.Novoselov et al., Science 306, 666 (2004)

[3]Michael S. Fuhrer Nature Materials, 9, 611-612 (2010)

[4]L. A. Ponomarenko et al., Science 320, 356 (2008)

[5]Sutter, P., Nature Materials 8 (3) (2009)

[6]Geim, A. K. MacDonald, A. H., Physics Today 60: 35-41 (2007)

[7]Brumfiel, G., Nature, doi:10.1038/news.2009.367 (2009)

[8]Kosynkin, D. V. et al., Nature 458 (7240) (2009)

[9]K. Nakada, M. Fujita, G. Dresselhaus, M.S. Dresselhaus, Phys. Rev. B54, 1795417961 (1996)

[10]A. H. Castro Neto, F. Guinea, N. M. R. Peres, K. S. Novoselov and A. K. Geim, RevModPhys. 81. 109 (2009)

[11]P. R. Wallace,PhysRev. 71. 622 (1947)

[12]Y. Alhassid Rev. Mod. Phys. 72, 895 (2000)

[13]A. V. Andreev, O. Agam, B. D. Simons, and B. L. Altshuler, Phys. Rev. Lett. 76, 3947 (1996)

[14]F. Haake, Quantum Signatures of Chaos, 2nd Edition, Springer (2000)

[15]Hideo Aoki Phys. Rev. B 33, 7310 (1986)

[16]V.I. Falko and K.B. Efetov, Europhys. Lett. 32, 627 (1995), Phys. Rev. B 52, 17413 (1995)

[17]Michael Schreiber and Heiko Grussbach, Phys. Rev. Lett. 67, 607 (1991)

[18]S. N. Evangelou, J. Phys. A: Math. Gen. 23 L317 (1990)

[19]Masatoshi Imada, Atsushi Fujimori, and Yoshinori Tokura, Rev. Mod. Phys. 70, 1039 (1998)

[20]Evangelou, S. N., Katsanos, D. E. Journal of Statistical Physics, Volume 85, Issue 5-6, pp. 525-550 (1996)

[21]P. W. Anderson, Phys. Rev. 109, 14921505 (1958)

[22]C. Weisbuch, B. Vinter, Academic Press, London (1991)

[23]L. A. Ponomarenko et al., Science 320, 356 (2008)

[24]M. V. Berry, R. J. Mondragon, Proc. R. Soc. London A 412, 53 (1987).

[25]Liang Huang, Ying-Cheng Lai, and Celso Grebogi, Phys. Rev. E 81, 055203(R) (2010)

[26]I. Amanatidis and S. N. Evangelou, Phys.Rev.B 79, 205420 (2009)

Chapter 2

Graphene

2.1 Introduction

Graphene is a monolayer of carbon atoms arranged in a honeycomb lattice structure. It was fabricated, for the first time in 2004 by the Manchester group of A. Geim and K. Novoselov[1,2]. They have been awarded the Nobel prize in physics for 2010. This one atom thick material is the first real 2d metal ever made. It is a basic candidate for replacing silicon[15] and is expected to have a major impact in nanotechnology and nanomaterials since it can been produced very easily[16]. It's extraordinary electronic properties involve relativistic band structure and topology dependent effects like electronic edge states whose existence depends strongly on the choice of boundary conditions.

In the tight binding formalism(see Appendix) graphene has a unit cell which consists of two carbon atoms A and B as can be seen in Fig. 2.1.

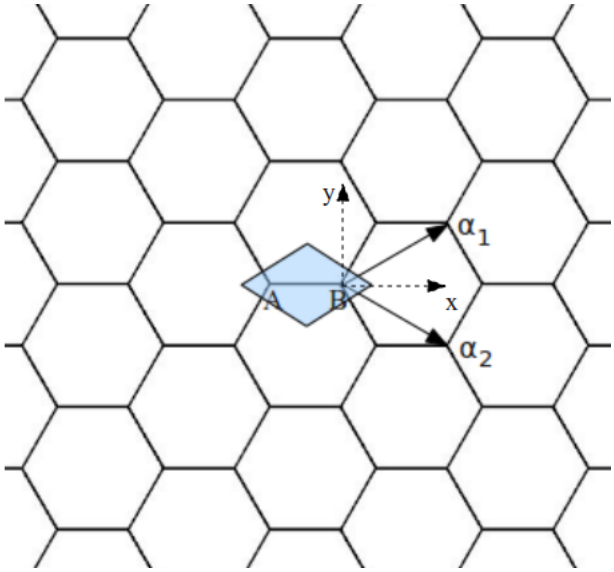

Figure 2.1: Graphene has characteristic honeycomb lattice structure.

The distance between neighbouring carbon atoms is $a_{cc} = 0.142nm$. The major difference with a square lattice is the presence of two instead of one atoms in graphene's unit cell. In order to describe the honeycomb lattice structure we can define two basis vectors $\overrightarrow{a_1}$ and $\overrightarrow{a_2}$

$$\overrightarrow{a_1} = \frac{a\sqrt{3}}{2}\widehat{x} + \frac{a}{2}\widehat{y}$$

$$\overrightarrow{a_2} = \frac{a\sqrt{3}}{2}\widehat{x} - \frac{a}{2}\widehat{y}$$

which connect adjacent unit cells, $a = |a_1| = |a_2| = \sqrt{3}a_{cc}$. Using $\overrightarrow{a_1}$,$\overrightarrow{a_2}$, we can easily construct the whole honeycomb lattice by repeating the unit cell of the two carbon atoms A and B. This is done for the dimer in the Appendix, write down the Schrodinger difference equations corresponding to the two different carbon atoms in the unit cell and apply Bloch's theorem.

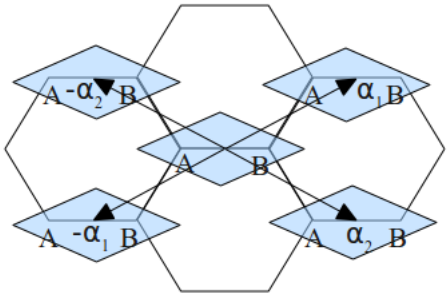

Figure 2.2: Unit cells of the honeycomb lattice.

As seen in Fig. 2.2 type A atom belonging to the central unit cell is connected with three type B atoms. One of those atoms is part of the same unit cell while the other two belong to the unit cells on the left, described by the vectors $-\overrightarrow{a_1}$ and $-\overrightarrow{a_2}$. So the tight binding equation centered on atom A inside the central unit cell by using the Bloch's theorem (see Appendix) becomes

$$E\Psi_A = -t(\exp(-i\,\overrightarrow{k}\,0) + \exp(-i\,\overrightarrow{k}\,\overrightarrow{a_1}) + \exp(-i\,\overrightarrow{k}\,\overrightarrow{a_2}))\Psi_B \Rightarrow$$

$$\Rightarrow E\Psi_A = -t(1 + \exp(-i\,\overrightarrow{k}\,\overrightarrow{a_1}) + \exp(-i\,\overrightarrow{k}\,\overrightarrow{a_2}))\Psi_B.$$

The corresponding equation is for the B atom

$$E\Psi_B = -t(1 + \exp(i\,\overrightarrow{k}\,\overrightarrow{a_1}) + \exp(i\,\overrightarrow{k}\,\overrightarrow{a_2}))\Psi_A.$$

This system of two equations with two unknowns Ψ_A,Ψ_B can be written in a matrix form as

$$\begin{bmatrix} 0 & f_1(\overrightarrow{k}) \\ f_1^*(\overrightarrow{k}) & 0 \end{bmatrix} \begin{bmatrix} \Psi_A \\ \Psi_B \end{bmatrix} = \begin{bmatrix} E & 0 \\ 0 & E \end{bmatrix} \begin{bmatrix} \Psi_A \\ \Psi_B \end{bmatrix} \Rightarrow H\Psi = E\Psi \qquad (2.1)$$

where $f_1(\overrightarrow{k}) = -t(1 + \exp(-i\overrightarrow{k}\overrightarrow{a_1}) + \exp(-i\overrightarrow{k}\overrightarrow{a_2}))$. So the graphene hamiltonian can be written as a two dimensional matrix

$$H = \begin{bmatrix} 0 & f_1(\overrightarrow{k}) \\ f_1^*(\overrightarrow{k}) & 0 \end{bmatrix}, \tag{2.2}$$

whose eigenvalues are

$$E = \pm\sqrt{\left|f_1(\overrightarrow{k})\right|^2} = \pm\left|f_1(\overrightarrow{k})\right| =$$

$$= \pm\left|1 + \exp(-ik_x\frac{\sqrt{3}}{2}a)(\exp(ik_y\frac{a}{2}) + \exp(-ik_y\frac{a}{2}))\right| = \pm\left|1 + 2\exp(-ik_x\frac{\sqrt{3}}{2}a)\cos(k_y\frac{a}{2})\right| =$$

$$= \pm\sqrt{(1 + 2\cos(k_x\frac{3}{2}a_{cc})\cos(ik_y\frac{a}{2}))^2 + 4\sin^2(k_x\frac{3}{2}a_{cc})\cos^2(k_y\frac{a}{2})} =$$

$$= \pm\sqrt{1 + 4\cos^2(k_x\frac{\sqrt{3}}{2}a)\cos^2(ik_y\frac{a}{2}) + 4\cos(k_x\frac{\sqrt{3}}{2}a)\cos(k_y\frac{a}{2}) + 4\sin^2(k_x\frac{\sqrt{3}}{2}a)\cos^2(k_y\frac{a}{2})} \Rightarrow$$

$$E_\pm(k_x, k_y) = \pm t\sqrt{1 + 4\cos(\frac{ak_y}{2})\cos(\frac{\sqrt{3}ak_x}{2}) + 4\cos^2(\frac{ak_y}{2})}, k_x, k_y \in [-\pi, \pi]. \tag{2.3}$$

Eq. (2.3) is the energy dispersion relation of graphene plotted in Fig. 2.3. The energy dispersion is consisted of two branches, for positive and negative energies respectively. They touch at six K points, known as valleys, lying on the corners of the first brillouin zone which has the form of a hexagon(see Fig 2.4). The Fermi level is at zero energy, making graphene a zero gap semiconductor. The energy dispersion has a cone like structure at those six K points with the energy being proportional to the absolute value of the wavevector $\overrightarrow{k}$,

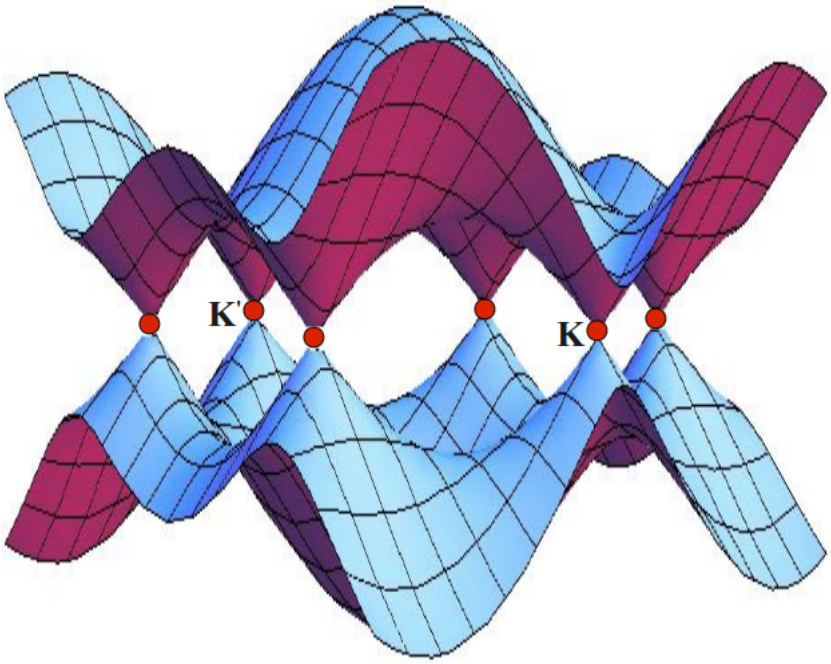

Figure 2.3: Energy dispersion of graphene. The six K points corresponding to zero energy can be distinguished, the two K,K' are non-equivalent

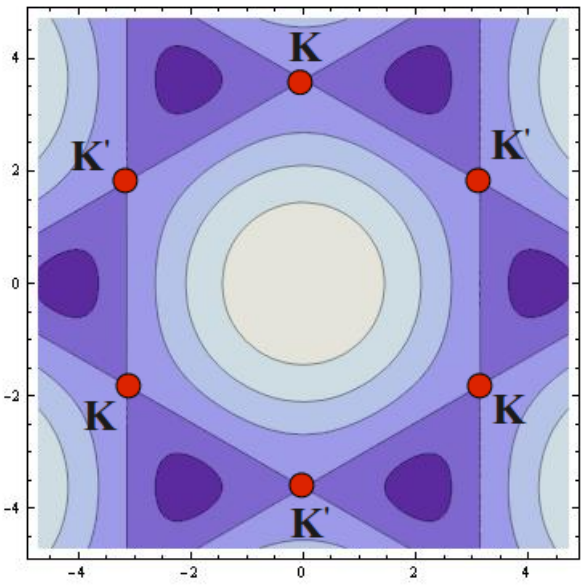

Figure 2.4: Contour plot of the energy dispersion of graphene. The points along the lines have equal energies so that different lines correspond to different energies.The sik K points can be distinguished along with the first Brillouin zone which has the form of a hexagon.

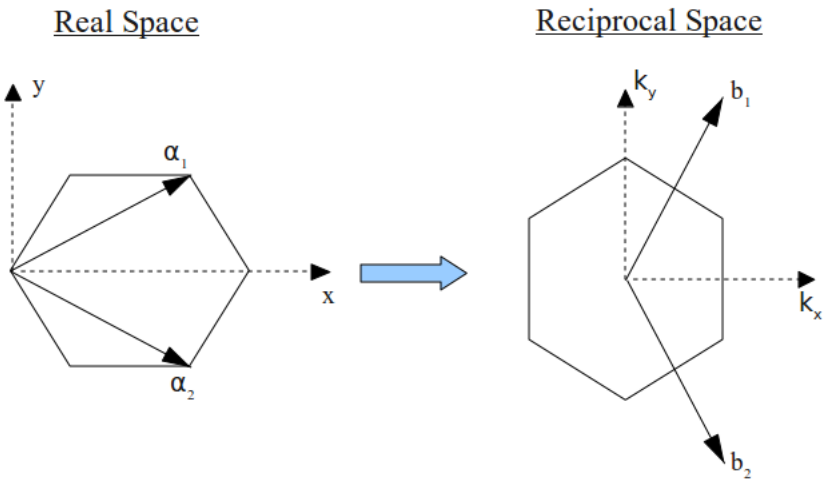

Figure 2.5: Real and reciprocal space of graphene.

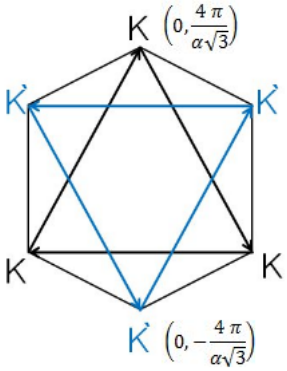

Figure 2.6: The two non-equivalent K points of graphene.

$$E = \frac{t\sqrt{3}a}{2}\left|\overrightarrow{k}\right|. \tag{2.4}$$

The linear energy relation of Eq. (2.4) resembles relativistic massless particles described by the Dirac equation.

The reciprocal space of graphene can be described by the the two reciprocal lattice vectors $\overrightarrow{b_1} = \frac{2\pi}{a\sqrt{3}}\widehat{x} + \frac{2\pi}{a}\widehat{y}$, $\overrightarrow{b_2} = \frac{2\pi}{a\sqrt{3}}\widehat{x} - \frac{2\pi}{a}\widehat{y}$. As seen in Fig 2.6 by using $\overrightarrow{b_1}$ and $\overrightarrow{b_2}$ it is possible to make a transition from one of the six K points only to two others

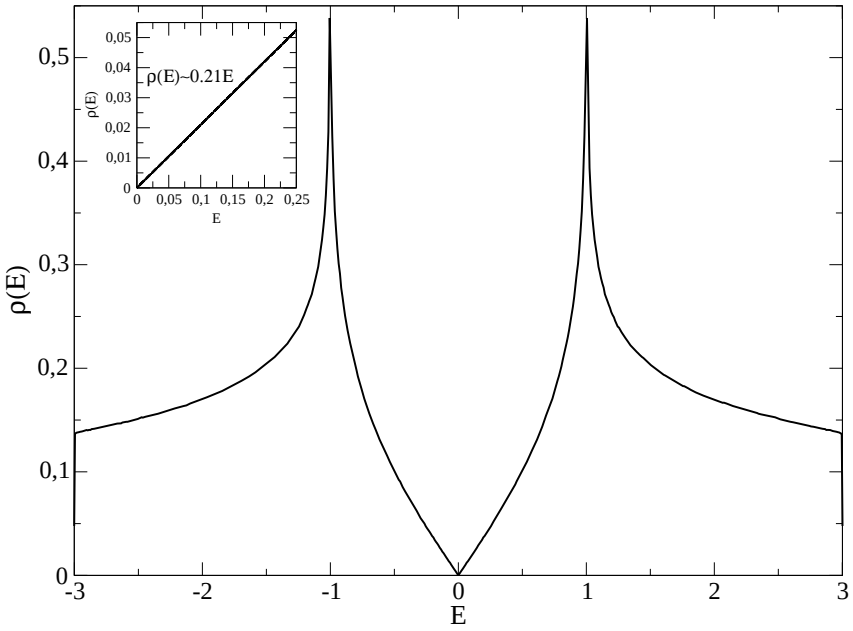

Figure 2.7: Density of states of graphene for $t = 1$ and $a = 1$.

which implies that only two of them are non-equivalent. We choose those points to be $K(0, \frac{4\pi}{a\sqrt{3}})$ and $K'(0, -\frac{4\pi}{a\sqrt{3}})$. They are sufficient in order to reproduce the remaining four K points and consequently the first brillouin zone of graphene.

The density of states of graphene is shown in Fig 2.7. It extends in the energy interval $-3t$ to $3t$ since in the honeycomb lattice structure every site is connected with it's three nearest neighbours. We observe that it is singular at $-1t$ and $1t$ and that it increases linearly at zero energy, in the six Dirac cones. We can prove this by using the definition for the density of states Eq. (A.4) and the polar coordinates $dk_x dk_y = k dk dk_y$ as follows

$$\rho(E) = \frac{1}{(2\pi)^2} \int dk_x \int dk_y \delta(E - E(k)) = \frac{1}{(2\pi)^2} \int_0^{2\pi} d\theta \int_0^{\infty} k dk \delta\left(E - \frac{t\sqrt{3}a}{2}k\right) =$$

$$\frac{2}{3\pi(at)^2}\int_0^\infty kdk\delta\left(E-k\right)=\frac{2}{3\pi(at)^2}E$$

$$\Rightarrow \rho\left(E\right)=\frac{2}{3\pi(at)^2}E. \tag{2.5}$$

A very important remark is that energy dispersion Eq. (2.3) does not have the simple form of the square lattice dispersion relation Eq. (A.18) where energy is split in two equal terms corresponding to the x and y spatial directions respectively. In the square lattice the two spatial directions are equivalent, being an isotropic model.

We can represent graphene by it's topologically equivalent brickwall lattice model shown in Fig. 2.8. It is obtained by removing every second bond along one of the spatial directions of the square lattice. The tight binding hamiltonian of the brickwall lattice is the same as graphene's and consequently the dispersion Eq. (2.3) holds. It clearly introduces a spatial anisotropy which makes the two spatial directions non-equivalent.

A brickwall lattice has also another feature mixing of k_x, k_y directions reflected in Eq. (2.3). A simple way to introduce spatial anisotropy in a square lattice model would be to assume different hoppings along the x and y directions, respectively. The corresponding square lattice dispersion relation becomes

$$E(k_x,k_y)=-2t_x\cos(k_x)-2t_y\cos(k_y),$$

split in two inequal terms due to the introduced anisotropy. This lattice however does not mix k_x, k_y and thus preserves the independency of the two spatial directions. Therefore, anisotropy and direction mixing are two mechanisms both present in graphene which play an important role in its peculiar electronic properties.

The eigenvectors of the graphene hamiltonian Eq. (2.2) can be obtained by solving

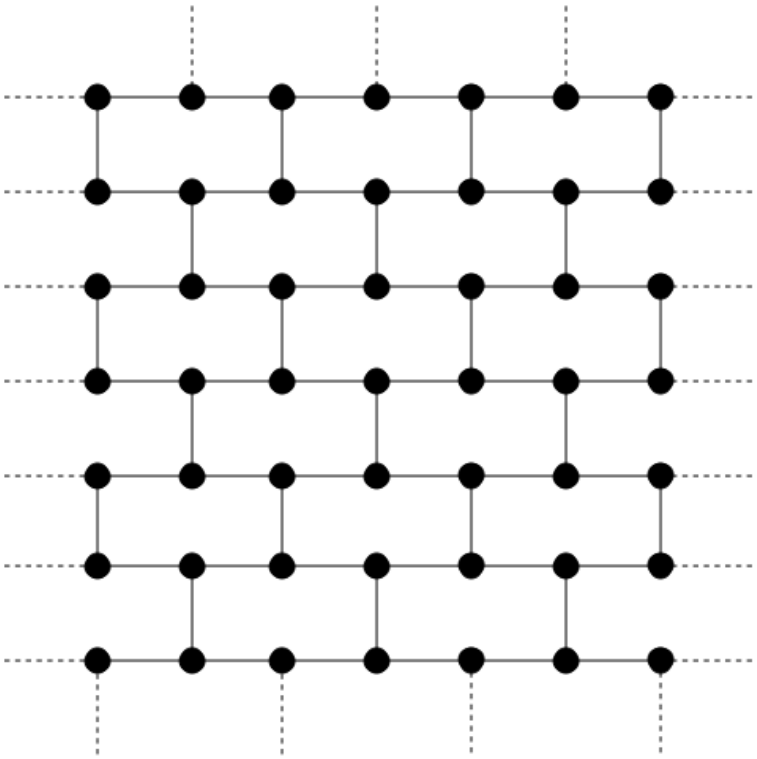

Figure 2.8: A brickwall lattice.

the system of linear equations

$$\begin{bmatrix} -E & f_1(\overrightarrow{k}) \\ f_1^*(\overrightarrow{k}) & -E \end{bmatrix} \begin{bmatrix} \Psi_A \\ \Psi_B \end{bmatrix} = 0,$$

for the eigenvalue $E_+ = t\sqrt{f_1(\overrightarrow{k}) f_1^*(\overrightarrow{k})}$ we get the equation

$$-t\sqrt{f_1(\overrightarrow{k}) f_1^*(\overrightarrow{k})}\Psi_A + t f_1(\overrightarrow{k})\Psi_B = 0 \Rightarrow \Psi_B = \frac{f_1^*(\overrightarrow{k})}{\sqrt{f_1(\overrightarrow{k})}}\Psi_A$$

so that the corresponding eigenvector can be written in the form

$$\Psi_{E_+} = \Psi_A \begin{bmatrix} 1 \\ \frac{f_1^*(\overrightarrow{k})}{\sqrt{f_1(\overrightarrow{k})}} \end{bmatrix}$$

and the normalization gives $\left|\Psi_{E_+}\right|^2 = 1$ as

$$\Psi_{E_+} = \sqrt{\frac{1}{1 + \left|f_1(\overrightarrow{k})\right|}} \begin{bmatrix} 1 \\ \frac{f_1^*(\overrightarrow{k})}{\sqrt{f_1(\overrightarrow{k})}} \end{bmatrix}.$$

Following the same procedure for energies $E_- = -t\sqrt{f_1(\overrightarrow{k}) * f_1^*(\overrightarrow{k})}$. the eigenvectors of Eq. (2.2) can be written in a general form as

$$\Psi_{E_\pm} = \sqrt{\frac{1}{1 + \left|f_1(\overrightarrow{k})\right|}} \begin{bmatrix} 1 \\ \pm\frac{f_1^*(\overrightarrow{k})}{\sqrt{f_1(\overrightarrow{k})}} \end{bmatrix} \tag{2.6}$$

which gives the amplitudes on A and B atomic sites. From Bloch's theorem ampli-

tudes on all the other unit cells will be given by $\Psi_{E_\pm}$ multiplied by a phase factor $\exp\left(i\,\overrightarrow{k}\,\overrightarrow{R}\right)$ depending on the position $\overrightarrow{R} = n\overrightarrow{a_1} + m\overrightarrow{a_2}$ of each unit cell. We can interpret this factor as simply the product of two traveling waves along the two spatial directions $\exp(ik_x x), \exp(ik_y y)$ as in the case of the square lattice model, with variables x and y denoting the coordinates of each unit cell this time.

The interesting point here is that for positive energies E_+ the amplitudes on B type sites differ by just a minus sign from the corresponding amplitudes for negative energies E_-. This fact along with the symmetric spectrum around zero energy are both consequence of a general property called chiral symmetry, which characterizes the so called bipartite lattices. The chiral symmetry combined with the fact that the unit cell of graphene consists of two atoms is to a great extent responsible for its highly unconventional electronic properties.

2.2 Relativistic effects

One of the most remarkable things about graphene is that electrons with energies near the Fermi energy $E_f = 0$ can be effectively described by the Dirac equation for free massless particles[1,3,4]. Close enough to the six K points of the first brillouin zone the band structure of graphene has a cone like form and the energy near there is proportional to the absolute value of the wavevector $\overrightarrow{k}$

$$E = \pm\hbar v_f \left|\overrightarrow{k}\right|, \tag{2.7}$$

where $v_f = 10^6 \frac{m}{s}$ is the fermi velocity of electrons. Energy-momentum relation for relativistic massless particles has the form

$$E^2 = \sqrt{c^2p^2 + m^2c^4} \Rightarrow E = \pm cp \Rightarrow E = \pm \hbar ck.$$

The speed of light c is replaced by the fermi velocity of electrons v_f, so that they behave like photons with a modified universal constant v_f instead of c. The velocity v_f has a very high value, notably higher than any conventional semiconductor. It is not however high enough comparable with the actual speed of light $c = 3\text{x}10^8 \frac{m}{s}$, so it is not essential using the Dirac equation to describe electron motion in graphene. We shall see that the Dirac equation is simply reproduced by the tight binding Schrodinger equation near the Fermi energy. This makes graphene a very useful effective model for studying relativistic massless particles. Both the discrete tight binding and the continuous Dirac approach can be used to study graphene near the Fermi energy, with the Dirac approach being more favorable for analytical calculations.

Let's see how the dispersion relation Eq. (2.3) is linearized close to the Fermi energy. It is enough to linearize at one of the six K points say $K_1(0, \frac{4\pi}{3a})$. We must first deal with the term $f_1(\overrightarrow{k}) = -t(1 + \exp(-i\overrightarrow{k}\overrightarrow{a_1}) + \exp(-i\overrightarrow{k}\overrightarrow{a_2}))$ in Eq. (2.2). We can make a small variation from $\overrightarrow{K_1}$ via $\overrightarrow{k} = \overrightarrow{K_1} + \overrightarrow{\delta k}$. The direction of $\overrightarrow{\delta k}$ doesn't play any role because of the cone like band structure at this point. We can write

$$f_1(\overrightarrow{k}) = -t(1 + \exp(i\overrightarrow{K_1}\overrightarrow{a_1}) \exp(i\overrightarrow{\delta k}\overrightarrow{a_1}) + \exp(i\overrightarrow{K_1}\overrightarrow{a_2}) \exp(i\overrightarrow{\delta k}\overrightarrow{a_2}))$$

because δk is small we can write $\exp(i\overrightarrow{\delta k}\overrightarrow{a_1}) = 1 + i\overrightarrow{\delta k}\overrightarrow{a_1}$. Also $\overrightarrow{K_1}\overrightarrow{a_1} = -\overrightarrow{K_1}\overrightarrow{a_2} = \frac{2\pi}{3}$.

Substituting in the previous relation we get

$$f_1(\overrightarrow{k}) = -t(1+(-\frac{1}{2}+i\frac{\sqrt{3}}{2})(1+i\overrightarrow{\delta k}\overrightarrow{a_1})+(-\frac{1}{2}-i\frac{\sqrt{3}}{2})(1+i\overrightarrow{\delta k}\overrightarrow{a_2})) = -\frac{\sqrt{3}a}{2}(i\delta k_x+\delta k_y).$$

For convenience we can move the origin of our coordinate system on $K_1(0, \frac{4\pi}{3a})$ measuring this way the wavevector $\overrightarrow{k}$ from K_1 replacing $\overrightarrow{\delta k}$ with $\overrightarrow{k}$. So the Hamiltonian of graphene close to the Fermi energy $E_f = 0$ can be written in the form

$$H_{k_1} = -\frac{t\sqrt{3}a}{2}\begin{bmatrix} 0 & ik_x + k_y \\ -ik_x + k_y & 0 \end{bmatrix}.$$

Using also the realistic value of the hopping $t = 2.8eV$ for graphene and the value of the lattice constant $a = a_{cc}\sqrt{3} = 0.246nm$ we can replace $\frac{t\sqrt{3}a}{2}$ with $\hbar v_f$ and write,

$$H_{k_1} = -\hbar v_f\begin{bmatrix} 0 & ik_x + k_y \\ -ik_x + k_y & 0 \end{bmatrix}.$$

The eigenvalues of H_{k_1} reproduce the linear dispersion relation (2.4)

$$|H_{k_1}| = \begin{vmatrix} -E & -\hbar v_f(ik_x + k_y) \\ -\hbar v_f(-ik_x + k_y) & -E \end{vmatrix} = E^2-(\hbar v_f\,|ik_x + k_y|)^2 = 0 \Rightarrow E = \pm\hbar v_f\left|\overrightarrow{k}\right|.$$

In order to be able compare with the Dirac Hamiltonian we have to rotate the original coordinate system ninety degrees anti-clockwise transforming the coordinates as $x \to y$ and $y \to -x$ resulting in $k_x \to k_y$ and $k_y \to -k_x$. The Hamiltonian of graphene

then transforms to

$$H_{k_1} = \hbar v_f \begin{bmatrix} 0 & k_x - ik_y \\ k_x + ik_y & 0 \end{bmatrix}. \tag{2.8}$$

It can be written in a more compact form via the Pauli matrices σ_i as

$$H_{k_1} = \hbar v_f \overrightarrow{\sigma}\,\overrightarrow{k},$$

while its eigenvectors are of the form of (2.6) with $f_1(\overrightarrow{k}) = k_x - ik_y$, each component corresponds to the two type of atoms A and B.

Following the same procedure for the other non equivalent K point, $K_2(0, -\frac{4\pi}{3a})$ we obtain a hamiltonian of the form

$$H_{k_2} = -\hbar v_f \begin{bmatrix} 0 & k_x + ik_y \\ k_x - ik_y & 0 \end{bmatrix}.$$

We can also write it in a compact form similar to the previous one as

$$H_{k_2} = -\hbar v_f \overrightarrow{\sigma}^* \overrightarrow{k}.$$

Its eigenvectors are the complex conjugate of the ones corresponding to K_1 due to a difference π in their phases.

The Dirac equation for relativistic quantum particles can be cast in the same form as the Schrodinger equation $H\Psi = E\Psi$, with H replaced by the four by four matrix

$$H_D = \begin{bmatrix} mc^2 I & c\overrightarrow{\sigma}\overrightarrow{p} \\ c\overrightarrow{\sigma}\overrightarrow{p} & mc^2 I \end{bmatrix}.$$

For massless particles, like photons, the Dirac hamiltonian becomes

$$H_D = \begin{bmatrix} 0 & c\overrightarrow{\sigma}\,\overrightarrow{p} \\ c\overrightarrow{\sigma}\,\overrightarrow{p} & 0 \end{bmatrix} = \hbar c \begin{bmatrix} 0 & \overrightarrow{\sigma}\,\overrightarrow{k} \\ \overrightarrow{\sigma}\,\overrightarrow{k} & 0 \end{bmatrix}$$

and using the fact that

$$\overrightarrow{\sigma}\,\overrightarrow{k} = \sigma_x k_x + \sigma_y k_y = \begin{bmatrix} 0 & k_x - ik_y \\ k_x + ik_y & 0 \end{bmatrix}$$

we can write

$$H_D = \hbar c \begin{bmatrix} 0 & 0 & 0 & k_x - ik_y \\ 0 & 0 & k_x + ik_y & 0 \\ 0 & k_x - ik_y & 0 & 0 \\ k_x + ik_y & 0 & 0 & 0 \end{bmatrix}.$$

In order to compare with the Hamiltonian of graphene near the Fermi energy we have to rearange its elements and write it us

$$H_D = \hbar c \begin{bmatrix} 0 & k_x - ik_y & 0 & 0 \\ k_x + ik_y & 0 & 0 & 0 \\ 0 & 0 & 0 & k_x - ik_y \\ 0 & 0 & k_x + ik_y & 0 \end{bmatrix}.$$

This is a block diagonal matrix with both blocks having the same form. The block

diagonal Dirac Hamiltonian can be written as

$$H_D = \hbar c \begin{bmatrix} H_D^{'} & 0 \\ 0 & H_D^{'} \end{bmatrix}$$

with

$$H_D^{'} = \hbar c \begin{bmatrix} 0 & k_x - ik_y \\ k_x + ik_y & 0 \end{bmatrix}.$$

These parts actually describe particles and antiparticles, becoming equivalent in the massless case.The eigenvectors of each part are known as spinors and consist of two components corresponding to the two different spin orientations, up and down, of the described massless particle. The derived Dirac hamiltonian derived is exactly the hamiltonian of graphene Eq. (2.8) at $K_1(0, \frac{4\pi}{3a})$ if we just replace the speed of light c by the fermi velocity of electrons v_f. In order to reproduce the graphene Hamiltonian of graphene at $K_2(0, -\frac{4\pi}{3a})$ we have to make a different rearangement of the Dirac Hamiltonian resulting in

$$H_{DIRAC} = \hbar c \begin{bmatrix} 0 & k_x + ik_y \\ k_x - ik_y & 0 \end{bmatrix}.$$

The speed of light c in this case is replaced by $-v_f$ denoting massless fermions moving in the transverse direction of those at $K_1(0, \frac{4\pi}{3a})$, known as holes. So the two nonequivalent Dirac K points K_1 and K_2 correspond to electrons moving in transverse directions, electrons and holes respectively, each described by the Dirac equation for free massless particles with the speed of light c being replaced by the fermi velocity of electrons v_f.

2.3 Electronic properties of Graphene structures

Graphene can be cut experimentally in various shapes, for example long strips called ribbons[8,9,10] or nanometer sized confined structures known as flakes[11]. The electronic properties of those systems can be understood theoretically by applying the appropriate boundary conditions on an infinite sheet made of graphene.

2.3.1 Edge States

Edge states in graphene nanostructures were first discovered by the pioneering theoretical work of M. Fujita et al[5] and have been observed experimentally[7]. Imagine a semi-infinite sheet of graphene(see Fig 2.9) extending to infinity in the y direction and is semi infinite in the x direction. We observe a zigzag like orientation along the top.

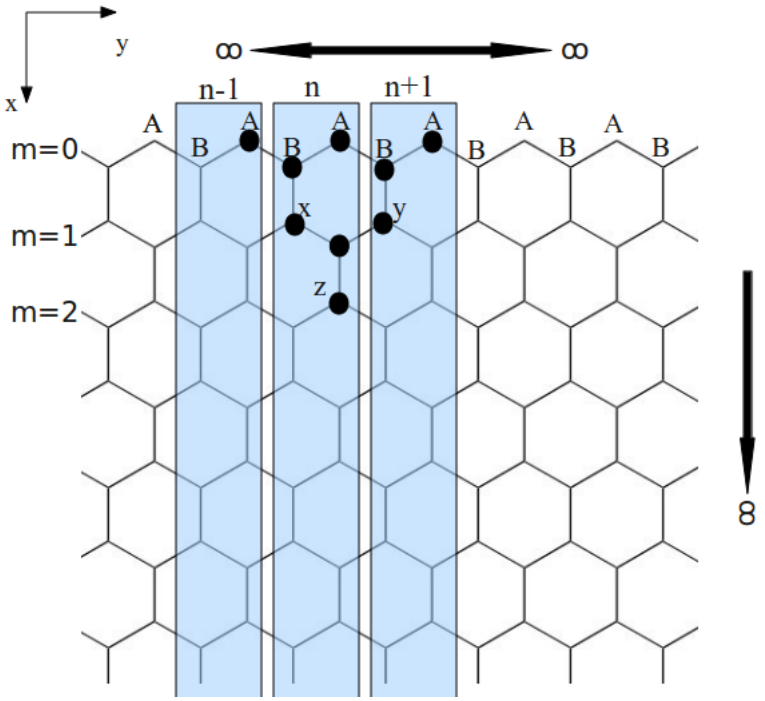

Figure 2.9: A semi infinite graphene sheet with one zigzag edge.

It can be viewed as an infinite sequence of horizontal zigzag chains each denoted by an index m=0,1,2,.. .It has just one edge with a zigzag like orientation. Equivalently It can be also split in vertical chains of infinite length (shadowed parts in Fig 2.9) to apply Bloch's theorem(see Appendix). Because of the sublattice chiral symmetry the corresponding wavefunctions for energy $E = 0$ have zero amplitudes on all the sites belonging to one of the sublattices A or B(see Chapter three). Assuming that the amplitude is zero for the B sublattice the tight-binding equations for the first zigzag chain (m=0) and n,$n+1$ unit cells, with $E = 0$ become (k is along the y direction)

$$\begin{aligned} 0 &= -t(\exp(ik(n-1)) + \exp(ikn))\Psi_A + \Psi_x \\ 0 &= -t(\exp(ik(n+1)) + \exp(ikn))\Psi_A + \Psi_y \end{aligned} \Rightarrow$$

$$\Rightarrow \begin{aligned} \Psi_x &= -2t\Psi_A \cos(\tfrac{k}{2}) \exp(i\tfrac{k}{2}) \exp(ikn) \\ \Psi_y &= -2t\Psi_A \cos(\tfrac{k}{2}) \exp(-i\tfrac{k}{2}) \exp(ikn) \end{aligned} .$$

The amplitude Ψ_z belonging to the chain with $m = 3$ on the unit cell n can be easily calculated via

$$\Psi_x + \Psi_y + \Psi_z = 0 \Rightarrow \Psi_z = -2t\Psi_B \cos^2(\frac{k}{2}) \exp(ikn).$$

For different values n give the amplitudes on A type atoms along the m zigzag chain are given according to the Bloch's theorem. We can continue for the rest of the zigzag chains and the corresponding propability for sites lying on the m zigzag chain away from the zigzag like top ($m = 0$) are

$$|\Psi_A^m|^2 = 4\Psi_A^2 \cos^{2m}(\frac{k}{2}). \tag{2.9}$$

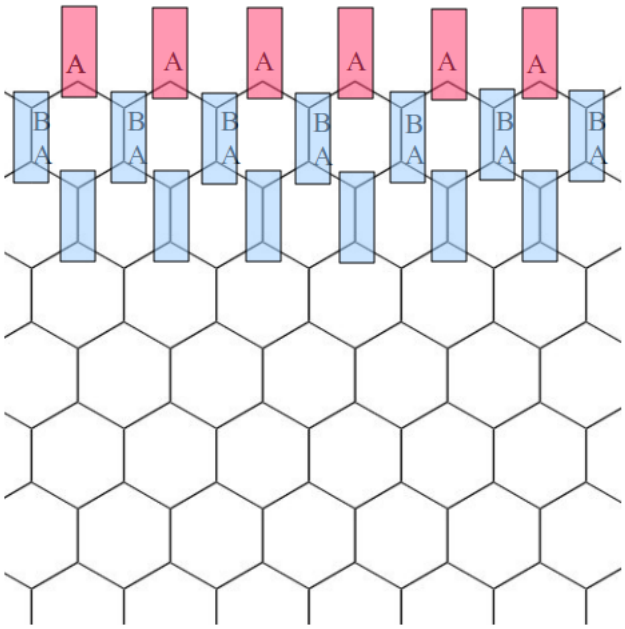

Figure 2.10: A zigzag edge breaks the periodicity of graphene. B sites missing along the edge.

For $k = \pi$ this is non-zero only on the first zigzag chain ($m = 0$). This gives a special edge state with zero energy and a corresponding wavefunction completely localized at the zigzag edge of the semi infinite graphene sheet ($m = 0$). For $k < \pi$ we have $\cos(\frac{k}{2})^2 < 1$ and the wavefunction propability penetrates inside the sheet with decaying amplitude $\left(cos^2(\frac{k}{2})\right)^m$ as the value of m increases, resulting again in edge states with zero energy, but with a smaller degree of localization. Note that we have not taken into account the analytical form for the graphene wavefunction (2.6). This is due to the fact that by forming a zigzag edge we have broken the $A-B$ sublattice symmetry, since for every edge site A it's counterpart site B belonging to the same unit cell is missing as can be seen in Fig. 2.10. This breaks the periodicity of the system destroying the validity of the wavefunction Eq. (2.6) and the dispersion

relation Eq. (2.3).

Edge states are a consequence of the special morphology of the honeycomb lattice which favors quantum destructive interference for zero energy. The honeycomb lattice, every site connected to three others, and as a result the tight binding equation written for each site will have four components. For zero energy the number of components reduces to three (one is multiplied by zero) giving an equation like the one used to derive Eq. (2.9). The corresponding equations for a zigzag edge be interpreted as the sum of two incident waves coming from the two A atoms belonging to the $n-1$ and n, unit cell respectively. They interfere with each other giving an outgoing wave at x. In the equation used to derive Eq. (2.9) we can see that the different phase factors $\exp(i\frac{k}{2})$ and $\exp(-i\frac{k}{2})$ for the amplitudes Ψ_x and Ψ_y give a destructive interference effect for Ψ_z. For $k=\pi$ complete destructive interference occurs with wavefunctions that have non-zero amplitude only at the edge of the graphene sheet. For example the tight-binding equation for the B type atom inside the n unit cell for $k=\pi$ gives

$$\Psi_x = -t(\exp(i(\pi n-\pi)) + \exp(i\pi n))\Psi_A.$$

This is the sum of two waves with a phase difference π canceling with each other.

A very important feature of graphene is that the existence of edge states depends on the orientation of the boundaries. For example we could take an infinite graphene sheet and cut it on a direction rotated by 30 degrees compared to the previous case a sheet with a zigzag edge. The sheet is again semi-infinite but with a different edge orientation , called armchair. The armchair edge preserves the $A-B$ symmetry unlike the zigzag sheet shown in Fig. 2.12. The wavefunctions of the semi-infinite system with an armchair edge will have the form of Eq. (2.6) multiplied by a factor

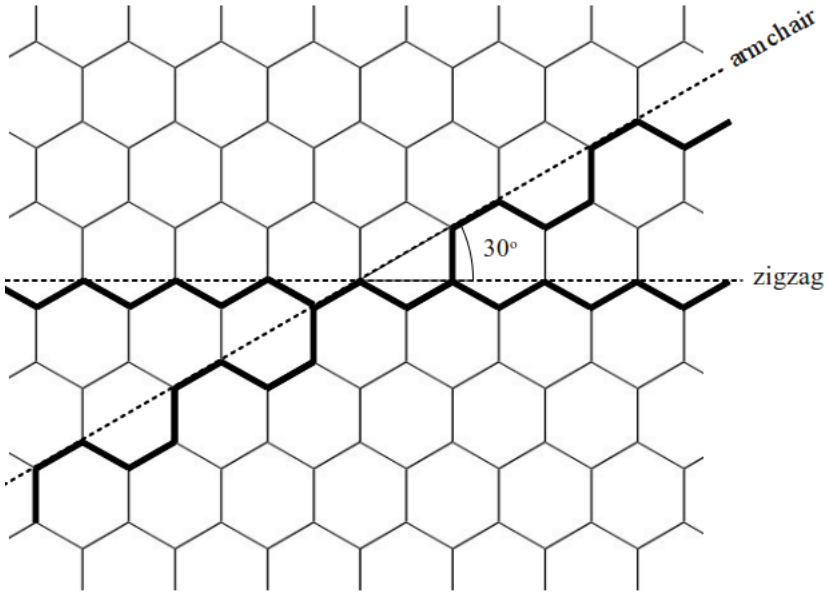

Figure 2.11: Two ways of cutting graphene in order to obtain a zigzag or an armchair edge.

concerning of a running wave in x direction and a standing wave in the y direction where the hardwall boundary conditions are applied, giving

$$\Psi_{E_\pm} = \sqrt{\frac{1}{1+\left|f_1(\overrightarrow{k})\right|}} \begin{bmatrix} 1 \\ \pm\frac{f_1^*(\overrightarrow{k})}{\sqrt{f_1(\overrightarrow{k})}} \end{bmatrix} exp(ik_x x)\sin(k_y y),$$

x and y being are the coordinates of each unit cell. It is evident from this form that edge states are absent for the armchair boundary morphology.

2.3.2 Nanoribbons(GNR)

Graphene nanoribbons(GNR) are infinitely long strips of graphene. They have been produced experimentally[8,9,10]. Their electronic properties are well known[5,6]. The destructive interference mechanism of the honeycomb lattice plays an important role

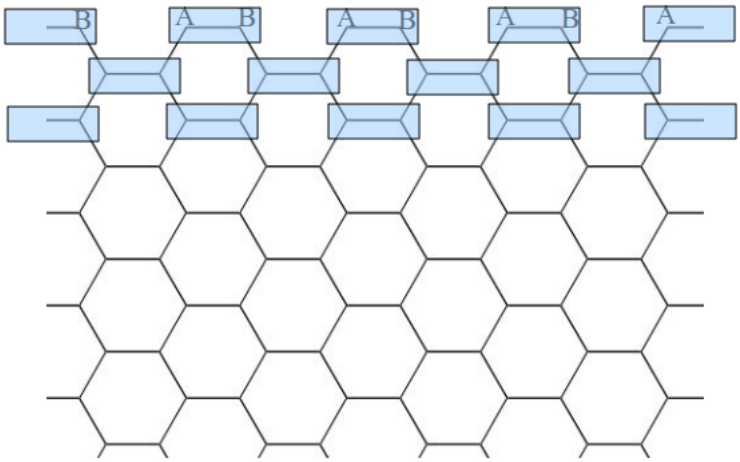

Figure 2.12: A semi infinite piece of graphene with an armchair edge.

in their electronic properties, contributing zero-energy edge states when zigzag edges are present (see section 2.3). The exact edge orientation (zigzag or armchair) of a GNR plays a definite role in their semi-conducting behavior.

Consider the GNR shown in Fig. 2.13. It is formed by applying hardwall boundary conditions on an infinite graphene sheet along the vertical x spatial direction and it has two zigzag like edges. It is called a zigzag ribbon. In Fig. 2.13 the number of horizontal zigzag chains is even the structure is symmetric along the x axis. If the number of zigzag chains is odd the resulting ribbon structure is not symmetric, giving an antizigzag ribbon (see Fig. 2.14). As stated already the inclusion of zigzag edges breaks the $A-B$ periodicity, so that the allowed energies of those ribbons can not be directly derived from the dispersion relation of graphene Eq. (2.3). However, we can calculate the allowed energies, called band structure(see Appendix), by using Bloch's theorem. In Fig. 2.13 we can see the unit cell (shadowed area) the ribbons is a chain. Consider a zigzag GNR consisting of two horizontal zigzag chains shown in Fig. 2.15. the tight-binding equations for atoms belonging in the nth unit cell are

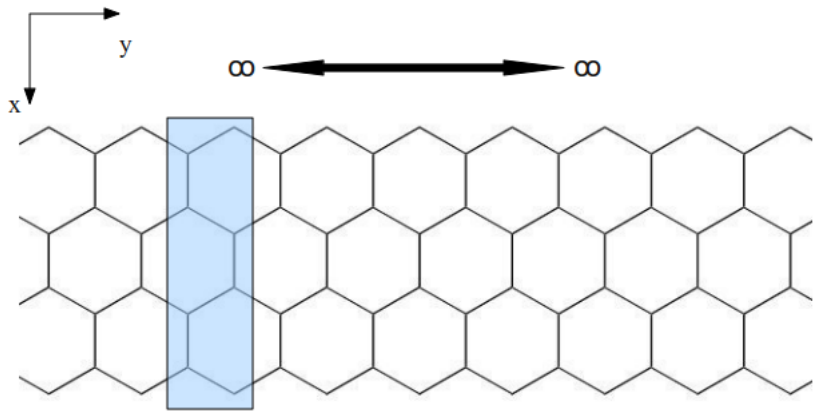

Figure 2.13: A zigzag ribbon.The shadowed area denotes its unit cell.

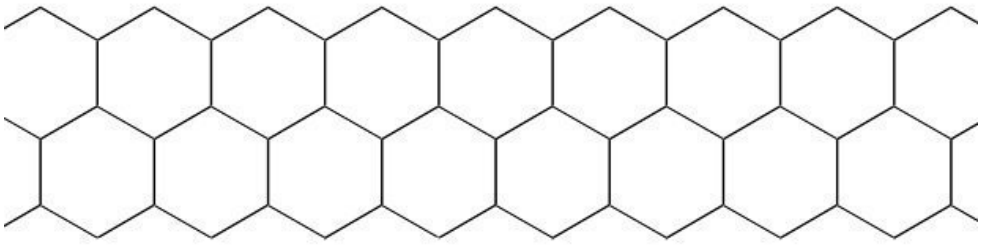

Figure 2.14: An antizigzag ribbon for N=3 zigzag chains.

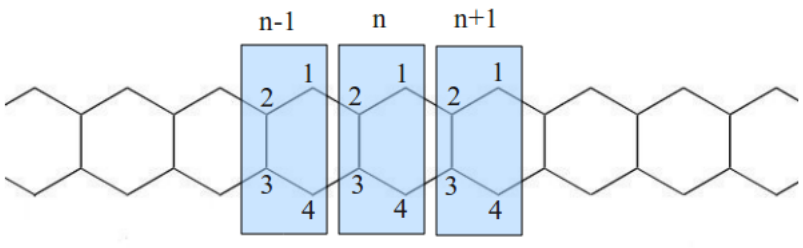

Figure 2.15: A zigzag ribbon for N=2.

$$E\Psi_1^n = -t(\Psi_2^n + \Psi_2^{n+1})$$

$$E\Psi_2^n = -t(\Psi_1^n + \Psi_1^{n-1} + \Psi_3^n)$$

$$E\Psi_3^n = -t(\Psi_4^n + \Psi_4^{n-1} + \Psi_2^n)$$

$$E\Psi_4^n = -t(\Psi_3^n + \Psi_3^{n+1})$$

via the Bloch's theorem (see Appendix) we can write $\Psi_j^n = \exp(ikn)\Psi_j, j = 1, 2, 3, 4.$ and substituting in the equations we get

$$E\Psi_1 = -t\Psi_2(1 + \exp(ik))$$

$$E\Psi_2 = -t(\Psi_1(1 + \exp(-ik)) + \Psi_3)$$

$$E\Psi_3 = -t(\Psi_4(1 + \exp(-ik)) + \Psi_2)$$

$$E\Psi_4 = -t\Psi_3(1 + \exp(ik)).$$

We solve this system of equations which is equivalent to obtaining the eigenvalues of the matrix(k is along the longitudinal directions)

$$H = \begin{bmatrix} 0 & ta & 0 & 0 \\ ta^* & 0 & t & 0 \\ 0 & t & 0 & ta^* \\ 0 & 0 & ta & 0 \end{bmatrix},$$

where $a = 1+\exp(ik)$. This is the tight-binding Hamiltonian of a linear chain with

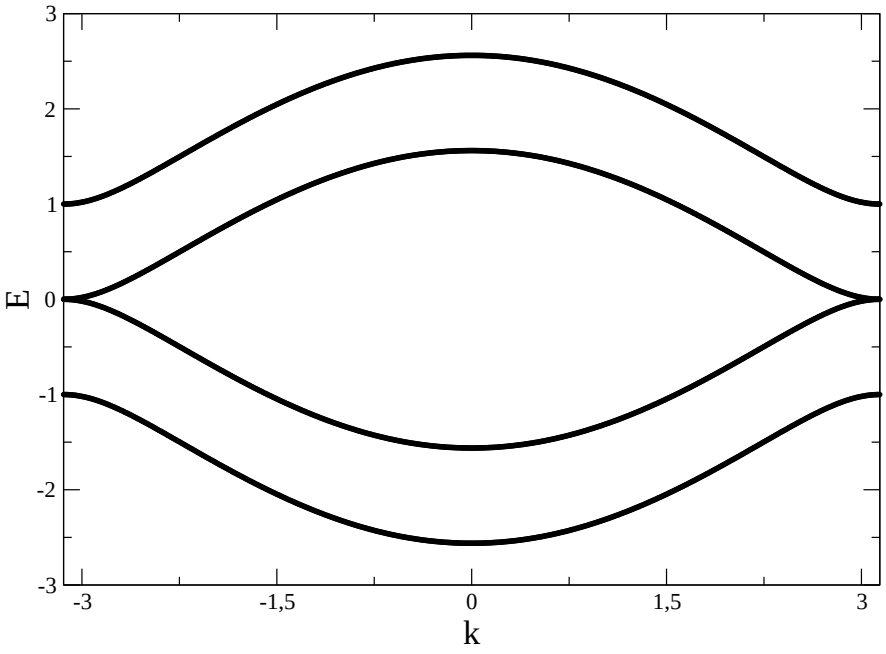

Figure 2.16: Band structure of a zigzag ribbon with two zig-zag chains and hopping $t = 1$.

modified hoppings connecting adjacent unit cells (see Appendix). Its eigenvalues are

$$E = \pm\frac{1}{2}t(1 \pm \sqrt{9 + 8\cos(k)}),$$

plotted for $t = 1$ in Fig. 2.16. It consists of four bands equal to the number of atoms inside the unit cell of the GNR. The two bands, valence and conduction respectively, closer to zero energy, touch each other near $k = \pi$ and $k = -\pi$ forming two small flat bands. Those states with zero energy, make the zigzag GNR a zero gap semiconductor. We can follow the same procedure for GNRs consisting of more than two horizontal zigzag chains and calculate their band structure numerically. For example for a ribbon

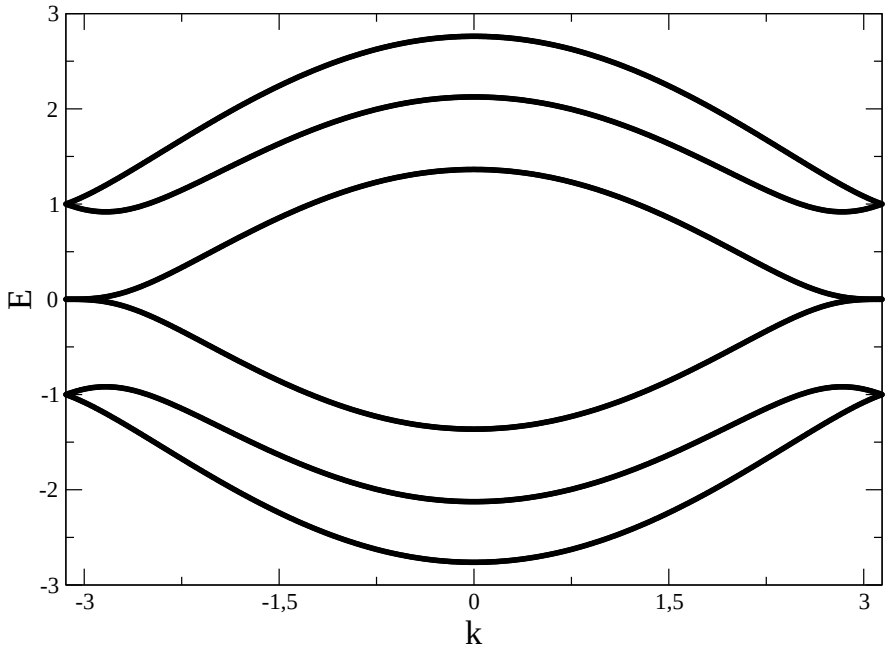

Figure 2.17: Band structure of a zigzag ribbon with six atoms in the unit cell.

with three horizontal zigzag chains and consequently six atoms inside its unit cell the corresponding Hamiltonian becomes

$$H = \begin{bmatrix} 0 & ta & 0 & 0 & 0 & 0 \\ ta^* & 0 & t & 0 & 0 & 0 \\ 0 & t & 0 & ta^* & 0 & 0 \\ 0 & 0 & ta & 0 & t & 0 \\ 0 & 0 & 0 & t & 0 & ta \\ 0 & 0 & 0 & 0 & ta^* & 0 \end{bmatrix}.$$

Its band structure is plotted in Fig. 2.17. Using this method we can calculate the

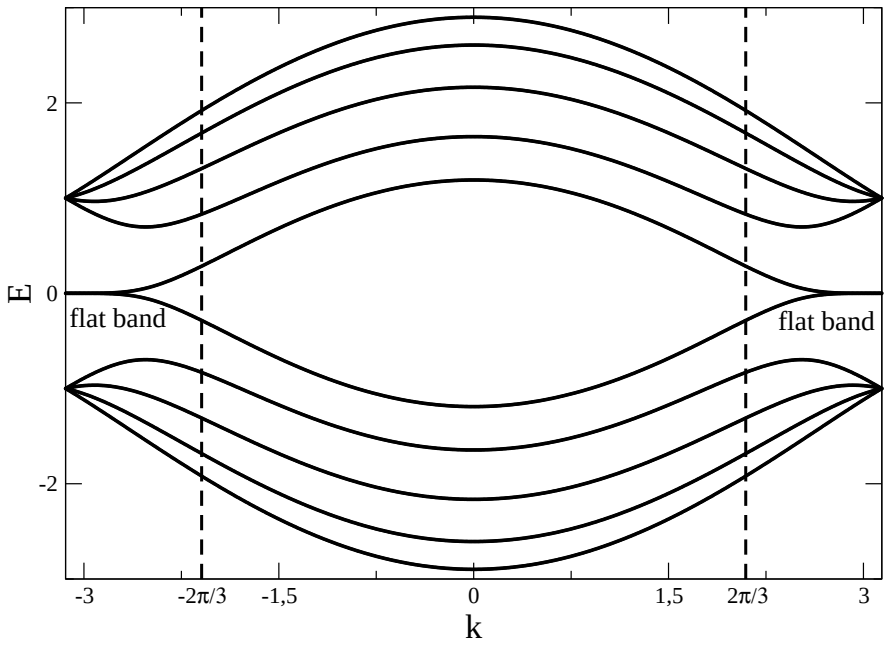

Figure 2.18: Band structure of a zigzag ribbon with ten atoms in the unit cell.

band structure of any zigzag or antizigzag GNR. In Fig. 2.18 and 2.19 we plot the band structure for different ribbon widths and $t = 1$, denoted by the number of atoms inside the unit cell.

As we increase the number of zigzag chains the band structure becomes denser in the energy interval $[-3, 3]$, reproducing gradually the energy dispersion of infinite unbounded graphene projected in the k_y plane. However the major difference with infinite graphene is the presence of two zero energy flat bands encountered in both Fig. 2.18 and Fig. 2.19. Their corresponding wavefunctions are edge states, localized at the edges of the GNRs. They have non-zero amplitudes only on the zigzag terminated edges in analogy with a semi infinite graphene sheet with one zigzag edge for $k =$

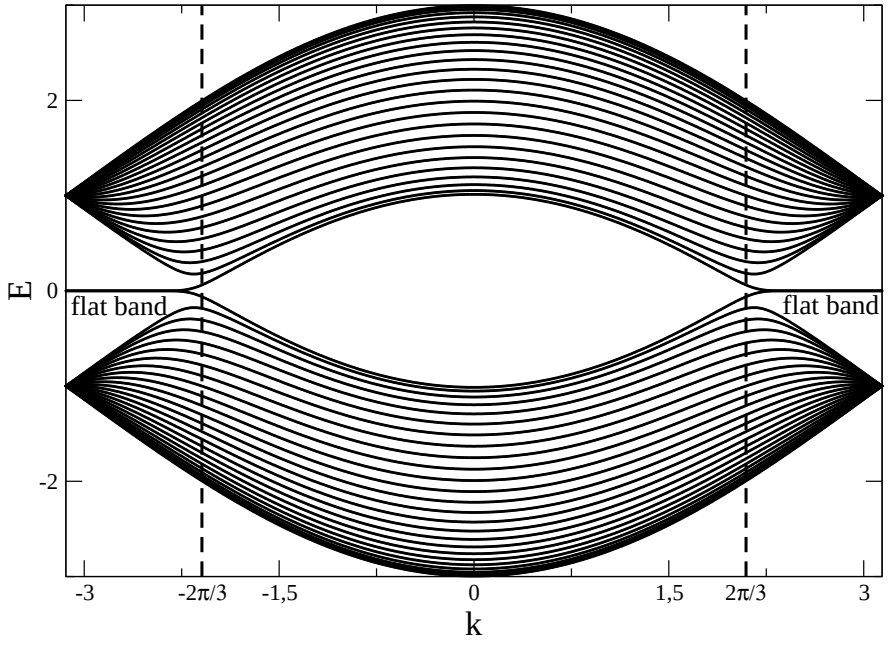

Figure 2.19: Band structure of a zigzag ribbon with fifty inside the unit cell.

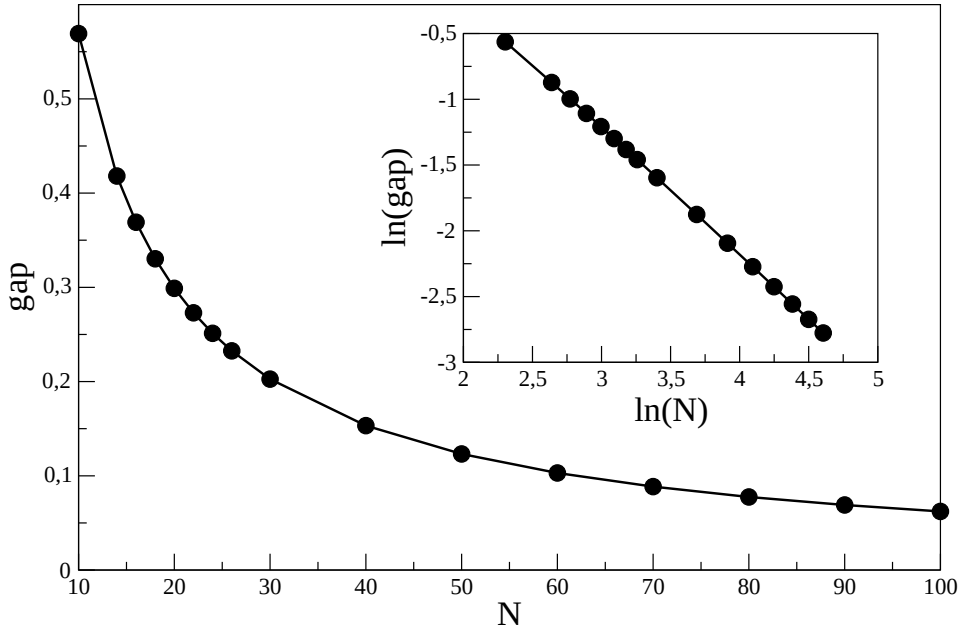

Figure 2.20: The gap at $k = \frac{2\pi}{3}$ for a zigzag GNR versus its length denoted by the number of horizontal zigzag chains N. As seen in the inset were we plot the logarithms, it decays as $\frac{1}{N}$ as N is increased.

$\pi, -\pi$. For $k \neq \pi, -\pi$ the edge states penetrate inside the GNRs, with decaying amplitude for $k \neq \pi, -\pi$ along the flat bands. The two lower bands closer to zero, valence and conduction, to whom the flat bands belong, begin to touch each other at two k points, which gradually approach $k = \frac{2\pi}{3}$ and $k = -\frac{2\pi}{3}$. The width of the flat bands increases as the size becomes larger.

This behavior can be seen in Fig. 2.20 where we plot the energy difference of the valence and conduction bands at $k = \frac{2\pi}{3}$ versus the length of the GNR. In the limit N the flat bands extend in the areas $[-\pi, \frac{-\pi}{-2\frac{\pi}{3}}]$ and $[\frac{-\pi}{-2\frac{\pi}{3}} - \pi]$. So even at the infinite width limit, the two flat bands and consequently zero energy edge states are always

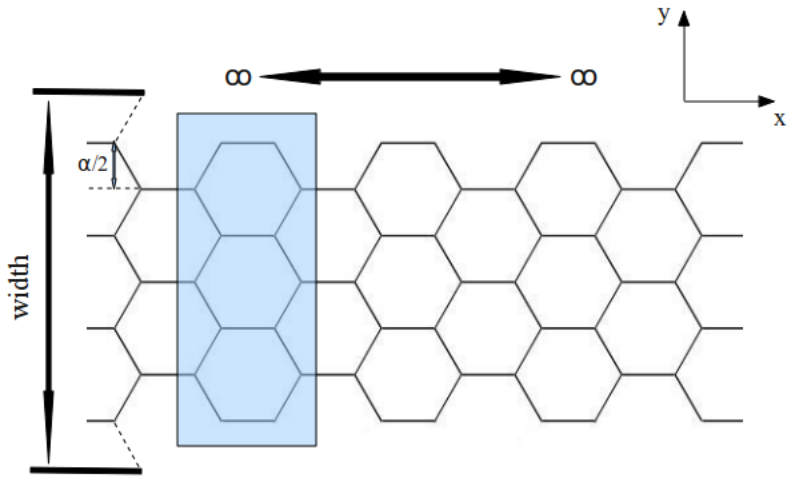

Figure 2.21: An armchair GNR with $N = 7$. The shadowed area denotes its unit cell.

present for zigzag GNRs. The zigzag GNRs behave as zero gap semiconductors. In general, zigzag edges play an important role in the semiconducting behavior of any bounded graphene system contributing edge states at the Fermi level[12,13,14].

Another simple case of GNRs can be formed by cutting graphene in a direction rotated by thirty degrees, compared to the direction used to produce zigzag or antizigzag ribbons (see Fig. 2.12). The resulting GNRs will have a completely different electronic behavior. They are called armchair since both their edges follow an armchair orientation. An armchair ribbon along with it's unit cell is shown in Fig. 2.21.

The band structure in this case can be derived analytically from Eq. (2.3). The width of the ribbon is equal to $(N+1)\frac{a}{2}$ where N is the number of sites along any vertical zigzag chain, that is half the number of sites inside each unit cell. The wavevector k_y will take discrete values according to the simple formula (hard wall BC)

$$k_y = \frac{\pi j}{(N+1)\frac{a}{2}}, j = 1, 2, ..., N,$$

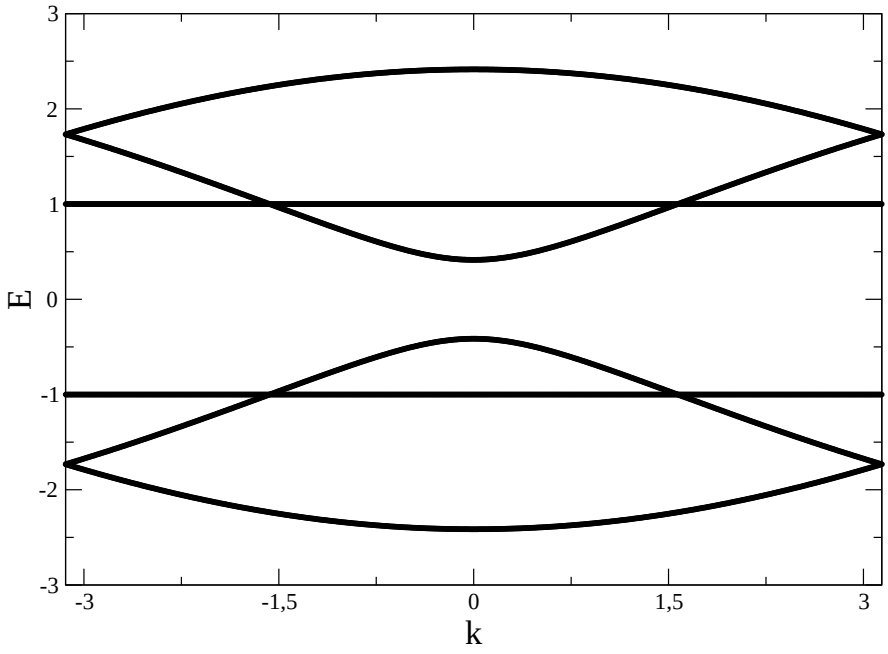

Figure 2.22: Band structure of an armchair GNR with six atoms inside its unit cell(N=3). There is a gap at the Fermi energy $E_f = 0$.

in complete analogy with a finite 1d chain. Substituting in Eq. (2.3) we get the dispersion relation of armchair GNRs

$$E_{\pm}(k_x, j) = \pm t\sqrt{1 + 4\cos(\frac{\pi j}{N+1})\cos(\frac{\sqrt{3}ak_x}{2}) + 4\cos^2(\frac{\pi j}{N+1})}, j = 1, 2, ..., N$$

The band structure of armchair ribbons of increasing width is shown in Fig. 2.22,Fig. 2.23 and Fig. 2.24. All the curves have been multiplied by the length of the unit cell $3a_{cc} = \sqrt{3}a$ in order to scale the first brilouin zone from $-\pi$ to π with $a = 1$ and $k = k_x$).

Armchair GNRs show a completely different semi-conducting behavior compared

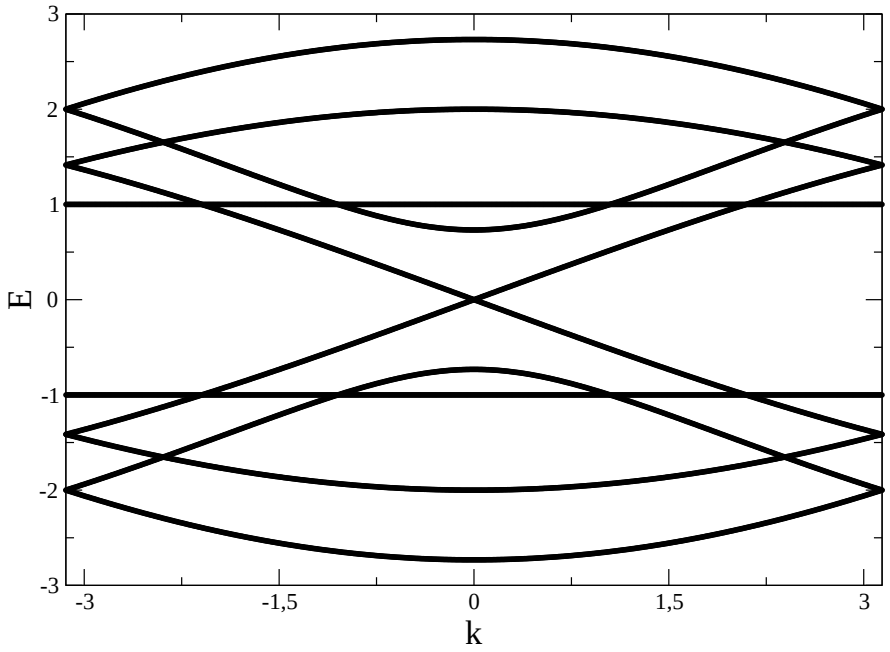

Figure 2.23: Band structure of an armchair GNR with ten atoms inside its unit cell(N=5).There is no gap at the Fermi energy according to Eq. (2.10).

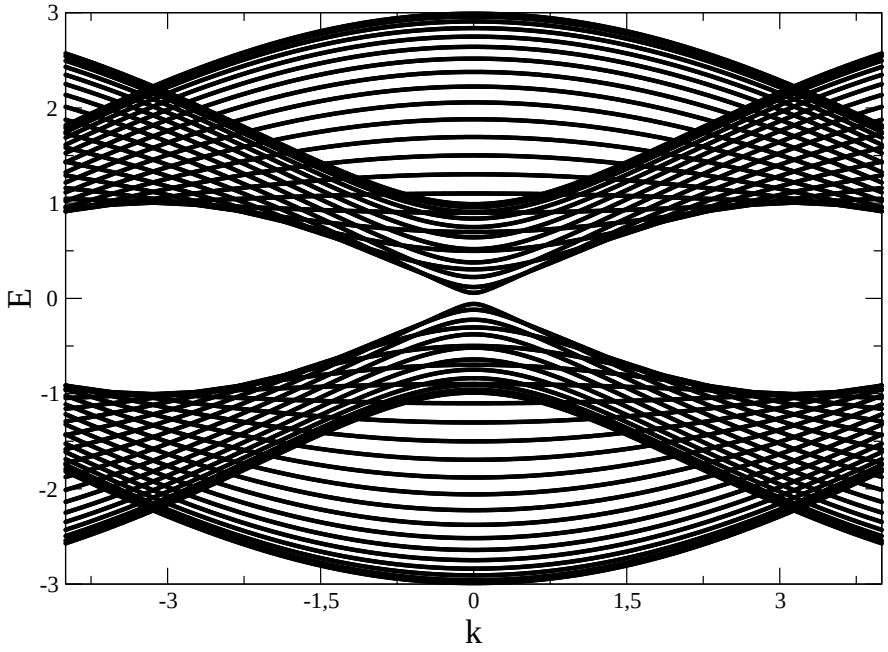

Figure 2.24: Band structure of an armchair GNR with sixty atoms inside its unit cell(N=30). There is a gap at the Fermi energy, which decreases with increasing width.

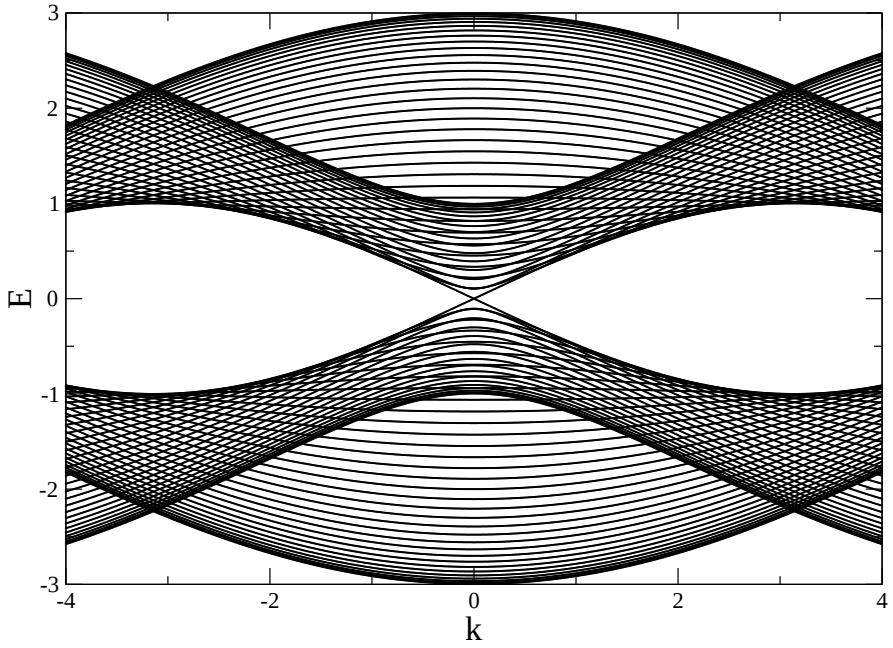

Figure 2.25: Band structure of an armchair GNR with one hundred atoms inside its unit cell(N=50). There is no gap at the Fermi energy.

to the zigzag or antizigzag ones. Specifically the value of N determinates whether they behave as zero-gap or as conventional semiconductors. This behavior can be understood by setting the derived energy dispersion relation for hardwall BC along the y direction, equal to zero at $k_x = 0$ where the valence crosses the conduction band for zero-gap GNRs. We obtain

$$1 + 4\cos(\frac{\pi j}{N+1}) + 4\cos^2(\frac{\pi j}{N+1}) = 0 \Rightarrow 1 + 4x + 4x^2 = 0 \Rightarrow x = -\frac{1}{2} \Rightarrow$$

$$\Rightarrow \cos(\frac{\pi j}{N+1}) = -\frac{1}{2} \Rightarrow \frac{\pi j}{N+1} = \frac{2\pi}{3} \Rightarrow N = \frac{3}{2}j - 1, j = 1, 2, ...$$

N is integer only for even values of $j = 2n, n = 1, 2, ...$ taking values

$$N = 3n - 1, n = 1, 2, ... \tag{2.10}$$

For the N values of Eq. 2.10 valence and conduction bands touch each other at $k = 0$, contributing zero energy states resulting in zero-gap semiconducting GNRs. The armchair GNRs behave as conventional semiconductors for every other value of N since there is a gap at the fermi energy. As the width is increased the gap decreases reproducing gradually the energy dispersion of an infinite graphene sheet projected in the k_x direction this time. It is clear that armchair oriented edges can either contribute zero energy states at $k = 0$ or leave a gap at the fermi level. At the limit of infinite ribbon width the armchair edges do not affect the band structure, unlike the zigzag edges which contribute two flat bands of zero energy states. The wavefunctions of armchair GNRs will have the same form as those corresponding to

a semi infinite graphene sheet with an armchair edge,

$$\Psi_{E_\pm} = \sqrt{\frac{1}{1+\left|f_1(\overrightarrow{k})\right|}} \begin{bmatrix} 1 \\ \pm\frac{f_1^*(\overrightarrow{k})}{\sqrt{f_1(\overrightarrow{k})}} \end{bmatrix} exp(ik_x x)\sin(k_y y),$$

The k_y takes discrete values according to the formula

$$k_y = \frac{\pi j}{(N+1)\frac{a}{2}}, j = 1, 2, ..., N,$$

multiplied by the normalization factor $\sqrt{\frac{2}{(N+1)\frac{a}{2}}}$. Edge states clearly do not exist for armchair GNRs.

2.3.3 Flakes

Graphene can be also cut in confined structures known as flakes[11]. They are can be studied theoretically by applying hardwall boundary conditions on an infinite graphene sheet. Flakes are usually characterized by high degree of edge irregularity[12,14,18], mixing the two possible edge types, zigzag and armchair. A third type of edge, known as dangling bond or Klein edge[15] also appears. In this case every atom is connected by a single bond only. An example of a circular graphene flake can be seen in Fig. 2.26 where we can clearly distinguish the three different type of edges.

It is interesting to see how the exact edge morphology affects the electronic properties of graphene flakes, for example whether edge states exist or not in these finite systems[12,13,14,18]. Moreover, edge states have been shown to play an important role in the chaotic behavior of graphene flakes[18].

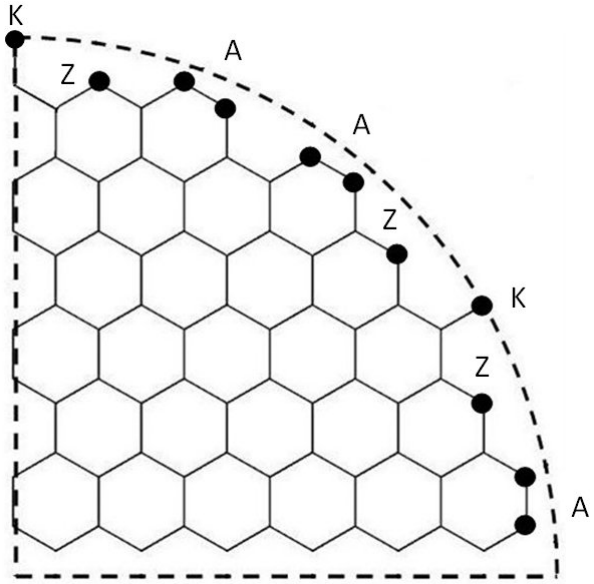

Figure 2.26: A quarter of a circular graphene flake. The three different type of edges, zigzag(Z), armchair(A) and Klein(K) can be distinguished.

We can choose the simplest possible example of a confined graphene system a flake with regular edges, in a square shape shown in Fig. 2.27. This system has a quite regular edge morphology with two parallel zigzag oriented edges the two other being armchair. It can be characterized by its width $w = \frac{N_c}{2}\sqrt{3}$ and its linear scale length $L = \frac{N_{sc}-1}{2}$, where N_c is the number of horizontal zigzag chains and N_{sc} the number of sites along each chain. We choose the aspect ratio $w/L \approx 1$.

In analogy with the ribbons already studied we expect the zigzag edges to contribute edge states with zero energy. We check this by plotting the wavefunction propability for different energies of the square sample consisting of 1760 sites. A wavefunction corresponding to zero energy is shown in Fig. 2.28. This is an edge state to a great extent localized at the zigzag oriented edges of the sample. This type of wavefunction exists also for energies different than zero, an example shown in Fig. 2.29. They are characterized by a smaller degree of localization than the

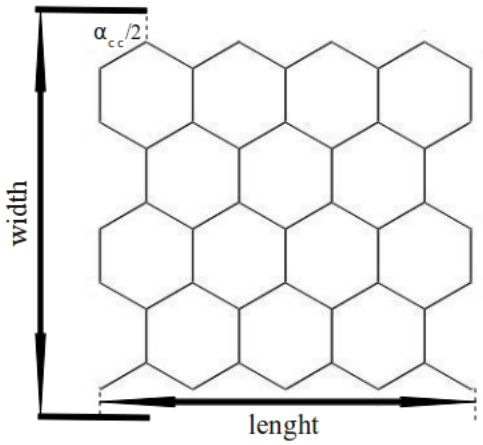

Figure 2.27: A square graphene flake.

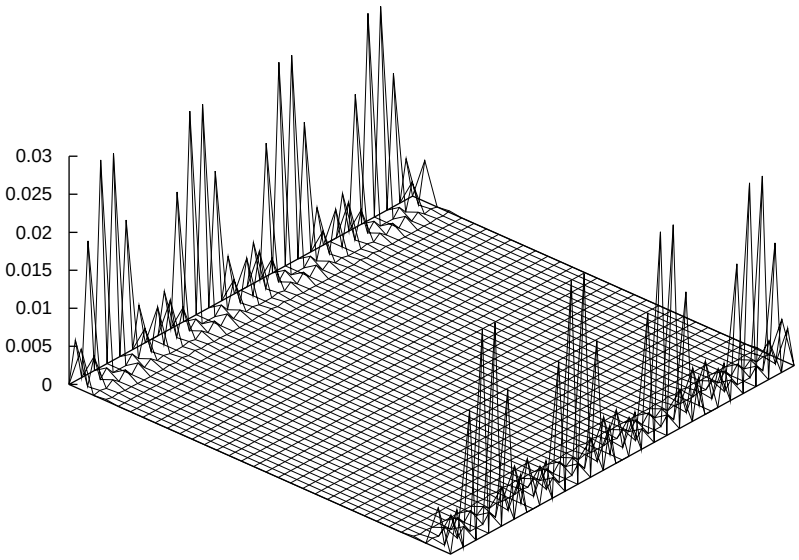

Figure 2.28: Wavefunction propability corresponding to $E = 0$ for a square flake of graphene consisting of 1760 sites. For simplicity the honeycomb lattice sites are arranged on a square lattice. The wavefunction is shown to be localized at the zigzag edges of the sample.

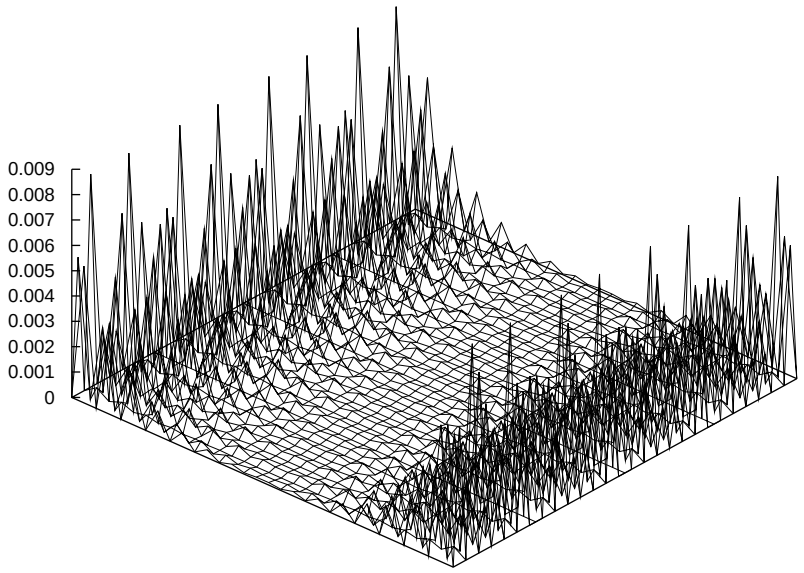

Figure 2.29: Wavefunction propability corresponding to $E \approx 0.0026$ for a square sample consisting of 1760 sites. The wavefunction localized at the zigzag edges penetrates more inside the sample.

zero energy edge states. The presence of edge states at non-zero energies is an extra feature compared with the zigzag GNRs. In that case edge states exist only for zero energy and their degree of localization is determined by the value of the wavevector k along the direction of the GNR which is infinite.

The edge states create degeneracy at the Fermi level which introduces a small peak at the otherwise zero density of states $\rho(E)$ at $E = 0$. The height of the $\rho(E)$ decreases with increasing size, and diminishes gradually, recovering the linear $\rho(E) \sim E$ law for large L, as shown in Fig. 2.30. In the inset the number of zero energy edge states for $|E| < 10^{-3}$ increases linearly with L. The $\rho(0)$ is this number divided by the total number of states $\frac{N(0)}{L^2}$ which is approximately L^2, giving the $\frac{1}{L}$ decay shown. A similar behavior for$\rho(0)$ is encountered for zigzag GNRs[5] or flakes of various formations[12,14,18].

We can consider a more complicated flake edge morphology and see how it affects the electronic properties of graphene at the Fermi level. A general way of doing this is by cutting graphene in a circular form by keeping the carbon atoms whose coordinates fulfill the following condition[18]

$$\sqrt{x^2 + y^2} \leq r,$$

where r is the radius of the circular flake. An example of this condition applied on graphene can be seen in Fig. 2.26 where the three possible types of edges are encountered. This condition was applied on a topologically equivalent brickwall lattice instead of honeycomb, resulting in a graphene flake with a non circular but a general highly irregular edge[18]. We also restrict ourselves to a quarter of the circular flake only for symmetry reasons. We plot the wavefunctions corresponding to different

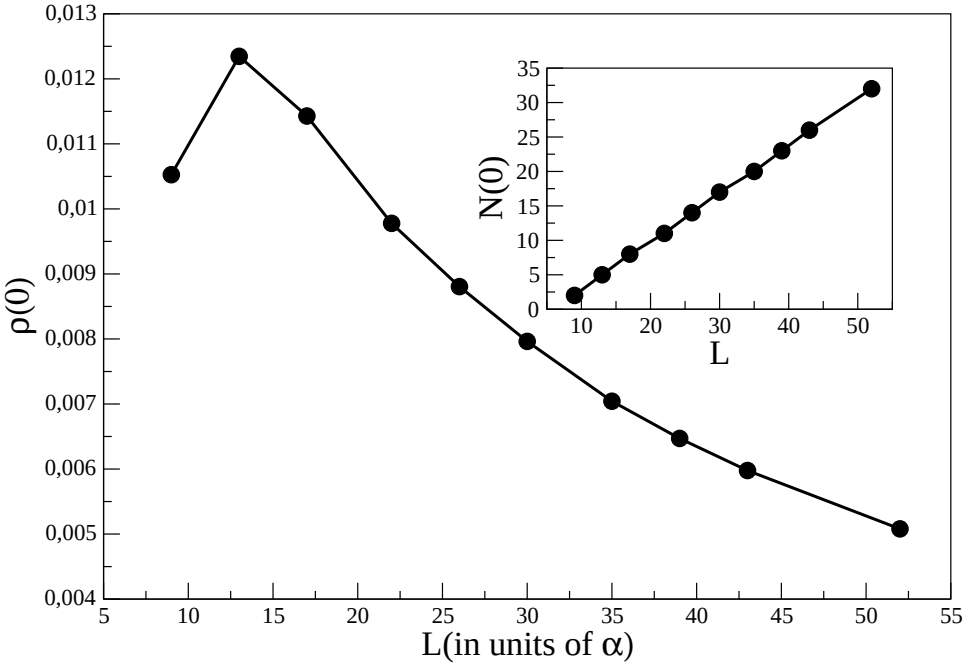

Figure 2.30: Density of states of a square sample of graphene as a function of it's linear length scale L for energies $|E| < 10^{-3}$. In the inset we show also the number of states that fullfill this condition.

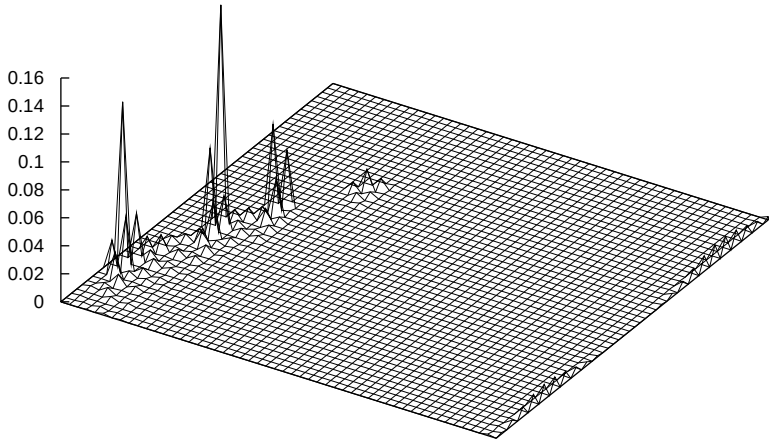

Figure 2.31: Wavefunction propability distribution corresponding to $E \approx 0$ for a quarter of a circular brickwall lattice flake consisting of 2095 sites. For plotting simplicity the brickwall lattice sites are arranged on a square lattice. The wavefunction is mostly localized along the circular edge of the flake and also along the lower edge. From Fig. 2.26 both have zigzag type of edges

energies shown in Fig. 2.31, Fig. 2.32 and Fig. 2.33.

Even in this case of highly irregular edge morphology which mixes zigzag, armchair and klein edges, the edge states survive for zero energy with wavefunctions remaining localized at the boundaries of the flake as shown in Fig. 2.31. Due to irregularity edge states appear at higher energies even for energies at the order of magnitude 10^{-1} than in the square geometry of Fig. 2.27. Edge states with non zero energy[12,18] are shown in Fig2.32 and Fig. 2.33. In Fig. 2.34 the behavior of the density of states at $E = 0$ is more abrupt, because of the irregular flake edge morphology which introduces some kind of weak disorder.

In general the presence of zigzag edges at the boundaries of any finite graphene

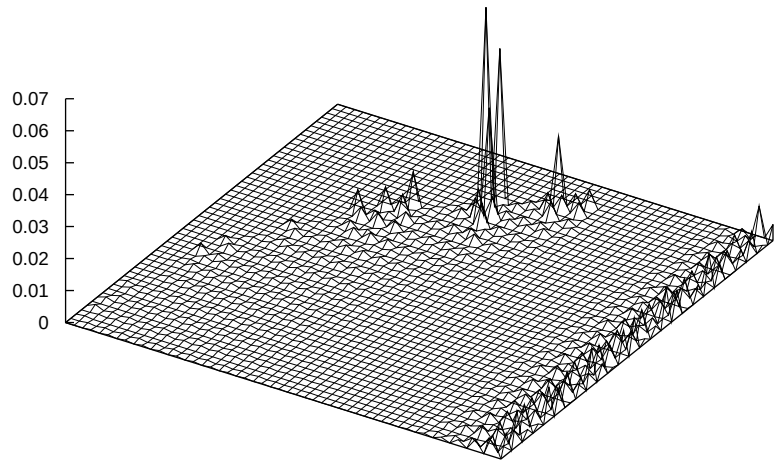

Figure 2.32: Wavefunction propability distribution corresponding to $E \approx 0.0015$ for a quarter of a circular brickwall lattice flake consisting of 2095 sites. The brickwall lattice sites are arranged on a square lattice. The wavefunction is again mostly localized along the circular edge of the flake and the lower zigzag edge.

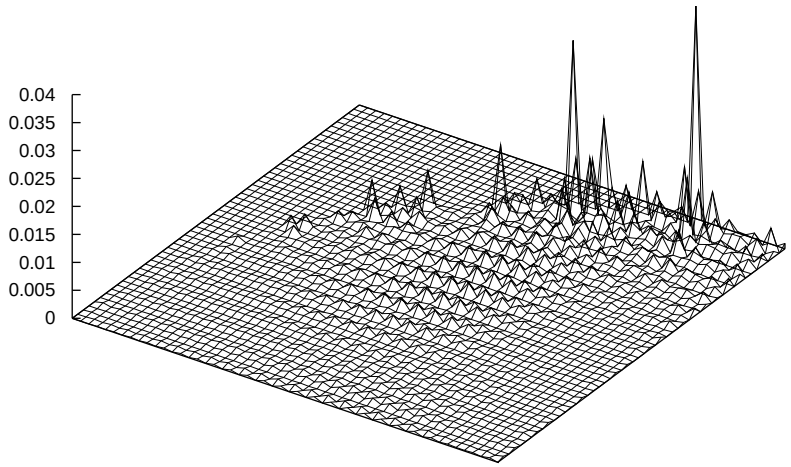

Figure 2.33: Wavefunction propability distribution corresponding to $E \approx 0.122$ for a quarter of a circular brickwall lattice flake consisting of 2095 sites. The brickwall lattice sites are arranged on a square lattice. The wavefunction is localized along the circular edge of the flake but at a smaller degree compared to zero energy edge states.

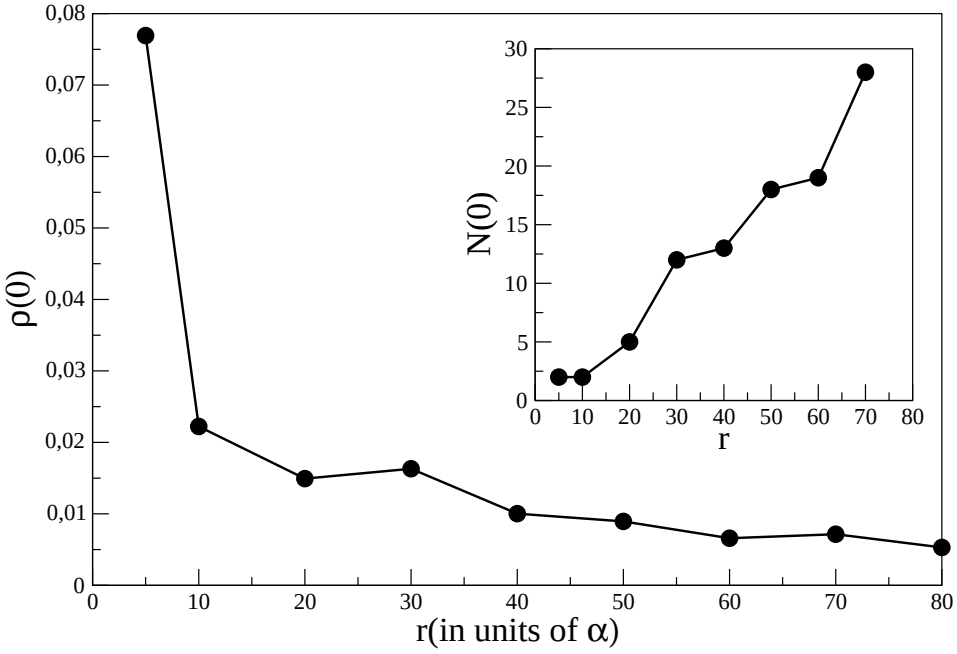

Figure 2.34: Density of states of a quarter of brickwall circle as a function of it's linear length scale L for energies $|E| < 10^{-3}$. Inset shows the corresponding number of zero energy states.

system affects to a great extend its electronic properties contributing edge states at the fermi level, making these systems behave as zero-gap semiconductors[12,13,14,18].

2.4 Conclusions

Graphene's linear dispersion near the Fermi energy along with the fact that its unit cell consists of two atoms makes electrons behave as relativistic massless particles described by the Dirac equation. This is combined with the chiral sublattice symmetry and the spatial anisotropy giving the highly unconventional electronic properties of graphene. Moreover, the special honeycomb lattice structure favors destructive interference effects which give zero energy edge states. In this thesis their existence is examined for various structures. The edge states exist for zigzag or antizigzag nanoribbons(GNRs) and flakes of different boundary arrangements e.g square and circular flakes mixing zigzag and armchair edges. It is shown that they strongly affect the electronic properties of graphene near the Fermi level, having consequences on their semiconducting behavior.

Bibliography

[1]Geim, A. K. and Novoselov, K. S, Nature Materials 6, 183-191 (2007).

[2]K.S.Novoselov et al., Science 306, 666 (2004).

[3]Geim, A. K. MacDonald, A. H., Physics Today 60: 35-41 (2007)

[4]A. H. Castro Neto, F. Guinea, N. M. R. Peres, K. S. Novoselov and A. K. Geim, RevModPhys. 81. 109 (2009)

[5]K. Nakada, M. Fujita, G. Dresselhaus, M.S. Dresselhaus, Phys. Rev. B54, 17954 (1996).

[6]Wakabayashi K., Fujita M., Ajiki H. and Sigrist M., Phys. Rev. B 59, 8271 (1999)

[7]Chenggang Tao et al, Nature Physics doi:10.1038/nphys (2011)

[8]Brumfiel, G., Nature, doi:10.1038/news.2009.367 (2009)

[9]Kosynkin, D. V. et al., Nature 458 7240 (2009)

[10]Michael S. Fuhrer Nature Materials, 9, 611-612 (2010)

[11]L. A. Ponomarenko et al., Science 320, 356 (2008)

[12]H P Heiskanen, M Manninen1 and J Akola, New Journal of Physics 10 103015 (2008)

[13]J. Akola, H. P. Heiskanen, and M. Manninen, Phys. Rev. B 77, 193410 (2008)

[14]Espinosa-Ortega, T., LukYanchuk, Igor A., Rubo, Yuri G. , doi: 10.1016/j.spmi.2010.06.018 (2010)

[15]D. J. Klein. Chem. Phys. Lett. 217, 261 (1994)

[16]Sutter, P., Nature Materials 8 (3) (2009)

[17]Segal, Michael, Nature Nanotechnology 4 (10) (2009)

[18]I. Amanatidis, I. Kleftogiannis, D. Katsanos, S.N. Evangelou (to be submitted)

Chapter 3

Fractal States in Disordered Graphene

3.1 Introduction

3.1.1 Fractals

There is a wide variety of objects encountered in nature that the usual Euclidean geometry fails to describe. These objects usually have extraordinary properties like self-similarity which attract people's attention. Fractal geometry was discovered for the first time by Benoit B. Mandelbrot[1] as a convenient way of characterizing those properties and can be used to describe these non Euclidean objects. The important property of every fractal object, self-similarity has to do with scaling invariance meaning that the object has the same structure on every possible order of magnitude. In rough terms if we were using a magnifying glass to examine it we would observe the same structure no matter of the zooming factor of the glass. This important property

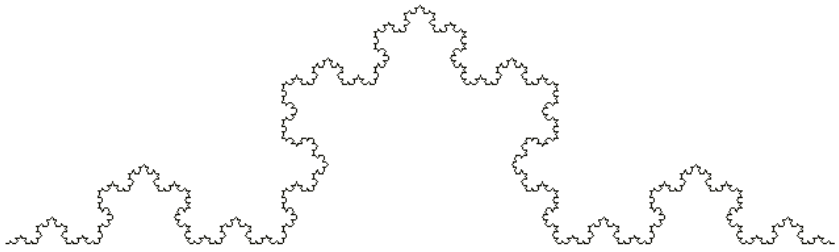

Figure 3.1: The Koch curve.

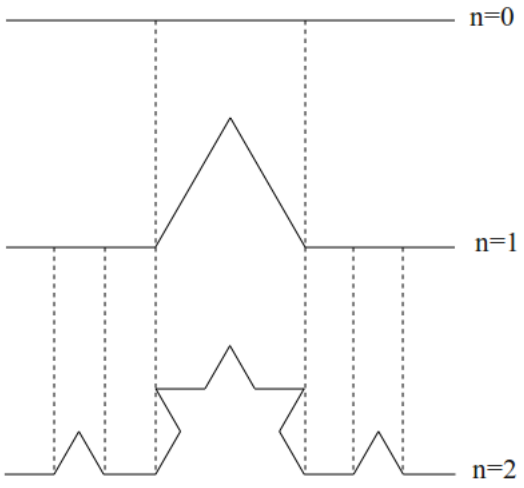

Figure 3.2: The steps to construct the Koch curve.

can be understood by a simple example usually used to introduce fractals, the Koch curve shown in Fig. 3.1 The steps in order to construct it are shown in Fig. 3.2. At the initial step $n = 0$ we take a line segment of length one and divide it into three equal ones. Then we add another segment forming the structure shown at step $n = 1$ and after repeating the same procedure for every different line segment this time we get the structure at step $n = 2$.

After infinite repetitions of this procedure we get the Koch curve. It's impossible, however, to draw the actual curve since the structure at step $n = 1$ is infinitely repeated at each order of magnitude resulting in the extraordinary property of a

line of infinite length enclosed in a finite space, a fact that owns it's existence to selfsimilarity. The structure shown in Fig. 3.1 is not the actual Koch curve it is just the result of repeating the construction procedure a finite number of times, this is called a prefactal. Koch curve is a very characteristic example of a fractal object with an Euclidean dimension $D_T = 1$ also known as topological dimension. In general all one dimensional fractals characterized by self similarity have another common characteristic, infinite length.

In order to discriminate between fractals we can use scaling theory. By scaling we mean to examine how a quantity changes as we vary for example the system size. A common way is to examine how the length of the fractal curve(L) changes as we change the length of the ruler used to measure it. This can be easily accomplished for the Koch curve by the help of the steps used to construct it. For a ruler of length $l = 1$ we would simply measure a curve length $L = 1$. As can be understood from steps $n = 1$ and $n = 2$ for $l = \frac{1}{3}$ the length becomes $L = 4l = \frac{4}{3}$ while for $l = \frac{1}{9}$,$L = 16l = \frac{16}{9}$ and so on.

In general the length of the curve will be given by $L = 4^n l$ where 4^n is the number of segments and $l = \frac{1}{3^n}$ the corresponding ruler length at each step. By writing $n = -\frac{\ln(l)}{\ln(3)}$ we get

$$L = \exp\left(-\ln(4)\frac{\ln(l)}{\ln(3)}\right)\exp(\ln(l)) = \exp\left(\ln(l)\left(1-\frac{\ln(4)}{\ln(3)}\right)\right) = l^{1-\frac{\ln(4)}{\ln(3)}} \Rightarrow$$

$$L = l^{1-d_f}. \tag{3.1}$$

The exponent $d_f = \frac{\ln(4)}{\ln(3)} \sim 1.2618$ is the fractal dimension of the Koch Curve, different from it's topological dimension $D_T = 1$. Examples of objects having the

same topological and fractal dimensions $d_f = D_T$ are common Euclidean shapes like a line, a square or a cube with dimensions $d_f = 1, 2, 3$ respectively. An other alternative way of obtaining the fractal dimension is box counting. This is achieved by trying to cover the Koch curve with a finite number of line segments or boxes N and then examine how this number scales with the their length l. As stated already $N = 4^n$ and $l = \frac{1}{3^n}$ at each step of the Koch curve construction resulting in

$$N = 4^{-\frac{\ln(l)}{\ln(3)}} = \exp\left(-\ln(4)\frac{\ln(l)}{\ln(3)}\right) = l^{-\frac{\ln(4)}{\ln(3)}} \Rightarrow$$

$$N = l^{-d_f}, \tag{3.2}$$

with $d_f = \frac{\ln(4)}{\ln(3)} \sim 1.2618$ the fractal dimension. The scaling rate is obviously constant so it is enough to consider only two sets of points (l, N) for example $(1, 1)$ and $\left(\frac{1}{3}, 4\right)$ in order to calculate the scaling exponent $d = \frac{\ln(4)-\ln(1)}{\ln(3)-\ln(1)} = \frac{\ln(4)}{\ln(3)}$,which is a convenient way of calculating the fractal dimension of such simple objects. In general the fractal dimension characterizes the scaling behavior related with self-similarity, denser fractal objects will have higher fractal dimension.

3.1.2 Multifractals

Fractals can exist also in the quantum world[7,8,9,10]. Well-known examples are the wavefunctions of electrons in the presence of disorder, at the metal-insulator transition for example in disordered mesoscopic systems[11,12,13]. In the case of graphene the geometric support of the wavefunctions is a honeycomb lattice. They can be multifractal objects [3,4,5] and define a whole spectrum of fractal dimensions.

This spectrum of dimensions is

$$D_q = -\frac{1}{q-1}\lim_{L\to\infty}\frac{\ln\sum_{i=1}^{N}\left(\left|\Psi_i\right|^2\right)^q}{\ln \text{Ł}}, q\in[-\infty,\infty]\,, \tag{3.3}$$

where $\left|\Psi_i\right|^2$ is the propability for the electron being at site i of the supporting lattice also called measure in the multifractal formalism. L is the linear length scale characterizing the size of the system and N the total number of sites. $N \sim L^D$ in general where D is the space dimension of the lattice, being two ($D = 2$) for both honeycomb and square. Every fractal dimension $D_q, q \in [-\infty, \infty]$, describes a different scaling behavior of the multifractal wavefunction. Compared with the Koch curve we follow an inverse approach for obtaining the scaling rates, by increasing the linear size L(scale). The fractal dimension D_0, coincides with the space dimension of the supporting lattice. The fractal dimension, for $q = 2$

$$D_2 = -\lim_{L\to\infty}\frac{\ln\sum_{i=1}^{N}\left|\Psi_i\right|^4}{\ln L}. \tag{3.4}$$

This is called the correlation dimension and describes the scaling of the quantity $\sum_{i=1}^{N}\left|\Psi_i\right|^4$, known as the inverse participation ratio

$$IPR = \sum_{i=1}^{N}\left|\Psi_i\right|^4. \tag{3.5}$$

IPR characterizes the localization properties of a wavefunction. An extended wavefunction which has equal amplitudes $\Psi_i = \frac{1}{\sqrt{N}}$ on all the lattice sites $IPR = \sum_{i=1}^{N}\left(\frac{1}{\sqrt{N}}\right)^4 = \sum_{i=1}^{N}\frac{1}{N^2} = \frac{1}{N}$ goes to zero as $N \to \infty$, being inversely proportional to the number of lattice sites. In the opposite case, a completely localized wavefunction on one lattice site has $IPR = 1$.

So the calculation of the inverse participation ratio gives a rough estimation about a wavefunction's degree of localization. The scaling of IPR with the system size gives information about the self-similar nature of a wavefunction in analogy with the simple fractals, where there is only one scaling dimension characterizing the structural scale invariance. For an extended wavefunction with equal propability $\left|\Psi_i\right|^2$ on all the sites from Eq. (3.3) all D_q coincide in the fractal dimension of the supporting lattice which is two in the case of graphene or the square lattice and one for a linear chain. The simple fractal objects are a special case of multifractals, when the measure is equally distributed over the geometric support. If the wavefunction is completely localized then $D_2 = 0$. Non integer values of D_2 imply multifractal wavefunctions.

3.2 Chiral Symmetry

Chiral lattice symmetry[6] plays an important role in the electronic properties of graphene. It is also related with the fractal nature of wavefunctions. Specifically it is responsible for multifractal wavefunctions for the midband states of a disordered square lattice[8,9] and of small length chains. Chiral symmetry has to do with a mirror symmetry present.

Consider a square lattice with zero potential on all its sites split into two sublattices A and B as shown in Fig. 3.3. We clearly see connections only between sites belonging to the two different sublattices. The chiral symmetry implies that one sublattice is the mirror image of the other. A square lattice can be thought consisting of two identical layers one of A and the other of B atoms, with every atom on each layer being connected with four atoms of the other, mirrored one. The honeycomb lattice of graphene preserves chiral symmetry. The only difference is the lattice connectivity,

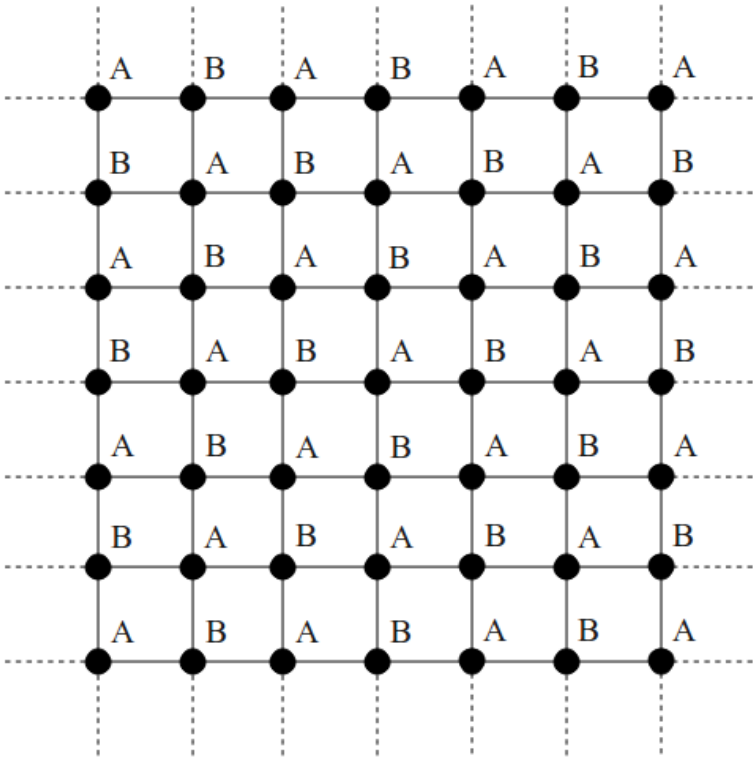

Figure 3.3: Square lattice represented as two sublattices A and B.

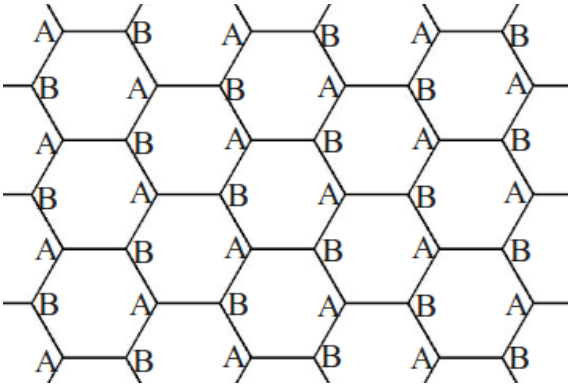

Figure 3.4: The honeycomb lattice can be represented also as two interconnected sublattices A and B.

for the honeycomb lattice is three(Fig. 3.4) instead of four for the square. Both the square and honeycomb lattices belong to a general class called bipartite lattices. In general, a lattice is bipartite if it can be made to consist of two sublattices A and B, with nonzero hoppings connecting only A sites and B sites.

The chiral symmetry remains for off-diagonal disorder which means random connections(hoppings) between the two A, B sublattices. The diagonal disorder is when site potentials are random. In the absence of diagonal disorder the Hamiltonian of a bipartite lattice can be written in the A-B basis as

$$H = \begin{bmatrix} 0 & H_{AB} \\ H_{AB}^{+} & 0 \end{bmatrix}, \tag{3.6}$$

where H_{AB} contains the hoppings between the two sublattices. The chiral symmetry of H can be expressed by the anti-commutation relation $[H, \sigma_3] = 0$,where σ_3 is the pseudospin matrix $\begin{bmatrix} 1 & 0 \\ 0 & -1 \end{bmatrix}$. Let's assume we have a state with energy E

and wavefunction $\Psi = \begin{bmatrix} \Psi_A \\ \Psi_B \end{bmatrix}$, so that $H\Psi = E\Psi$. By using the above anti-commutation relation we easily prove that $H\sigma_3\Psi = -\sigma_3 H\Psi = -E\sigma_3\Psi$ meaning that there is also a state corresponding to energy $-E$ with wavefunction $\sigma_3\Psi = \begin{bmatrix} 1 & 0 \\ 0 & -1 \end{bmatrix} \begin{bmatrix} \Psi_A \\ \Psi_B \end{bmatrix} = \begin{bmatrix} \Psi_A \\ -\Psi_B \end{bmatrix}$. Therefore for a bipartite lattice energies always appear in pairs $E, -E$ with corresponding wavefunctions $\Psi, \sigma_3\Psi$. and the chiral symmetry manifests itself as a symmetric energy spectrum around zero.

The chiral symmetry allows to write the Schrodinger equation for the square of the Hamiltonian

$$H^2\Psi = E^2\Psi \Rightarrow \begin{bmatrix} H_{AB}H_{AB}^{+} & 0 \\ 0 & H_{AB}^{+}H_{AB} \end{bmatrix} \begin{bmatrix} \Psi_A \\ \Psi_B \end{bmatrix} = E^2 \begin{bmatrix} \Psi_A \\ \Psi_B \end{bmatrix} \Rightarrow$$

$$\begin{aligned} H_{AB}H_{AB}^{+} &= E^2\Psi_B \\ H_{AB}^{+}H_{AB} &= E^2\Psi_A \end{aligned} .$$

The eigenvalues of H can be obtained by diagonalizing either $H_{AB}H_{AB}^{+}$ or $H_{AB}^{+}H_{AB}$ which are of reduced size (by half) compared to H. For zero energy $E = 0$

$$\begin{bmatrix} \Psi_A \\ \Psi_B \end{bmatrix} = \begin{bmatrix} \Psi_A \\ -\Psi_B \end{bmatrix} \Rightarrow \begin{cases} \Psi_A \neq 0 \\ \Psi_B = 0 \end{cases}$$

the wavefunctions have zero amplitudes on one of the sublattices (A or B). For N_A number of sites for sublattice A and N_B number of sites for sublattice B with $N_A > N_B$, it can be proven[6] that there are at least $N_A - N_B$ states corresponding to zero energy, having zero amplitudes on the sublattice with the smallest number of sites

(B in this case). If $N_A = N_B + 1$ at least one zero energy state always will be present in the middle of the energy spectrum. This is easily understood if we think that the total number of sites is $N = N_A + N_B$, consequently the corresponding number of energies is odd, combined with the presence of a symmetric spectrum around zero.

The wavefunction of this $E = 0$ state will have zero amplitudes on sites of the B sublattice. In order to prove this we can write down the tight binding equations for $E = 0$

$$H\Psi = 0 \Leftrightarrow \begin{bmatrix} 0 & H_{AB} \\ H_{AB}^{+} & 0 \end{bmatrix} \begin{bmatrix} \Psi_A \\ \Psi_B \end{bmatrix} = 0 \Leftrightarrow \begin{cases} H_{AB}\Psi_B = 0 \\ H_{AB}^{+}\Psi_A = 0 \end{cases} \tag{3.7}$$

The term $H_{AB}\Psi_B = 0$ is a system of N_A linear homogeneous independent equations with N_B unknowns, it's actually the set of Schrodinger equations centered on all the A type atoms. On the other hand the term $H_{AB}^{+}\Psi_A = 0$ on the other hand is a system of N_B equations with N_A unknowns. There is also one more equation obtained by the normalization condition for the wavefunction, namely $\sum^{N_A} |\Psi_A|^2 + \sum^{N_B} |\Psi_B|^2 = 1$. If we assume that $\Psi_A = 0$ then the system of equations $H_{AB}^{+}\Psi_A = 0$ is trivially satisfied while $H_{AB}\Psi_B = 0$ is only satisfied when $\Psi_B = 0$ since the number of equations is larger than the number of unknowns in this case, resulting in a zero amplitude wavefunction as the only possible solution. Assuming on the other hand that $\Psi_B = 0$ equations $H_{AB}\Psi_B = 0$ are trivially satisfied while equations $H_{AB}^{+}\Psi_A = 0$ along the normalization condition $\sum^{N_B} |\Psi_A|^2 = 1$ will allow us to calculate the amplitudes Ψ_A.

3.3 Lattices with off-diagonal disorder

Multifractal wavefunctions are almost exclusively encountered in disordered quantum systems under certain conditions[7,8,9,10,11,12]. Their multifractal nature is charac-

terized by non-trivial scaling behavior described by the spectrum of fractal dimensions (Eq. (3.3)).

Disorder which might own it's existence to high impurity concentration in realistic systems, can be simulated easily in the tight binding framework by introducing random parameters,like random on-site potential or random hopping propability between the different sites of the lattice called off-diagonal disorder. These disordered systems follow a class of universal behaviors independent of the underlying details, like the lattice morphology for instance.

A characteristic example is Anderson localization[2] occurring when there is enough randomness of the disordered parameters present or if the dimensionality is low. For 1d and 2d systems, a linear chain and a square lattice for example all states for every allowed energy and all possible strengths of disorder exhibit Anderson localization. The corresponding wavefunctions become localized at a certain space and their amplitude decays exponentially $\exp\left(-\frac{1}{\xi}|r|\right)$ at distance r from its maximum characterized by the localization length ξ.

There is an exception to this universal behavior however, which is disordered systems that preserve the chiral symmetry[6,8,9], introducing random hoppings only between the two underlying sublattices, preserving this way the mirror symmetry of each other. We study the fractal nature of the wavefunctions belonging to mid-band states for systems that preserve the chiral symmetry, graphene with off-diagonal disorder in conjunction with a square and a chain also with off-diagonal disorder.

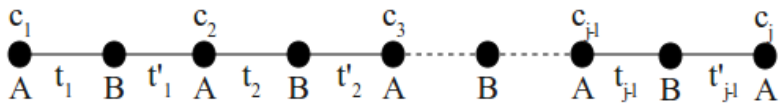

Figure 3.5: a linear chain represented as two sublattices A and B

3.3.1 Linear chain

The simplest model with off-diagonal disorder is a linear chain with random nearest neighbour hoppings called off-diagonal disorder. Again this lattice can always be represented by two interconnected sublattices A and B being the mirror image of each other. If the number of sites is odd there is always a state corresponding to zero energy at the middle of the otherwise symmetric energy spectrum of this system. There is a convenient way of calculating the wavefunction of this state. Consider the chain labeled as shown in Fig. 3.5 with Ψ_j denoting the amplitude on site j of the B sublattice and $t_j, t_{j'}$ the random hoppings, the amplitudes on A sublattice are all equal to zero. Writing down the Schrodinger equations centered on all the B sites where the wavefunction amplitude is zero we get the amplitude on site j of the B sublattice

$$\Psi_j = (-1)^{j-1} \frac{t_{j-1}t_{j-2}...t_1}{t'_{j-1}t'_{j-2}...t'_1} \tag{3.8}$$

and the zero energy wavefunction without the need of diagonalizing the corresponding Hamiltonian. The Schrodinger tight binding equations for the sites of the B sublattice can be also written in a general recursive form as

$$\Psi_j t_j + \Psi_{j+1} t'_j = 0, j = 1, 2, ..., N-1 \Rightarrow |\Psi_{j+1}| = \left|\Psi_j \frac{t_j}{t'_j}\right| \Rightarrow \ln|\Psi_{j+1}| = \ln|\Psi_j| + \left[\ln|t_j| - \ln\left|t'_j\right|\right]$$

The logarithm of the amplitude at distance r (one unit of r is two lattice spacings

long in this case) from the site with amplitude Ψ_j will be

$$\ln|\Psi_{j+r}| = \ln|\Psi_j| + \sum^{r} \left[\ln|t_j| - \ln\left|t'_j\right|\right] \Rightarrow \ln|\Psi_{j+r}| - \ln|\Psi_j| = \sum^{r} \left[\ln|t_j| - \ln\left|t'_j\right|\right]$$

quantity $g(r) = \ln|\Psi_{j+r}| - \ln|\Psi_j|$describes the behavior of the wavefunction as we move away from a starting site j. We expect it to oscillate abruptly due to the introduced disorder, we can get an average estimation however by simply calculating the variance

$$< (\Delta g(r))^2 >=< \left(\Delta \left(\sum_{j=1}^{r} \left[\ln|t_j| - \ln\left|t'_j\right|\right]\right)\right)^2 >$$

The hoppings $t_j, t_{j'}$ for $j = 1, 2, ..., N-1$ are random variables which can be obtained by a specific propability distribution $P(t)$ characterized by the strength of disorder W . We can also consider them as completely uncorrelated meaning that the random value of one doesn't depend in any way on the values of the other hoppings. For off-diagonal disorder we can choose a special propability distribution called logarithmic ensuring that all hoppings take positive non-zero values replacing$|t|$ with t while the propabilities of the logarithms for the random numbers obtained $P(\ln t)$ become equal. The exact form of the propability $P(t)$ that satisfies the above requirements can be easily obtained as follows. Consider that $\ln t$ belongs to the interval $\left[-\frac{W}{2}, \frac{W}{2}\right]$ resulting in the so called box distribution $P(\ln t) = \frac{1}{W}$ The required distribution can be calculated as

$$P(t)\, dt = P(\ln t)\, d\ln|t| = \frac{P(\ln t)}{t} dt \Rightarrow$$

$$P(t) = \frac{1}{Wt}, t \in \left[\exp\left(-\frac{W}{2}\right), \exp\left(\frac{W}{2}\right)\right] \tag{3.9}$$

This is the so called logarithmic propability distribution. The term $\left[\ln|t_j| - \ln\left|t'_j\right|\right]$ now, is a random variable also with zero mean value and finite variance, as long as

the random hoppings $t_j, t_{j'}$ follow the logarithmic distribution. This is very easy to prove, take for example the mean value

$$< \ln t - \ln t'_j >=< \ln t > - < \ln t >$$

$$< \ln t >= \int_{e^{-\frac{W}{2}}}^{e^{\frac{W}{2}}} \ln t P(\ln t)\, dt = \int_{e^{-\frac{W}{2}}}^{e^{\frac{W}{2}}} \ln t \frac{1}{Wt} dt = \frac{1}{W} \int_{-\frac{W}{2}}^{\frac{W}{2}} \ln t d \ln t = \frac{1}{W} \int_{-\frac{W}{2}}^{\frac{W}{2}} x dx = 0$$

$$< \ln t - \ln t'_j >= 0$$

while for the variance we have($X = \ln t_j - \ln t'_j$)

$$variance =< (X - < X >)^2 >=< X^2 > - < X >$$

since $< X >= 0$ the variance becomes

$$\sigma^2 =< \left(\ln t_j - \ln t'_j\right)^2 >=< \ln^2 t_j > + < \ln^2 t'_j >$$

$$< \ln^2 t >= \int_{e^{-\frac{W}{2}}}^{e^{\frac{W}{2}}} \ln^2 t P(\ln t)\, dt = \frac{1}{W} \int_{-\frac{W}{2}}^{\frac{W}{2}} x^2 dx = \frac{W^2}{12}$$

so that the variance of $\left[\ln t_j - \ln t'_j\right]$ becomes equal to $\frac{W^2}{6}$. Returning to the equation for $g(r)$ now due to the fact that the different terms inside the sum are independent random variables we can use the basic property $Var\left(\sum_{i=1}^{N} X_i\right) = \sum_{i=1}^{N} Var(X_i)$ and write

$$< (\Delta g(r))^2 >= \sum^{r} < \left(\Delta\left(\left[\ln|t_j| - \ln\left|t'_j\right|\right]\right)\right)^2 >$$

as proved above $\Delta\left(\left[\ln|t_j| - \ln\left|t'_j\right|\right]\right) = \frac{W^2}{6}$ independent of r so that the required

variance of the wavefunction amplitude at distance r from the starting site j becomes

$$< (\Delta g(r))^2 >= \frac{W^2}{6} r \sim r \Rightarrow$$

$$\sqrt{< (\Delta g(r))^2 >} \sim \sqrt{r}$$

Since $g(r) = \ln|\Psi_{j+r}| - \ln|\Psi_j|$ this implies that the amplitude of the wavefunction corresponding to zero energy decays in average as

$$\exp\left(-\lambda\sqrt{r}\right) \tag{3.10}$$

at distance r from it's maximum value with $\lambda \sim W^2$[8]. Despite the fact we have used a specific propability distribution for the random hoppings the obtained result is independent of the distribution's exact form as long as it has zero mean value and finite variance. The decay behavior is also essentially different and slower from the pure exponential decay $\exp\left(-\frac{1}{\xi}|r|\right)$ characterizing localized wavefunctions.

The problem described is a characteristic example of a random walk process. The term $\ln|c_j|$ can be interpreted as the starting position of the walker while the role of the additional random displacement at each iteration is played by the random variable $\left[\ln|t_j| - \ln\left|t'_j\right|\right]$ with mean value and finite variance. The average distance x of the walker from his starting position after r iterations will be $x \sim \sqrt{r}$ a diffusive behavior similar to the one derived for the amplitudes of the zero energy wavefunction.

We can also verify the above result numerically[8] by using Eq. (3.8) in order to calculate the amplitudes Ψ_j. First we have to consider a chain of finite size with N number of sites and then apply the normalization condition $\sum_{j=1}^{N} \Psi_j = 1$. Then we can check the validity of Eq. (3.10) by calculating the average of the correlation

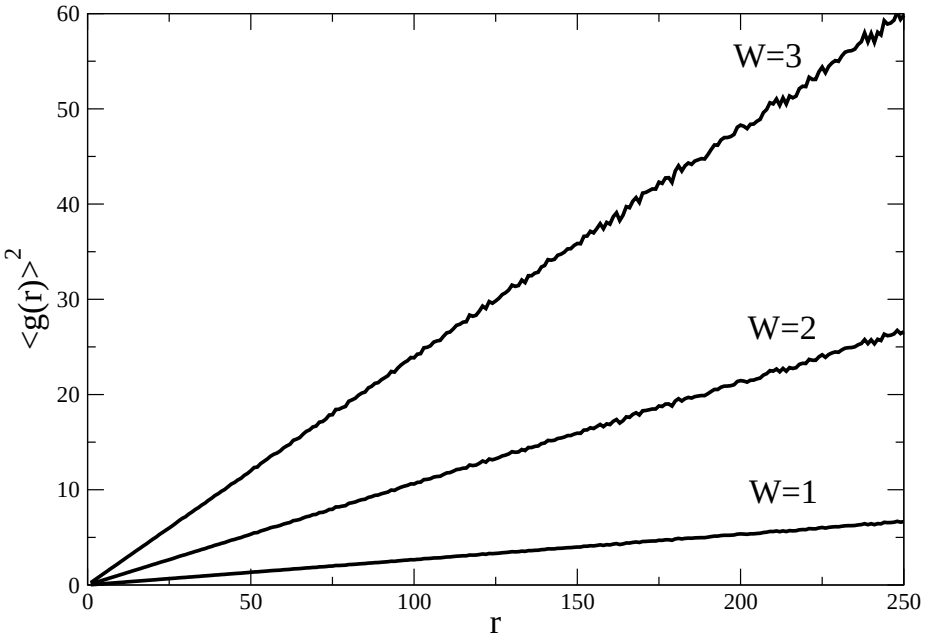

Figure 3.6: The square of the correlation function $g(r)$ ploted as a function or correlation distance r for a chain of $N = 2001$ sites varying j in the interval for different stenghts of disorder W and 10000 realizations. The analytical result is reproduced.

function $g(r) = [\ln|\Psi_{j+r}| - \ln|\Psi_j|]$ over the different j sites of the chain and over different realizations of the random hoppings, varying also the correlation distance r. Below we show the result of this procedure for a chain of $N = 2001$ sites with j chosen for sites belonging to the middle part of the chain in order to eliminate the edge scattering effects introduced by the system's boundaries

As seen in Fig. 3.6 $g(r)$ appears to be in average analogous to r in complete agreement with the behavior obtained analytically. In Fig. 3.7 the propability distribution of the correlation function is plotted for different disorder strengths W

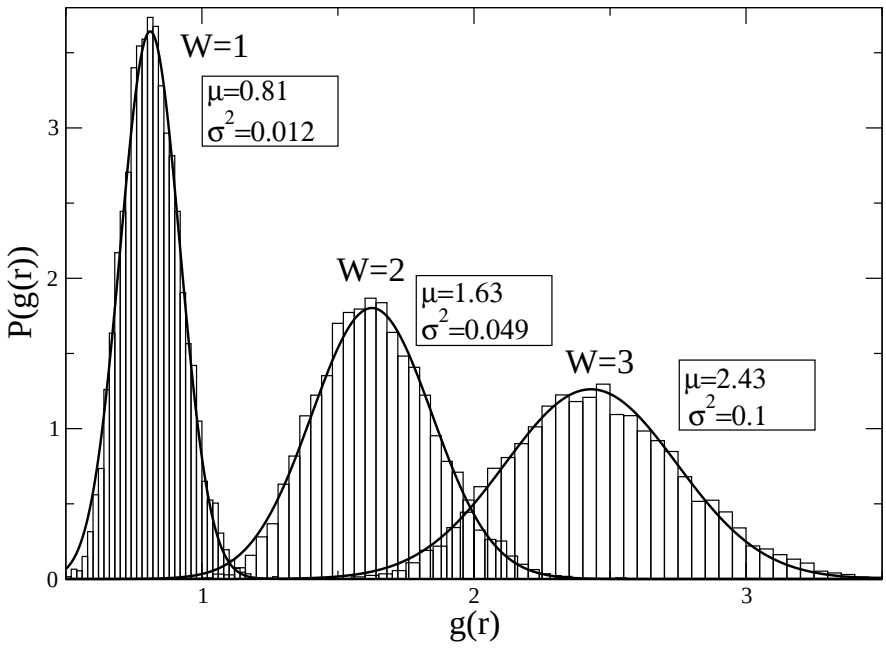

Figure 3.7: Propability distribution of $g(r)$ for correlation distance $r = 25$, 10000 realizations, fit with gauss distribution $P(g) = \frac{1}{\sqrt{2\pi\sigma^2}} \exp\left[-\frac{(g-<g>)^2}{2\sigma^2}\right]$

All curves follow the gaussian form a direct consequence of the special form of the wavefunction amplitude Eq. (3.8). It's logarithm can be written as $\ln|c_j| = (\ln t_{j-1} + \ln t_{j-2} + ... + \ln t_1) - \left(\ln t'_{j-1} + \ln t'_{j-2} + ... + \ln t'_1\right)$ a sum of $N-1$ independent random variables. According to the central limit theorem of statistics the propability distribution of $\ln|c_j|$ approaches the Gaussian form as the number of the summed random variables increases ($N \to \infty$). The increasing also of the disorder strength W leads to the broadening of the Gaussian distribution expressed through the increasing of it's variance σ^2.

The linear chain with off-diagonal disorder is the simplest disordered tight binding

model for which multifractal wavefunctions exist. The logarithm of the wavefunction amplitude for the midband states corresponding to zero energy at each site, undergoes a random walk, leading to the power law decay of Eq. (3.10) which is different from Anderson exponentially localized states. The scaling of the inverse participation ratio, $IPR = \sum_{i=1}^{N} \left|\Psi_i\right|^4$, with the system size N the length of the chain, gives the characteristic correlation dimension D_2. This can be accomplished easily, the chiral symmetry is preserved for off-diagonal disorder and using Eq. (3.7) we calculate the wavefunction amplitudes. We then plot the logarithm of the average $< IPR >$, taken over different realizations as a function of $\ln(N)$. The result is shown in Fig. 3.9 for different strengths of disorder W. The whole propability distributions of $\ln(IPR)$ are shown in Fig. 3.8.

The expected power law decay Eq. (3.10) for the $E = 0$ wavefunction leads to zero amplitude at large distances(r) with a decay slower than exponential. The fractal dimension D_2 of this power-law localized wavefunction will eventually be zero, that is the fractal dimension of a point. Accordingly, we expect the scaling rate of $\ln(< IPR >)$ vs $\ln(N)$, for any disorder strength W, to approach zero for large enough chain lengths as confirmed in Fig. 3.9. For small lengths, however, we observe linear scaling, indicating the existence of a fractal dimension D_2 which decreases as the strength of disorder W is increased. Small values of W result in values for D_2 close to the integer dimension of a line indicating a wavefunction extended along the chain. As we increase W the D_2 approaches non integer values indicating that the $E = 0$ wavefunction has a multifractal form.

A typical multifractal wavefunction can be seen in Fig. 3.10. We notice immediately the signs of self similarity ,characteristic of fractal objects. As seen in the inset where log-linear plot is used, the propability amplitude fluctuates wildly along the

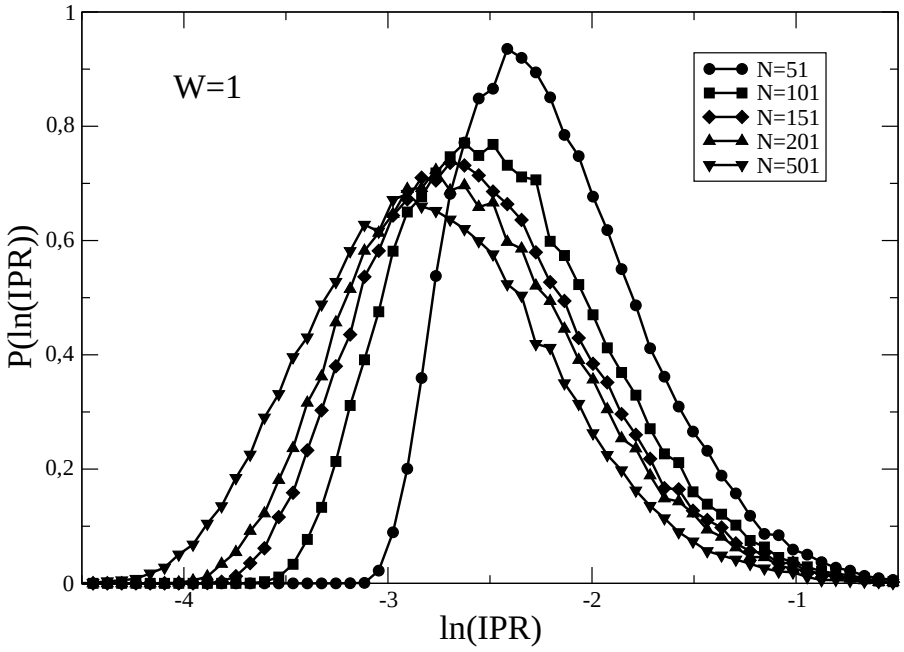

Figure 3.8: Propability distributions of $\ln(IPR)$ at $E = 0$ for a chain with off-diagonal disorder, $W = 1$ and 50000 realizations.

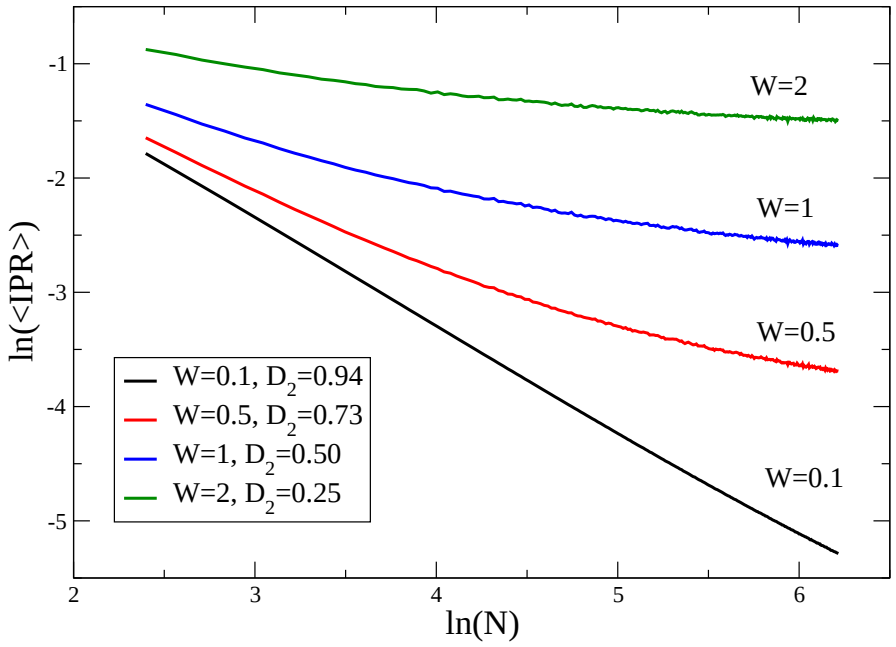

Figure 3.9: The scaling of IPR with the system size N for a chain at $E = 0$ averaging over 10000 realizations for different strenghts of disorder W. The fractal dimension D_2 exists only for small sizes and diminishes as the disorder increases.

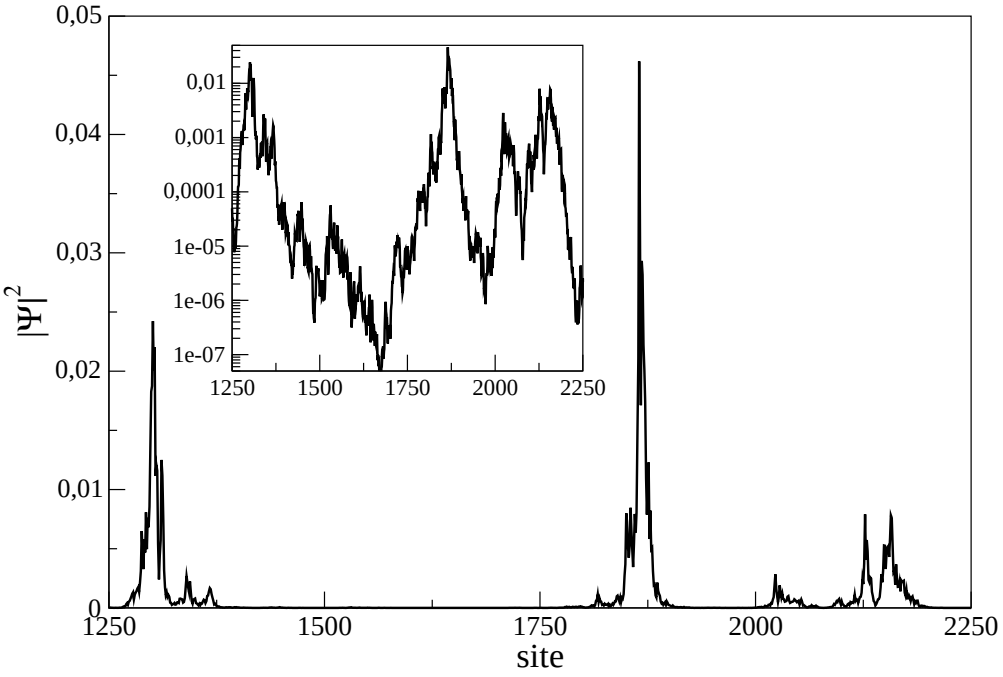

Figure 3.10: Plot of the propability $|\Psi|^2$ for the chiral multifractal wavefunction at $E = 0$ for a chain of 5001 sites and disorder strength $W = 0.5$. The plot is done for sites at the range $[1250, 2250]$. In the inset logarithmic scale is used.

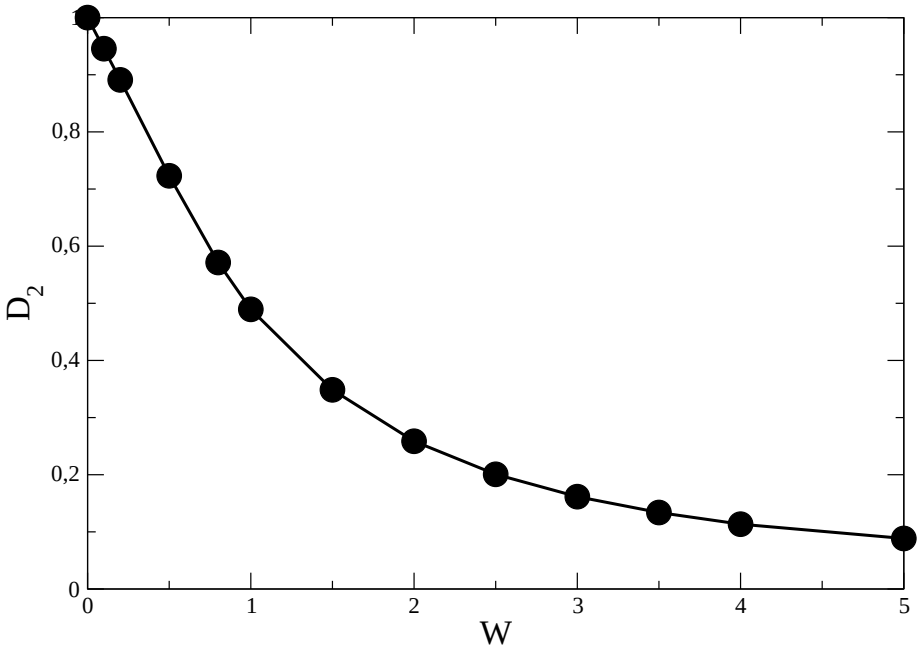

Figure 3.11: D_2 as a function of the off-diagonal disorder with strength W, for a zero energy chiral wavefunction of a chain.

chain, while on the other hand it shares the properties of both, extended and localized wavefunctions. For example, it is localized along different isolated regions in the chain, expected to lead to extreme sensitivity of the system's transport properties like conductance depending on the choice of boundary conditions. Therefore, although the power law decay localizes the wavefunctions, a fractal nature is encountered when we examine small enough regions (scales) of the chain. These regions reduce in size if the disorder is increased and the wavefunction becomes more power-law localized.

In Fig. 3.11 we show the behavior of D_2 with increasing W. The D_2 approaches asymptotically zero as W increases.

3.3.2 Square lattice

We can can easily apply the multifractal method on a square lattice model with off-diagonal disorder in order to check the existence of midband multifractal states. We consider again the hopping as uncorrelated real random variables distributed in the logarithmic form Eq. (3.9) with W denoting the strength of the disorder. The chiral symmetry is preserved since there are two identical underlying sublattices, one being the mirror image of each other.

For convenience we can choose a square sample with $N = L^2$ number of sites reducing this way the scaling parameters to just the linear length scale L. By demanding it also to take odd values only so that N is also odd we ensure the presence of at least one zero energy state in the middle of the energy spectrum of this system. The scaling of IPR with L will give the fractal dimension D_2 of this midband state. For this calculation we use the system described by Eq. (3.7), the amplitudes lie on sites of the A sublattice. The wavefunction has zero amplitude on the sites of the B sublattice, which has the smallest number of sites. In Fig. 3.13 we have studied the scaling of two different quantities. The first is the geometric mean $\exp(< \ln(IPR) >)$ while the second is the arithmetic mean $< IPR >$ of IPR. For the geometric mean it is enough to plot $< \ln(IPR) >$ as a function of $\ln(L)$ in order to get it's scaling dimension D_2 and for the arithmetic mean we plot $\ln < IPR >$ as a function of $\ln(L)$.

The two curves are shown in Fig. 3.14. They imply that the studied zero energy midband state undergoes an interesting crossover. For example, for low values of disorder $W = 0.1$, the value D_2 is close to two meaning that the wavefunction is completely extended. For large enough disorder, for example $W = 50$, the value of D_2 is close to zero, and clearly the wavefunction becomes localized. For intermediate

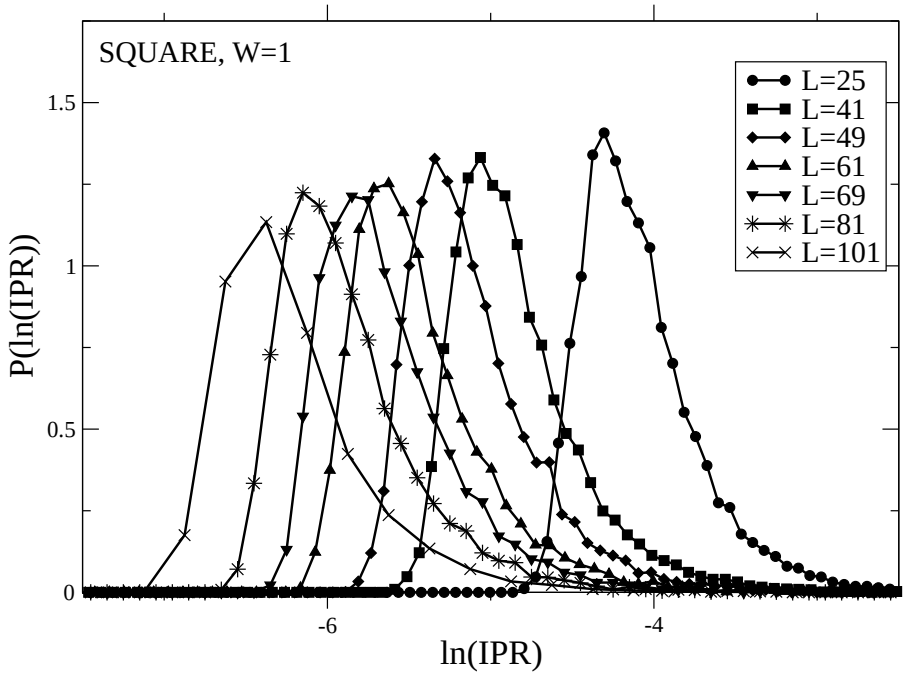

Figure 3.12: Distribution of ln(IPR) for strength of disorder $W = 1$ and different lenght scales L using 10000 realisations.

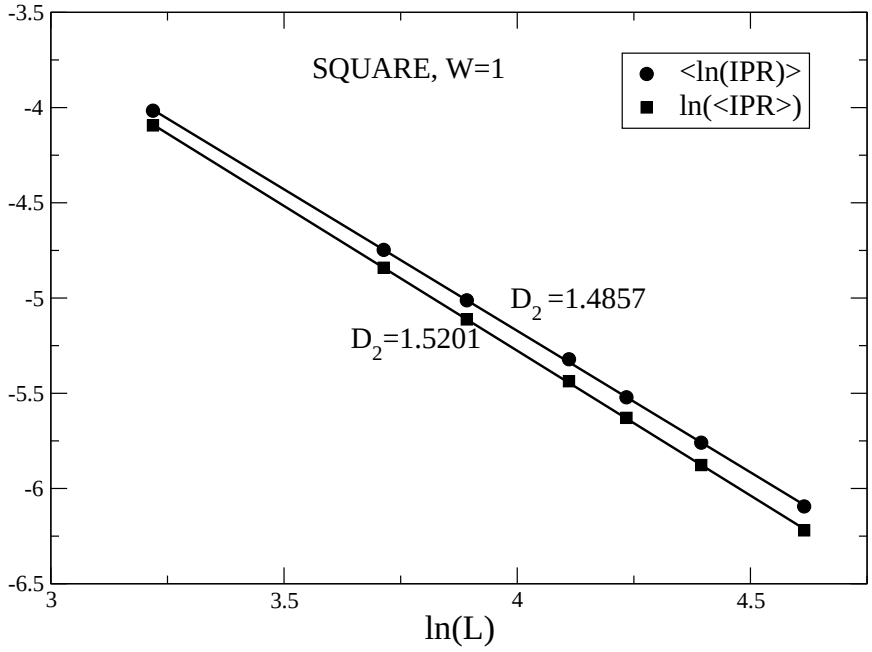

Figure 3.13: Scaling with L of two different quantities the geometric and the arithmetic mean of IPR , for disorder strength $W = 1$ and 10000 realizations. The curves allow us to calculate the fractal dimensions D_2 describing the scaling of both those quantities.

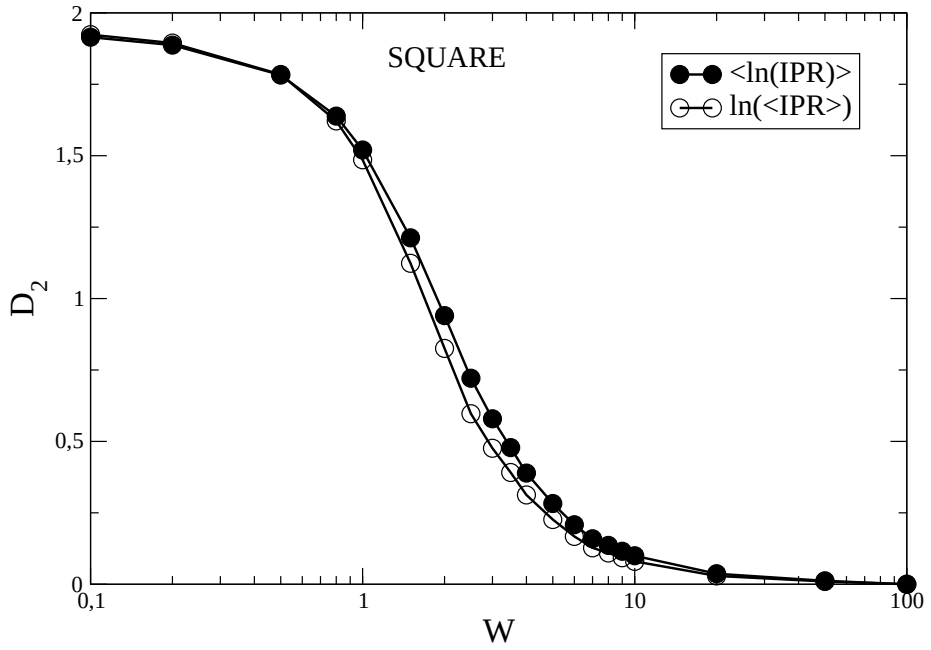

Figure 3.14: Fractal dimension D_2 as a function of the disorder strength W for both the arithmetic and the geometric mean of IPR.

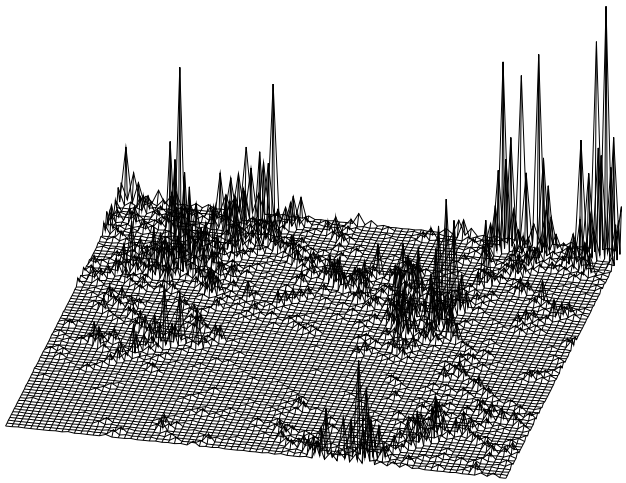

Figure 3.15: A multifractal wavefunction propability at $E = 0$ for a square lattice of linear length $L = 81$ with 6561 sites for off-diagonal disorder strength $W = 1$.

values of disorder the wavefunction has a non integer fractal dimension D_2 between two and zero indicating a typical multifractal distribution.

The amplitude $|\Psi|^2$ seen in Fig. 3.15 fluctuates wildly with signs of self-similarity, a characteristic example of a multifractal wavefunction. It can be understood from the point of view of phase transitions. There is a continuous second order phase transition in the asymptotic limit $W = 0$ only, the extended-chaotic phase occurring in the asymptotic limit $W = 0$, for $0 < W < \infty$ the state is fractal and Anderson localization occurs in the asymptotic limit($W \to \infty$). This is implied in Fig. 3.14 by the two scaling factors for the geometric and arithmetic mean as defined above. We clearly see that the two values of D_2 differ only for the fractal phase, while they coincide for the two other limiting phases. We can interpret their difference as some kind of order parameter that takes values from zero to some finite value as W increases

and the system jumps from one ordered state for small W to a more disordered one for large W. The two exponents become equal at the asymptotic limit.

3.3.3 Graphene

In order to check if midband multifractal wavefunctions exist in graphene with off-diagonal disorder we study also a square honeycomb lattice sample. This system (see Fig2.26) can be characterized by, the number of horizontal zigzag chains, N_c, and the number of sites on each one of those N_{sc} . The lattice has $N = N_c N_{sc}$ sites, width $w = \frac{N_c}{2}\sqrt{3}$ and length $L = \frac{N_{sc}-1}{2}$, both in units of $a = \sqrt{3}a_{c-c}$. As in the previous case of the square lattice we require N_c and N_{sc} to be both odd in order for N to become odd. We also require that $\frac{w}{L} \simeq 1$ to be talking about square graphene samples.

The Hamiltonian studied has again the chiral form (3.6), with the hopping elements given by logarithmic distribution Eq. (3.9). This graphene sheet will have two parallel boundaries containing only zigzag edges and two other also parallel boundaries containing only armchair edges. As in the case of zigzag graphene ribbons we expect the presence of zigzag edges to contribute edge states with zero energy. This results in high degeneracy at $E = 0$, increasing with the size of the graphene sample.

In order to calculate the amplitudes on A type sites of graphene We use Eq. (3.7). The IPR allows to study the fractal properties for one of those degenerate states. A very fundamental question we address is about the role of the destructive interference mechanism of the honeycomb lattice in this disordered graphene system, for example to see if edge states survive in this case.

As seen in Fig. 3.18 the conclusions derived for the square-lattice $E = 0$ state, hold also for the corresponding graphene $E = 0$ state . Their main difference is that

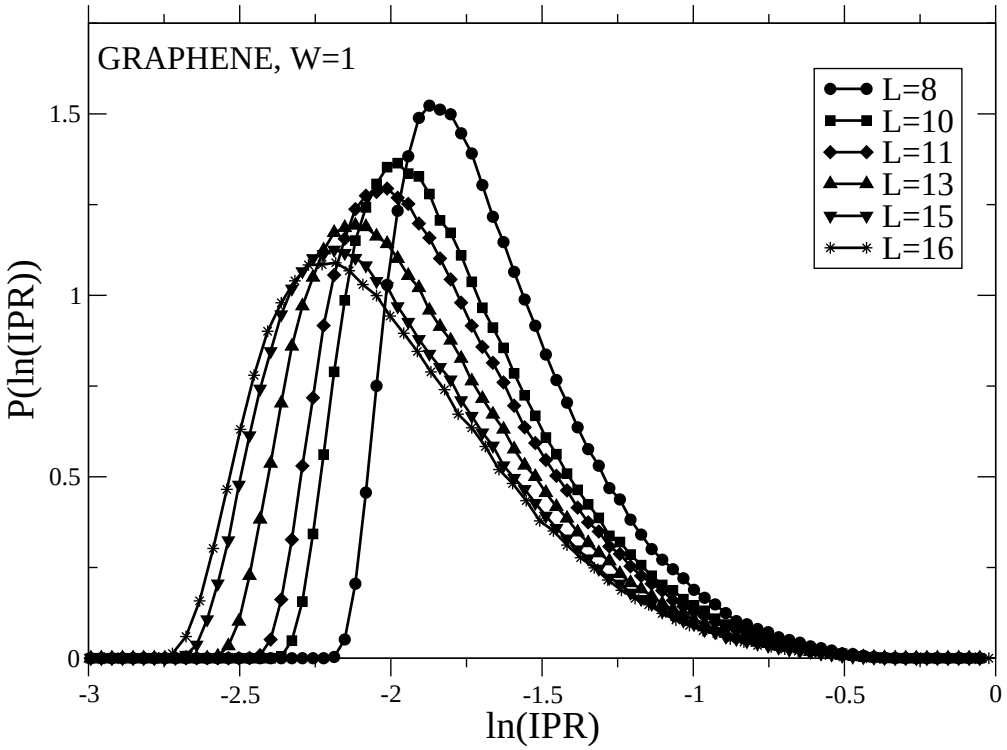

Figure 3.16: The distribution of ln(IPR) with w=1 for different lentgh scales L for 500000 realisations.

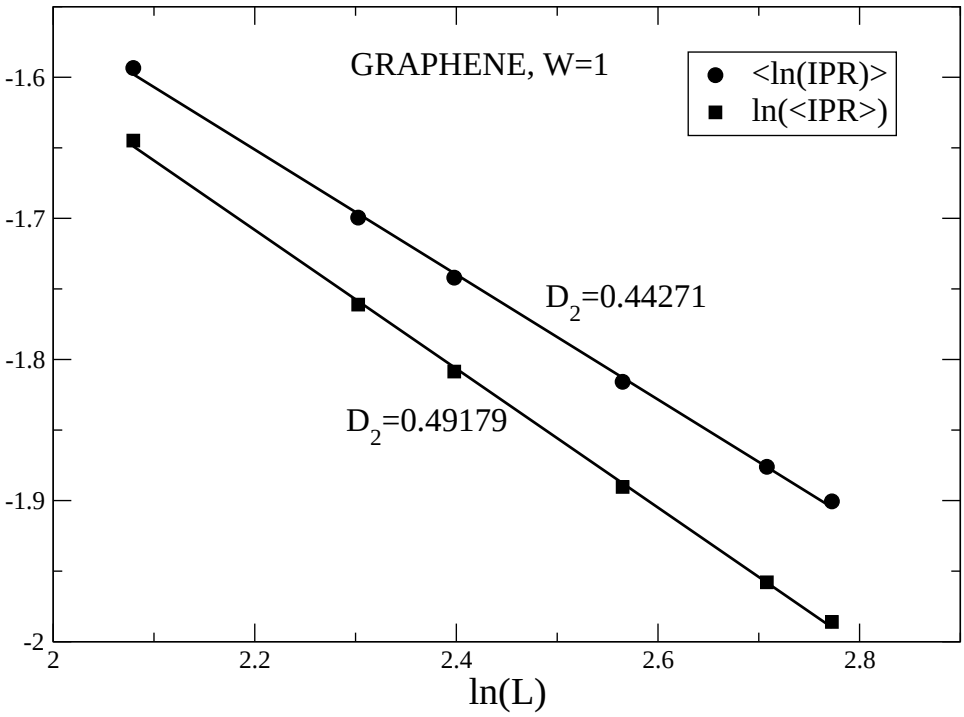

Figure 3.17: The scaling of two different quantities discussed in the text, with w=1 for 500000 realizations.The curves give us the fractal dimensions D_2 describing their scaling.

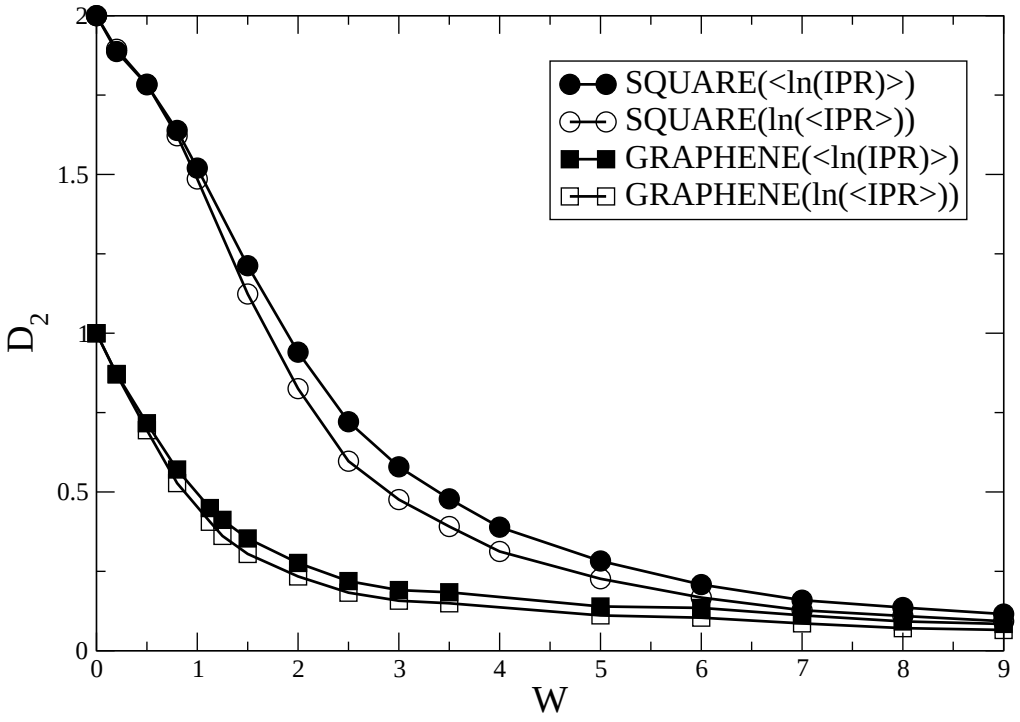

Figure 3.18: Fractal dimension D_2 as a function of the disorder strength W for the geometric $< ln(IPR) >$ and arithmetic mean $ln(< IPR >)$, in the case of both square and honeycomb lattices.

the midband state with zero energy has fractal dimension D_2 ranging from one to zero. This clearly indicates a wavefunction that remains localized along a line in space even in the presence of disorder and has a fractal structure characterized by the linear dependance of $\ln(IPR)$ on $\ln(L)$. This line corresponds to the zigzag edges of the graphene sheet and resembles the behavior of D_2 for the midband wavefunction of small length chains with off-diagonal disorder seen in Fig. 3.11. So even in the presence of off-diagonal disorder zero energy edge states survive in graphene. In other words the destructive interference mechanism, due to the special morphology of the honeycomb lattice structure, giving edge states with zero energy, is not destroyed by the introduced disorder which preserves chiral symmetry of the two underlying sublattices.

3.4 Conclusions

The wavefunctions of graphene at the Dirac point are shown to be fractal as long as the disorder preserves the chiral sublattice symmetry. This is common behavior for off-diagonal disorder encountered also in the square lattice and small length chains. In the case of a square lattice the fractal dimension D_2 ranges from two to zero as the disorder increases. For the graphene sample with off-diagonal disorder fractal states are also edge states and the value of the scaling dimension D_2 ranges from one to zero. This shows that the destructive interference mechanism in the honeycomb lattice of graphene survives in the the presence of off-diagonal disorder.

Bibliography

[1]Benoit B. Mandelbrot, The Fractal Geometry of Nature. New York: W. H. Freeman and Co., 1982.

[2]Anderson, P. W., Phys. Rev. 109 (1958)

[3]G. Paladin, A. Vulpiani, Phys. Rep. 4, 147 (1987)

[4]H. E. Stanley, P. Meakin, Nature 335, 405 (1988)

[5]H. G. E. Hentschel, I. Procaccia, Physica (Amsterdam) 8D, 435 (1983)

[6]M. Inui, S. A. Trugman, Elihu Abrahams Phys. Rev. B 49, 3190 (1994)

[7]Hideo Aoki Phys. Rev. B 33, 7310 (1986)

[8]S. N. Evangelou, J. Phys. A: Math. Gen. 23 L317 (1990)

[9]Evangelou, S. N., Katsanos, D. E. Journal of Statistical Physics, Volume 85, Issue 5-6, pp. 525-550 (1996)

[10]V.I. Falko and K.B. Efetov, Europhys. Lett. 32, 627 (1995), Phys. Rev. B 52, 17413 (1995)

[11]A. Bunde, S. Havlin, Springer Verlag, Berlin, Heidelberg, New York, (1991)

[12]Michael Schreiber and Heiko Grussbach, Phys. Rev. Lett. 67, 607 (1991)

[13]Masatoshi Imada, Atsushi Fujimori, and Yoshinori Tokura, Rev. Mod. Phys. 70, 1039 (1998)

[14]I. Kleftogiannis, S. N. Evangelou, (to be submitted)

Chapter 4

Quantum Chaos in Disordered Graphene

4.1 What is Quantum Chaos

4.1.1 Introduction

Chaos in the quantum world is completely different from the classical deterministic chaos. Classically chaotic systems are characterized by increased sensitivity to initial conditions, leading to extreme unpredictability expressed through an exponential growth of the error described by the distance between two chaotic orbits in their phase space. The unpredictability is characterized by a Lyapunov exponent from the exponential growth rate of the error. In classical dynamical systems chaos occurs even for a small number of degrees of freedom, with an essential condition for chaos the presence of the non-linearity in the deterministic equations.

In the quantum world the Schrodinger equation $i\frac{\theta}{\theta t}\Psi(x,t) = H\Psi(x,t)$ is linear,

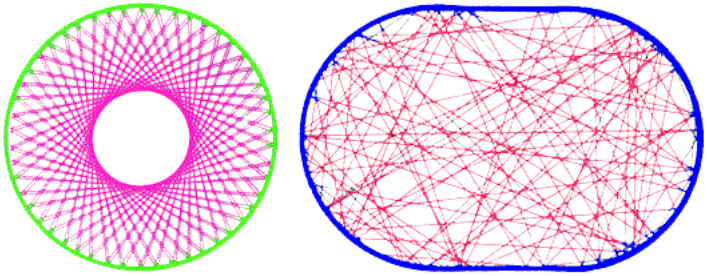

Figure 4.1: Two billiards of circular and stadium shape . The classical motion is periodic for the circular one, while it is chaotic for the stadium.

therefore the classical sense chaos is excluded. Quantum chaos is not related with dynamical evolution, instead, it is encountered in the the statistical properties of the eigenvalue energy spectrum. However, there is a strong relation between the classical and quantum manifestation of chaos acting as a bridge between the two worlds. A very striking example appears in systems commonly referred to as billiards[1]. For example, the circular billiard shown in Fig. 4.1 with a classical particle like a ball moving freely inside, by allowing elastic scattering with the walls. It can be proven[1] that the ball will follow a completely predictable orbit characterized by zero Lyapunov exponent. This result is related with the number of conserved physical quantities in conjunction with the number of the spatial degrees of freedom. Because of the elastic scattering the absolute value of the momentum is conserved after each scattering event which is equivalent to the conservation of the energy, while we can easily prove that the angular momentum is also conserved. The number of degrees of freedom (two) is equal to the number of conserved physical quantities.

In the quantum case a particle, e.g an electron, can be enclosed in this billiard geometry. The obtained energy eigenvalues for the quantum system will be distributed as completely random variables with zero spacing between successive energy levels having propability one. This surprising fact can be expressed through the Poissonian

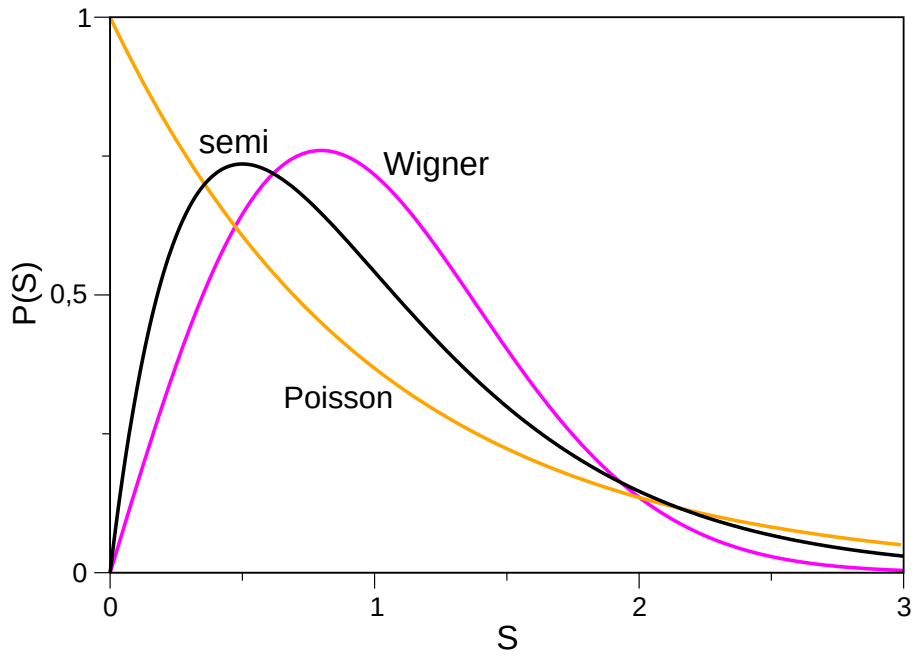

Figure 4.2: The Poisson, semi-poisson and Wigner distributions, characterizing integrable, semi-integrable and chaotic quantum systems respectively.

form

$$P(S) = \exp(-S), \tag{4.1}$$

which gives the propability of the spacing S between sucessive energy levels $S = E_j - E_{j-1}$. It is plotted in Fig. 4.2. The circular billiard is a characteristic example of a classically integrable system desplaying a non-cahotic quantum behavior.

Quantum Chaos occurs for more complex billiard geometries. We can consider the case of a classical particle enclosed in a stadium, shown in Fig. 4.1. This is characteristic non-integrable classical system, with the orbits of the enclosed particle being completely chaotic, having non zero Lyapunov exponent[1] leading to unpre-

dictability. The corresponding quantum system shows a statistical behavior of the eigenvalues completely different from the randomly distributed levels of the circular billiard[2,3]. The propability distribution $P(S)$ for the spacing of successive energy levels will follow a form known as Wigner[5]

$$P(S) = \frac{\pi}{2} S \exp\left(-\frac{\pi}{4} S^2\right), \tag{4.2}$$

plotted in Fig. 4.2. This gives zero propability to zero spacing S and a linear law for small S. It, somehow, means that the levels communicate with each other, this effect is called level-repulsion. This is in sharp contrast to what is happening for the uncorrelated random levels in the circular billiard. Moreover, the corresponding wavefunctions will have a characteristic structure with scars (concentrated amplitudes) where the periodic orbits of the chaotic classical system occur[3], in contrast to the perfect ballistic wave states for the integrable systems.

In general, there is a widely accepted conjecture[7,8,9,12] that quantum systems displaying classically integrable behavior, like the circular billiard, are expected to follow a universal behavior for their energy level statistics conveniently expressed through the Poissonian form of $P(S)$. For quantum systems whose classical counterparts display classically chaotic behavior, like the stadium billiard, $P(S)$ will follow universal Wigner statistics.

4.1.2 Random matrix theory

The Wigner distribution can be in general derived by the random matrix theory(RMT) [4,9], which has to do with the statistical properties of the eigenvalues of full infinite dimensional random matrices. These matrices can be regarded as hamiltonians of

disordered quantum systems with most of their possible symmetries being broken. There are, however, some basic symmetries preserved even in the case of completely chaotic systems. Time-reversal symmetry is the most fundamental one. H must be real[8] when time-reversal symmetry is preserved. The real time reversible hamiltonians of RMT are characterized by a definite statistical behavior of their energy levels, they show level-repulsion as in the case of the stadium billiard. This is clearly expressed through the special form of the nearest level spacing distribution $P(S)$ which has the Wigner form $\frac{\pi}{2}S\exp\left(-\frac{\pi}{4}S^2\right)$. The unique behavior of the time reversible hamiltonians of RMT, can be derived in the simple case of a two dimensional real, random, Hamiltonian[8]

$$H = \begin{bmatrix} H_{11} & H_{12} \\ H_{12} & H_{22} \end{bmatrix},$$

where we have taken account hermicity. We can also consider all the elements H_{11}, H_{22}, H_{12} as uncorrelated random variables with a propability distribution of the typical gaussian form $W(x) \sim \exp(-x^2)$. The difference between its eigenvalues is

$$E_2 - E_1 = \sqrt{(H_{11} - H_{22})^2 + 4H_{12}^2},$$

the terms $x = H_{11} - H_{22}$ and $y = 4H_{12}$ are again uncorrelated random variables distributed in the gaussian form, so that we can write the spacing between the two energy levels of the random Hamiltonian as

$$S = E_2 - E_1 = \sqrt{x^2 + y^2}.$$

The propability distribution of this spacing S can be derived from the following

formula

$$P\left(S\right)=\int\int dxdyW\left(x,y\right)\delta\left(S-\sqrt{x^{2}+y^{2}}\right),$$

which gives $P(S)$ if we know the propability distribution of each random variable. In our case we have two random variables described by the propability $W(x,y)\sim\exp\left[-A\left(x^{2}+y^{2}\right)\right]$ and we need to derive the propability distribution of their function $S=\sqrt{x^{2}+y^{2}}$. In polar coordinates $x=rdrd\theta$,$r=\sqrt{x^{2}+y^{2}}$ we have

$$P\left(S\right)=\int\int rdrd\theta\exp\left(-Ar^{2}\right)\delta\left(S-r\right)=2\pi S\exp\left(-AS^{2}\right),$$

An important remark is that $P\left(S\right)$ is a statistical measure of the fluctuations of the S around its mean value $<S>$ which does't hold any information about the chaotic nature of a quantum system. For convenience we require that $<S>=\int SP\left(S\right)dS=1$, along with the normalization condition $\int P\left(S\right)dS=1$ gives the Wigner distribution of Eq. [4.2].

In general the basic symmetries present in the systems described by the RMT theory enable us to categorize them into three basic universality classes, characterized by a level-repulsion between their energy levels. The ensemble of real symmetric random matrices which preserve the time reversal symmetry is called the gaussian orthogonal ensemble(GOE) and is characterized by $P\left(S\right)\sim S$ for small energy differences S.

When the time reversal symmetry is broken, e.g. in the presence of a magnetic field, the corresponding ensemble, called gaussian unitary (GUE), consists of complex hermitian random matrices. It is characterized by a universal level-repulsion of $P\left(S\right)\sim S^{2}$ when $S\rightarrow0$. This behavior can be derived again by considering the

simple case of a two dimensional complex random matrix

$$H = \begin{bmatrix} H_{11} & H_{12} \\ H_{12}^{*} & H_{22} \end{bmatrix}.$$

The spacing between its eigenvalues now becomes

$$S = E_2 - E_1 = \sqrt{(H_{11} - H_{22})^2 + 4Real\,(H_{12})^2 + 4Im\,(H_{12})^2},$$

S depends on three uncorrelated random variables this time $x = H_{11} - H_{22}$, $y = 2Real\,(H_{12})$ and $z = 2Im\,(H_{12})$ so that we can write

$$S = \sqrt{x^2 + y^2 + z^2}.$$

If we calculate $P\,(S)$ assuming that x, y, z are distributed in a typical gaussian form as in the gaussian orthogonal ensemble, by using also the spherical coordinates $dxdydz = r^2 \sin\theta dr d\theta d\phi$,$r = \sqrt{x^2 + y^2 + z^2}$

$$P\,(S) = \int\int dxdyW\,(x, y, z)\,\delta\left(S - \sqrt{x^2 + y^2 + z^2}\right) =$$

$$= \int\int dr d\theta d\phi r^2 \sin\theta \exp\left(-Ar^2\right)\delta\,(S - r) =$$

$$= 4\pi S^2 \exp\left(-AS^2\right).$$

By taking account the conditions $\int P\,(S)\,dS = 1$ and $< S >= \int SP\,(S)\,dS = 1$ we derive another type of Wigner distribution $\frac{32}{\pi^2}S^2 \exp\left(-\frac{4}{\pi}S^2\right)$, characterizing the gaussian unitary ensemble, with an increased level of repulsion $P\,(S) \sim S^2$ for $S \to 0$.

There is also a third universality class characterizing the so called gaussian symplectic ensemble which consists of full random matrices that preserve the time reversal symmetry but have spin orbit coupling. This ensemble shows a universal level of repulsion $P(S) \sim S^4$ for $S \to 0$.

Therefore, the chaotic nature of quantum systems can be found by fully random matrices which form the three elementary ensembles of RMT according to the basic symmetries present. All quantum chaotic cases show a universal level-repulsion between their energy levels

$$P(S) = S^{\beta}, S \to 0,$$

where $\beta = 1, 2, 4$ is called the universal class index, denoting orthogonal, unitary and symplectic universality classes, respectively.

4.2 Quantum chaos in disordered tight binding lattices

The universality classes of quantum chaos are also encountered in systems described by the tight binding model in the presence of disorder, like graphene or a square lattice. They are closely related with the localization properties of the corresponding wavefunctions. Such behavior is well known for the energy levels of a cubic lattice with on-site potential disorder denoted by the strength W[10,11,12], by introducing random variables on the diagonal matrix elements of the corresponding Hamiltonian. The levels show the typical characteristics of repulsion described by the Wigner distribution for $P(S)$ with universality class index $\beta = 1$. They are correlated having overlapping wavefunctions that diffuse in space, characterized by infinite localization

length. The corresponding chaotic wavefunctions are randomly fluctuating.

In the cubic lattice when the randomness on the diagonal exceeds a certain limit, that is for $W > W_c \approx 16.5$, where W_c is known as the critical point, then Anderson localization mechanism occurs[6] leading to localized wavefunctions with their finite localization length decreasing further as W is increased. The energy levels on this localized regime behave as completely uncorrelated random variables described by the Poissonian form of $P(S)$. That is resemble quantum systems that are classically integrable like the circular billiard (see Eq. (4.1)). The corresponding wavefunction are non-overlapping concentrated on sites suggested by the localization length. At the critical point W_c, where the transition between the chaotic and localized regime occurs, the propability distribution of the spacing between successive levels $P(S)$ is known to follow a form $4S\exp(-2S)$ called semi-poisson[10,11]. This intermediate distribution is characterized by a behavior intermediate between the Poisson and the Wigner, for small is analogous to S similar to Wigner, while for large S it decays with a Poissonian rate as $\exp(-2S)$. The semi-poisson distribution characterizes quantum systems that are classically semi-integrable, e.g a trigonal irrational billiard. The corresponding wavefunctions are multifractal sharing the properties of both extended and localized states with their amplitude wildly fluctuating in space (see Chapter two). For one and two-dimensional tight binding models with diagonal disorder, e.g. a linear chain or a square lattice, the critical value of $W_c = 0$ implies that $P(S)$ for the energy levels always follows the Poisson form with the wavefunctions being localized for any finite value of the disorder strength W.

The above results are valid in the limit of infinite system size only. In practice we can use numerical methods, like diagonalization, for finite systems and via scaling reproduce the chaotic behavior of the infinite systems. We can verify for example,

that the distribution of spacings $P(S)$ for a finite linear chain approaches gradually the Poisson form as the disorder strength W is increased. For a square lattice with on-diagonal disorder, however, $P(S)$ gives an almost scale and disorder invariant Wigner form, as long as we stay at the chaotic region for disorder W under W_C. The scale invariance of $P(S)$ also indicates multifractality of the corresponding wavefunctions[13]. As we increase the size the expected Poisson form is indeed, approached extremely slowly, it is obtained for very large sizes. In other words it is difficult to detect Poisson in practice for moderate values of W because of the large localization lengths of the corresponding wavefunctions.

In confined graphene systems recent experiments[16] ,pose the fundamental question about its chaotic nature. It is of great importance to see the role of edge states in the presence of disorder.

4.2.1 Square Lattice

In a finite square lattice sample with on-diagonal disorder quantum chaos occurs. We can show this by studying the statistics of just one spacing between two successive energy levels, at the the middle of the energy spectrum. We have done this for the simplest possible flake form, that is a square. The results are shown in Fig. 4.3.

We carried out the calculations for the distribution $P(S)$, by demanding that the mean value of the spacings is $< S >= 1$, obtained for different sizes and values of the disorder strength W. Clearly $P(S)$ follows a form close to Wigner, almost invariant under scaling, consistent with the multifractality of the wavefunctions corresponding to the two energy levels. The form of $P(S)$ is Wigner-like for every value of disorder strength W ($W < 1$), showing that the system remains at the chaotic region for

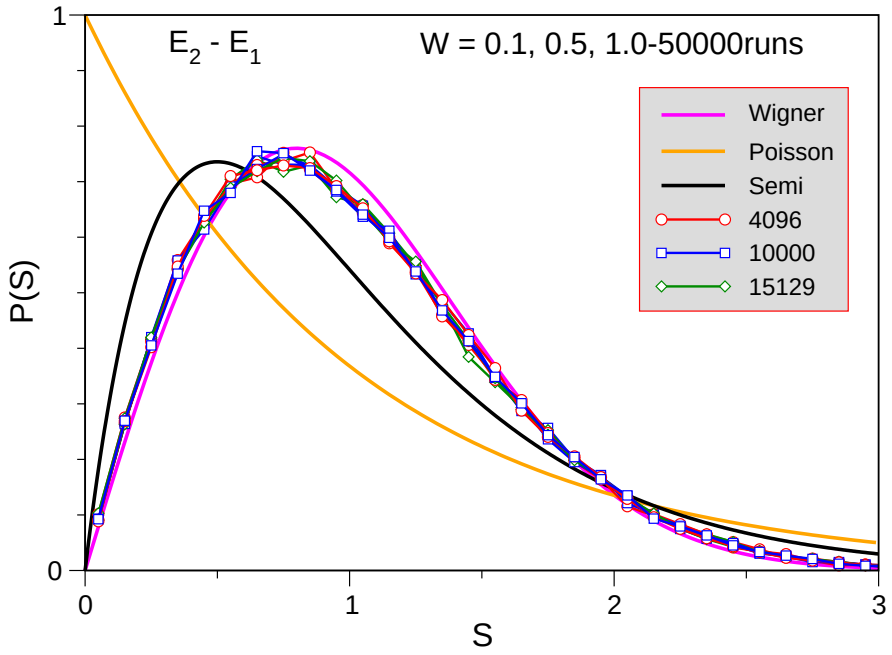

Figure 4.3: The distribution of the level spacing between two successive positive mid-band energy levels of a square lattice for different strengths of disorder W ,50000 realizations and different sizes. We plot also the Poisson[4.1] and Wigner[4.2] distributions. All the curves stay near the Wigner distribution showing the typical chaotic behavior derived by RMT for $\beta = 1$.

the disorder values. In order to be able to study the statistical behavior of the level spacings including more energy levels than two near zero energy we have to ensure that the mean value of the spacings $< S >= 1$. In this case we must apply a method called unfolding ensuring that the mean value becomes one and the fluctuations around this value which characterize quantum chaos. Our results are consistent with the presence of a chaotic region which crosses over to localized only for very large size.

There is a continuous crossover between the two different, chaotic and localized regions, a behavior known as crossover. For weak disorder there is a typical chaotic behavior where the energy levels show a considerable repulsion without ever crossing, well described by the Wigner form of $P(S)$ shown in Fig. 4.3. Despite the fact that for an infinite square lattice there is a trivial transition point at $W_c = 0$, localized wavefunctions exist for every non-zero disorder and every possible energy. The wavefunctions of the studied finite square lattice, however, look extended due to the finite system size. They display a chaotic region for sizes below the localization length. For large disorder strengths the energy levels gradually begin to fluctuate wildly resulting in high possibility of both crossings and large spacings, resembling the behavior of an ensemble of uncorrelated random numbers described by the Poisson $P(S)$.

4.2.2 Graphene

We have studied the level-spacing distribution near $E = 0$ for a finite square honeycomb lattice representing a graphene flake. The obtained results are similar those found in [17]. In particular the distribution of the spacing between two successive levels is shown in Fig. 4.4. The $P(S)$ between two successive positive levels stays near the semi-poisson distribution for all the sizes and weak disorder strengths studied.

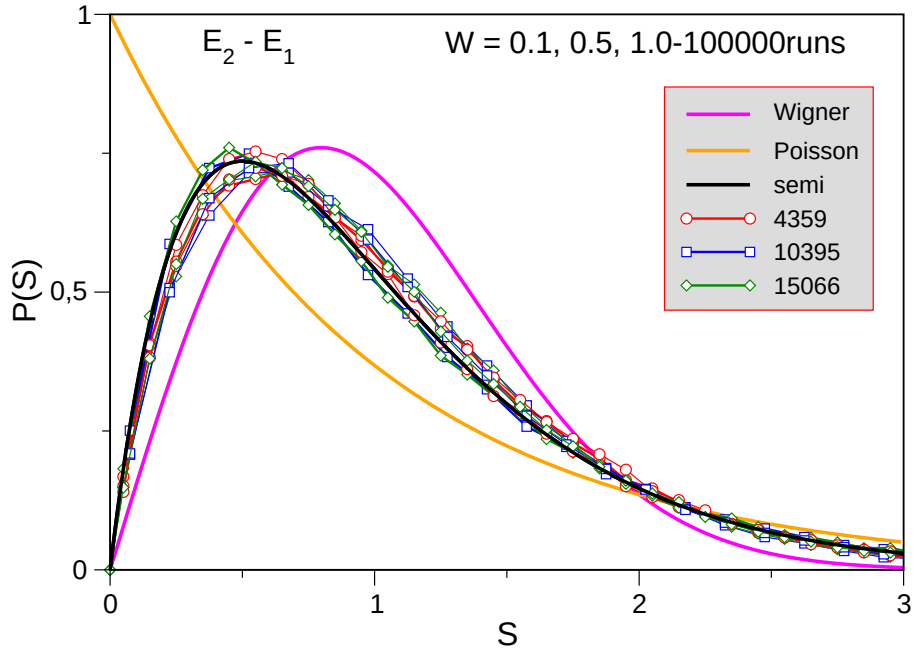

Figure 4.4: The distribution of the spacing between two successive midband energy levels of a square graphene flake for different strengths of disorder W ,100000 realizations and different sizes. All the curves stay near the Semi-poisson distribution for all weak W and sizes.

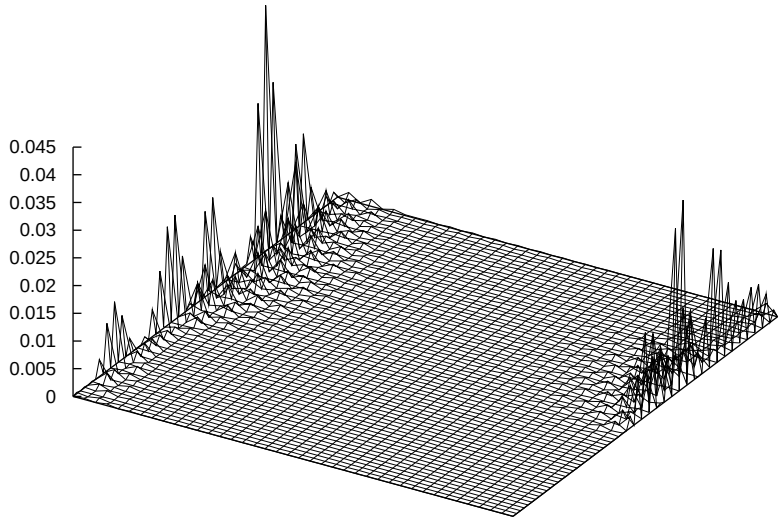

Figure 4.5: $E \approx 0.014$ wavefunction propability distribution of a square graphene flake with on-diagonal disorder ($W = 0.5$) consisting of 2840 sites. The honeycomb lattice sites are arranged on a square lattice. The wavefunction is shown to be localized at the zigzag edges of the flake.

This is a weakly chaotic behavior non existent in the square lattice with on-diagonal disorder. For higher disorder strengths we expect the usual Poisson distribution of $P(S)$ to be recovered, since Anderson localization mechanism prevails as for the square lattice. The Wigner distribution is not encountered at the Dirac point of graphene for the square flake geometry studied.

This weakly chaotic behavior is closely related with the localization properties of the wavefunctions. In graphene the edge states exist even in the presence of on-diagonal disorder, arising from the destructive interference mechanism of the honeycomb lattice. In order to verify this assumption in Fig4.5 we have plotted a wavefunction near the Dirac. Edge states are intermediate case between the diffusive wavefunctions of the disordered square lattice, that give chaotic behavior, and the

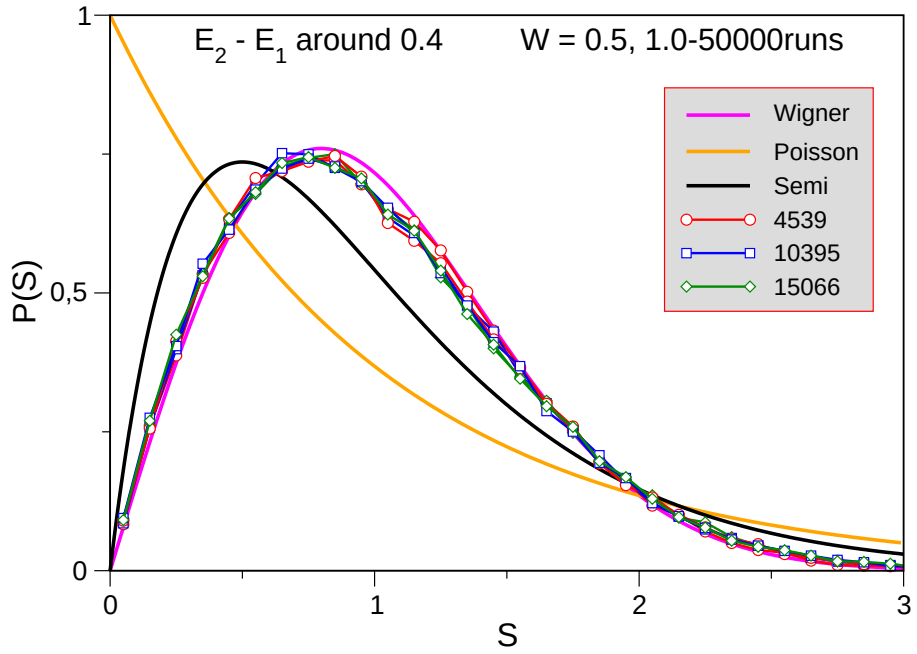

Figure 4.6: The the level spacing distribution between two successive energy levels at $E = 0.4$ of a square graphene flake for different strengths of disorder W ,50000 realizations and different sizes. The typical chaotic Wigner like behavior is recovered since edge states are absent.

localized states occuring in disordered 2d systems when the disorder strength becomes sufficiently large. They are approximately extended along the edge, without penetrating in the internal region of the flake. If this is combined with the diffusive mechanism of quantum chaos gives chaotic edge states and a form of $P(S)$ intermediate between the Wigner distribution characterizing repelled extended wavefunctions, and the Poisson distribution related with localized wavefunctions. According to this analysis we expect the propability distribution of spacings $P(S)$ for levels higher in the energy spectrum of graphene where edge states are absent to recover the usual chaotic behavior described by the Wigner form of $P(S)$. This is shown in Fig. 4.6 for

two successive energy levels at $E = 0.4$. The typical chaotic behavior corresponding to diffusive wavefunctions encountered in the square lattice is recovered. The form of $P(S)$ is Wigner like for the all weak disorder strengths and flake sizes studied.

4.3 Conclusions

Disordered Graphene flakes show a new quantum chaotic behavior not encountered in conventional disordered 2d systems like a square lattice. The propability distribution of spacings $P(S)$ near the Dirac point of graphene with on-diagonal disorder follows approximately the semi-Poisson distribution indicating a weakly chaotic behavior,as obtained in [17], intermediate between the typical chaotic behavior encountered in a square lattice with on-diagonal disorder, described by the Wigner form of $P(S)$, and the Poissonian form of $P(S)$ characterizing Anderson localization. This special chaotic behavior is strongly related with edge states present in graphene systems. For weak disorder the honeycomb lattice destructive interference mechanism of graphene survives giving edge states near the Dirac point, extended approximately along the edge of the finite graphene system, leading to the weakly chaotic behavior shown.

Bibliography

[1]Berry, M V, Eur.J.Phys 2, 91-102, (1981)

[2]H.-J. Stockmann and J. Stein, Phys. Rev. Lett. 64, 2215 (1990)

[3]Steven W. McDonald and Allan N. Kaufman, Phys. Rev. A 37, 3067 (1988)

[4]F. Haake, Quantum Signatures of Chaos, 2nd Edition, Springer (2000)

[5]Eugene Paul Wigner, Dirac, P. A. M. Proc. Cambr. Philos. Soc. 47: 790 (1951)

[6]Anderson, P. W., Phys. Rev. 109 (1958)

[7]O. Bohigas, M. J. Giannoni, and C. Schmit, Phys. Rev. Lett. 52, 1 (1984)

[8]B. D. Simons and B. L. Altshuler, Phys. Rev. B 48, 5422 (1993)

[9]A. V. Andreev, O. Agam, B. D. Simons, and B. L. Altshuler, Phys. Rev. Lett. 76, 3947 (1996)

[10]B. I. Shklovskii, B. Shapiro, B. R. Sears, P. Lambrianides, and H. B. Shore, Phys. Rev. B 47, 11487 (1993)

[11]Evangelou, S. N., Katsanos, D. E. Journal of Statistical Physics, Volume 85, Issue 5-6, pp. 525-550 (1996)

[12]I. Kh. Zharekeshev , M. Batsch and B. Kramer , Europhys. Lett, 34 (8), pp. 587-592 (1996)

[13]V.I. Falko and K.B. Efetov, Europhys. Lett. 32, 627 (1995), Phys. Rev. B 52, 17413 (1995)

[14]What is... Quantum Chaos by Zeev Rudnick (January 2008, Notices of the American Mathematical Society)

[15]Masatoshi Imada, Atsushi Fujimori, and Yoshinori Tokura, Rev. Mod. Phys. 70, 1039 (1998)

[16]L. A. Ponomarenko et al., Science 320, 356 (2008)

[17]I. Amanatidis, I. Kleftogiannis, D. Katsanos, S.N. Evangelou (to be submitted)

Chapter 5

Conclusions

The honeycomb lattice structure of graphene has important properties like chiral symmetry and spatial anisotropy. These are responsible for the highly topology dependent electronic properties shown. Graphene is also characterized by extreme sensitivity to boundary conditions. The underlying destructive interference mechanism plays a definite role. Its existence is due to the fact that the honeycomb lattice has every site connected to its three nearest neighbours. For finite systems with edges this mechanism leads to wavefunctions localized at the boundaries. These are well known as edge states and their existence is dependent on the morphology of the boundary. The so called zigzag type of edges contributes edge states near the Fermi energy for any confined graphene system. The other possible type of edge, armchair does not give edge states and consequently, the semiconducting behavior remains intact. We have demonstrated edge states in various systems, semi-infinite graphene sheets, zigzag nanoribbons, and flakes of square and circular formations where there exists mixing of zigzag and armchair edges.

We show how the topology sensitive electronic properties of graphene play an

important role in the fractal nature of the wavefunctions at the Dirac point. In the presence of off-diagonal disorder which preserves the chiral sublattice symmetry, the mechanism leading to edge states survives. The wavefunctions located at the boundaries of finite systems resemble the fractal states for small length chains with off-diagonal disorder. This is clearly indicated by the scaling dimension D_2 taking values from zero to one, instead of going from zero to two as for the midband multifractal wavefunctions of a square lattice with off-diagonal disorder. Zero value of D_2 means Anderson localization, $D_2 \approx 0$ means edge states and $D_2 \approx 2$ fully chaotic, diffusive or ballistic states.

We have shown also that the destructive interference mechanism plays an important role in the quantum chaotic behavior of disordered graphene. The energy levels at the Dirac point for square samples with on-diagonal disorder show a statistical behavior not encountered in conventional 2d-systems, like the square lattice. The form of the spacing distribution $P(S)$ is intermediate Semi-Poisson like, indicating a weakly chaotic behavior. This remains for many successive energy levels near the Dirac point where edge states exist for pure graphene. We argue that this behavior is due to the underlying mechanism of edge states which survives even in the presence on-diagonal disorder. It is clearly indicated by the comparison of the statistical behavior for the midband energy levels to a disordered square lattice, for which edge states are absent. For the latter case the well known Wigner like chaotic form for $P(S)$ is obtained.

Therefore,in both, off-diagonal and on-diagonal disorder, the destructive interference mechanism of the underlying honeycomb lattice of graphene prevails giving midband edge states, heavily affecting the fractal nature of the wavefunctions and the chaotic behavior of graphene. This mechanism is of extreme importance for the

construction on graphene based nanoelectronics. The weakly chaotic behavior at the Dirac point, implies a semi-metallic behavior intermediate between metals and insulators.

Appendix A

Lattice representation (tight binding method)

A.1 Introduction

Tight binding is a method widely used in condensed matter physics for modeling electronic quantum properties of various crystal lattice structures. The wavefunction of an electron inside a periodic lattice structure can be expressed as a superposition in the lattice site basis. In this sense the wavefunction for one electron can be written as a linear combination of the atomic site orbitals denoted by $\mid n >$ as

$$\mid \Psi >= \sum_{n=1}^{N} \Psi_n \mid n > \tag{A.1}$$

where N is the total number of atoms and $\Psi_n$the amplitude coefficients. The tight binding approximation is based on the simple assumption that each atomic orbital is strongly localized on the corresponding site position. $\mid n >$ denotes the positions

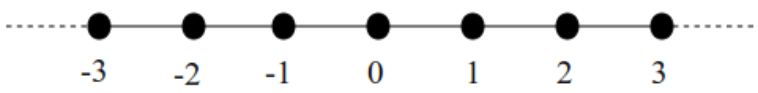

Figure A.1: An infinite linear chain.

of each atom in the lattice. The propability amplitude for finding the electron in position $\overrightarrow{r}$ would be $< r \mid \Psi >= \sum_{n=1}^{N} \Psi_n < r \mid n >= \Psi_n$. This is obviously non-zero only if there is an electron in the atomic position. In this case electrons are tightly bound in each atomic site which defines the term tight binding.

In otherwords, tight binding model is a discretization of real space into lattice site points where the atoms lie. The tight binding Hamiltonian can be derived by descretizing the Schrodinger equation in the lattice points. A simple continuous model of a particle in one dimension in the presence of a potential $V(x)$ is described by the Schrodinger equation

$$H\Psi(x) = E\Psi(x) \Rightarrow -\frac{\hbar^2}{2m}\frac{\theta^2\Psi(x)}{\theta x^2} + V(x)\Psi(x) = E\Psi(x)$$

We can easily transform this system into a set of discrete spatial points within distances equal to the lattice constant a,forming this way a chain extending from $-\infty$ to ∞ which can be seen in FigA.1 The position x in this case takes discretized values $x = na, n \in Integer\,[-\infty, \infty]$ while the second derivative $-\frac{\hbar^2}{2m}\frac{\theta^2\Psi(x)}{\theta x^2}$ assuming that a is small can be written as

$$\frac{\theta^2\Psi(x)}{\theta x^2} \mid_{x=na} \rightarrow \frac{1}{a}\left(\frac{\theta\Psi(x)}{\theta x} \mid_{x=\left(n+\frac{1}{2}\right)a} - \frac{\theta\Psi(x)}{\theta x} \mid_{x=\left(n-\frac{1}{2}\right)a}\right)$$

The first derivatives at points $x = \left(n + \frac{1}{2}\right) a$ and $x = \left(n - \frac{1}{2}\right) a$ are

$$\frac{\theta\Psi(x)}{\theta x} \mid_{x=\left(n+\frac{1}{2}\right)a} \rightarrow \frac{1}{a} \left(\Psi((n+1)\, a) - \Psi(na)\right)$$

$$\frac{\theta\Psi(x)}{\theta x} \mid_{x=\left(n-\frac{1}{2}\right)a} \rightarrow \frac{1}{a} \left(\Psi(na) - \Psi\left((n-1)a\right)\right)$$

and the second derivative is

$$\frac{\theta^2\Psi(x)}{\theta x^2} \mid_{x=na} \rightarrow \frac{1}{a^2} \left(\Psi((n+1)\, a) - 2\Psi(na) + \Psi\left((n-1)a\right)\right)$$

so that the difference tight binding equation for the chain becomes

$$-t \left[\Psi\left((n+1)\, a\right) + \Psi\left((n-1)a\right)\right] + \left(V(na) - 2t\right) \Psi(na) = E\Psi(na)$$

with $t = \frac{\hbar^2}{2ma^2}$. Although in the derivation we have assumed that the lattice spacing a is infinitesimally small ,this model can be easily generalized for any value of a. For simplicity we choose $a = 1$, and write

$$-t \left[\Psi_{n+1} + \Psi_{n-1}\right] + \left(V_n - 2t\right) \Psi_n = E\Psi_n \tag{A.2}$$

The discretized Scrodinger equation $H\Psi = E\Psi$ can be written also in matrix form as

$$\Rightarrow \begin{bmatrix} ... & -t & 0 & 0 & 0 \\ -t & V_{n-1} - 2t & -t & 0 & 0 \\ 0 & -t & V_n - 2t & -t & 0 \\ 0 & 0 & -t & V_{n+1} - 2t & -t \\ 0 & 0 & 0 & -t & ... \end{bmatrix} \begin{bmatrix} ... \\ \Psi_{n-1} \\ \Psi_n \\ \Psi_{n+1} \\ .. \end{bmatrix} = E \begin{bmatrix} ... \\ \Psi_{n-1} \\ \Psi_n \\ \Psi_{n+1} \\ .. \end{bmatrix}$$

The tight binding matrix H is written in the$|\ n>$orbitals basis which is exactly the discretised space. We see that neighbouring orbitals or sites, communicate via off-diagonal hopping terms $-t$ while in the diagonal there is an on site term $V_n - 2t$. In our calculations we usually neglect the extra diagonal term $-2t$ because it just shifts the whole energy spectrum by a constant factor. This result can be easily extended to more dimensions two and three and different lattice types, so that we can derive their electronic properties like the band structure, the density of states or the wavefunctions.

A.2 1d tight-binding lattices

A.2.1 Infinite systems

The tight-binding difference equation for an an infinite linear chain is

$$-t\left[\Psi_{n+1} + \Psi_{n-1}\right] + V\Psi_n = E\Psi_n$$

considering the on-site potential $V_j = V$ constant for all the sites of the chain. We can solve this equation in order to obtain the energies and the wavefunctions of this system by assuming a simple solution in the form of a plane wave $\Psi_n = \exp(ikn)$.

$$-t\left[\exp(ik) + \exp(-ik)\right] + V = E \Rightarrow$$

$$E = V - 2t\cos(k) \tag{A.3}$$

This is the dispersion relation of the infinite linear chain with nearest neighbor hopping $-t$ and constant potential V Eq. (A.3). It gives continuous energy values in the

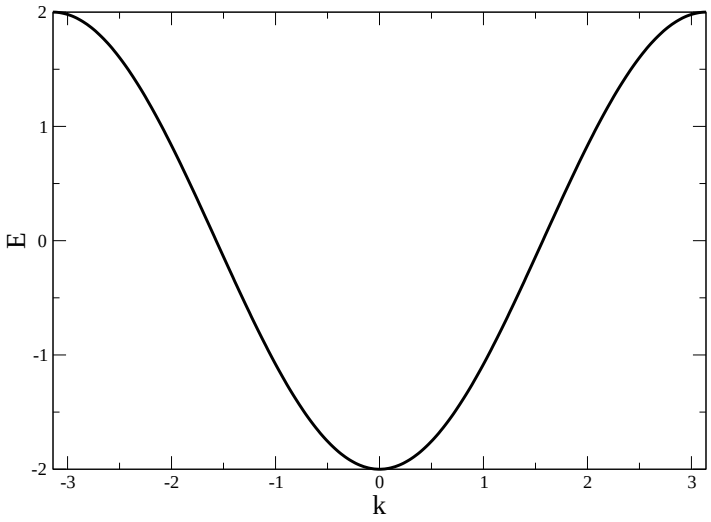

Figure A.2: The energy dispersion of a linear chain with hopping $t = 1$.

interval $[V - 2t, V + 2t]$. For $k \in [-\pi, \pi]$ which defines the first brillouin zone, there is double degeneracy, $E(k) = E(-k)$. It is plotted in Fig. A.2 for $V = 0$ and $t = 1$.

The eigenvector corresponding to energy $E(k)$ expressed in the lattice site basis $\mid n >$ is

$$\mid \Psi_k >= \sum_{n=-\infty}^{\infty} \exp(ikn) \mid n >$$

A basic quantity characterizing the electronic properties of a quantum system is the density of states $\rho(E)$. It is defined for a finite system as

$$\rho(E) = \frac{1}{N} \sum_k \delta(E - E(k)) \tag{A.4}$$

where N is the total number of states of the system. It is constructed by the sum

of individual delta functions localized around each allowed energy $E(k)$. The $\rho(E)$ gives the number of states which have a specific energy E and the density of states at this energy if we include the normalization factor $\frac{1}{N}$. For an infinite chain, since k takes continuous values in the interval $[-\pi, \pi]$, we can derive $\rho(E)$ by calculating the integral

$$\rho(E) = \int_{-\pi}^{\pi} \delta(E - E(k))dk$$

excluding the normalization term since $N \to \infty$ in this case. by using dispersion relation Eq. (A.3) we have

$$\frac{dE}{dk} = 2t\sin(k) \Rightarrow dk = \frac{dE}{2t\sin(k)} \Rightarrow dk = \frac{dE}{2t\sqrt{1-\cos^2(k)}} \Rightarrow dk = \frac{dE}{\sqrt{4t^2-(E-V)^2}}$$

By substituting dk into the integral and using the property of delta function $\int_{-\infty}^{\infty}\delta(x-a)f(x)dx = f(a)$ we get

$$\rho(E) = \int_{V-2t}^{V+2t} \delta(E - E(k))\frac{dE(k)}{\sqrt{4t^2-E(k)^2}} = \frac{1}{\sqrt{4t^2-(E-V)^2}}$$

while using also the normalization condition $\int_{V-2t}^{V+2t}\rho(E)dE = 1$ we get the result for the density of states

$$\rho(E) = \frac{1}{\Pi}\frac{1}{\sqrt{4t^2-(E-V)^2}} \tag{A.5}$$

It is symmetric around V and is defined only when $\mid E - V \mid \leq 2t$ since the density of states must be a real function. This is of course due to the fact that energies belong in the interval $[V - 2t, V + 2t]$. It is also singular at $E = V - 2t$ and $E = V + 2t$ .It is plotted in Fig. A.3 for $t = 1$ and $V = 0$.

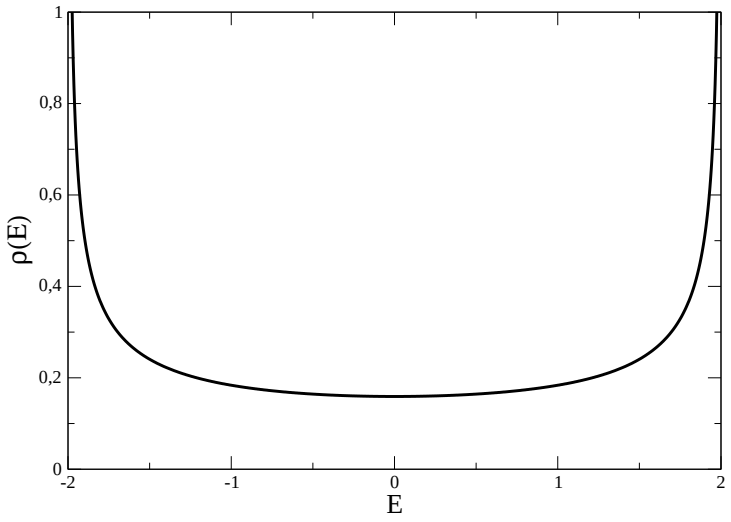

Figure A.3: The density of states $\rho(E)$ of a linear chain with $t = 1$.

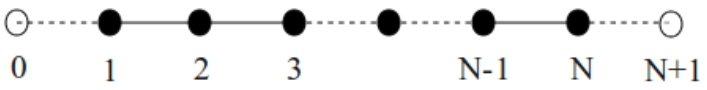

Figure A.4: Finite linear chain consisted on N atomic sites.

A.2.2 Finite systems with boundary conditions

In finite 1d systems formed by implying various types of boundary conditions we have hard wall boundary conditions whose equivalent model in continuous space would be an infinite quantum well. This type of boundary conditions requires the wavefunction of the electron to be zero at sites where the chain is terminated. The resulting system will be a finite chain of N sites shown in Fig. A.4 An important remark here is that we require the wavefunction to be zero at sites zero and $N + 1$ which seem to lie outside the chain. Those actually belong to the chain but the propability of finding the electron there is zero so we don't need to include them in the the total number

of sites. With the lattice being terminated at those sites solution of the tight binding equation must be in the form of a standing wave. This wave must have zero amplitude on $x = 0$. The only possible form fulfilling this condition is $\Psi_x^k = A\sin(kn)$ while the boundary condition at $n = N + 1$ gives

$$\Psi_{N+1} = A\sin(k(N+1)) = 0 \Rightarrow k = \frac{j\pi}{N+1}, j = 1, 2, .., N \tag{A.6}$$

Note that in the derivation of k we have excluded negative values of j so that it takes discrete values between zero and π only. Dispersion relation Eq. (A.5) becomes

$$E_j = V - 2tcos\left(\frac{j\pi}{N+1}\right) \tag{A.7}$$

This gives discrete energy values in the interval $[V - 2t, V + 2t]$. As $N \to \infty$ this set of energies becomes denser until it finally reproduces the positive part $k \in [0, \pi]$ of the first brillouin zone of the infinite chain. Negative values of j in the definition of k would give states that belong to the negative part of this brillouin zone. These states would have energies $E_{-j} = E_j$ and corresponding wavefunctions related with those for positive values of j by just a phase factor $\psi_n^{-j} = -\psi_n^j$.

Eigenvectors for this system are in the form of (A.1)

$$\mid k >= A\sum_{n=1}^{N} \sin(\frac{j\pi}{N+1}n) \mid n >$$

The factor A can be calculated by the normalization condition for the wavefunction

$$< k \mid k >= 1 \Rightarrow A^2 \sum_{n=1}^{N} \sin^2(\frac{n\pi}{N+1}n) = 1$$

the sum can be written also as$\sum_{n=0}^{N+1} \sin^2(\frac{j\pi}{N+1}x)$ since the wavefunction is zero for $n = 0$ and $n = N + 1$ .When $N \to \infty$ this can be approximated by an integral with $L = N + 1$ being the actual length of the chain

$$\int_0^L \sin^2(\frac{j\pi}{L}n)dn = \frac{L}{j\pi}\int_0^{j\pi} \sin^2(x)dx = \frac{L}{j\pi}\int_0^{j\pi} \frac{1-\cos(2x)}{2}dx = \frac{L}{2}$$

the normalization condition becomes then

$$A^2\frac{L}{2} = 1 \Rightarrow A = \sqrt{\frac{2}{L}}$$

as we would expect for an 1d infinite well of length L. So the normalized eigenvector is

$$\mid \Psi_j >= \sqrt{\frac{2}{N+1}}\sum_{n=1}^{N} \sin(\frac{j\pi}{N+1}n) \mid n > \tag{A.8}$$

We can also calculate the density of states of this system assuming it is large enough $N \to \infty$. In order to do this we can consider a small energy window dE and count the number of states dN (don't confuse with total number of sites) inside it. This is in principle the same as definition (A.4) when $dE \to 0$. By using also dispersion relation (A.7) we get

$$\rho(E) = \frac{dN}{dE} = \frac{dN}{dk}\frac{1}{\frac{dE}{dk}} = \frac{1}{2t\sin(k)} = \frac{1}{2t\sqrt{1-\cos^2(k)}} = \frac{1}{\sqrt{4t^2-(E-V)^2}}$$

$\frac{dN}{dk}$ gives us the number of states inside a windowdk in k space. It is also obvious From (A.6) that there is always only one state corresponding to a specific k so that $\frac{dN}{dk}$=1 . The normalization condition $\int_{V-2t}^{V+2t} \rho(E)dE = 1$ makes the derived relation for $\rho(E)$ the same as (A.5).

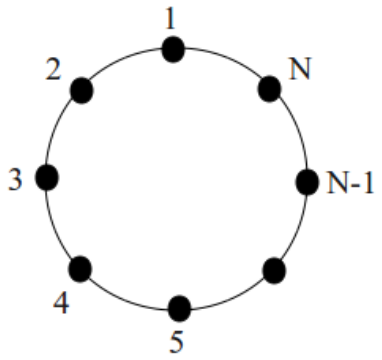

Figure A.5: A finite periodic linear chain consisted on N sites.

We now examine the case of periodic boundary conditions. In order to form a system of this kind we just take the 1d-finite chain discussed and connect it's edge sites one and N with a hopping. This way we form a closed chain as shown in Fig. A.5.

In this case the wavefunctions must be in the form of running waves. We choose the form $\Psi(n) = A\exp(kn)$ and apply the right conditions as before

$$\Psi_1 = \Psi_{N+1} \Rightarrow \exp(ikN) = 1 \Rightarrow k = \frac{2\pi j}{N}, j \in [1, 2, .., N] \tag{A.9}$$

The resulting dispersion relation

$$E_j = V - 2t\cos\left(\frac{2\pi j}{N}\right) \tag{A.10}$$

gives again discrete energy values in the interval $[V-2t, V+2t]$. An important remark here is that this energy spectrum has double degeneracy. For $j = N - j$

$$E_{N-j} = -2t\cos\left(2\pi - \frac{2\pi j}{N}\right) = -2t\cos\left(\frac{2\pi j}{N}\right) = E(j)$$

When N is even we only need values of $j = 1, 2, ..., N/2 - 1$ which give $N - 2$ states with double degeneracy. There are also two non degenerate states for $j = N/2$ and $j = N$ with their corresponding energies $E(N/2) = V - 2t$ and $E(N) = V + 2t$. For N odd $j = 1, 2, ..., (N - 1)/2$ gives $N - 1$ states with double degeneracy. The remaining state is for $j = N$ with energy $E(N) = V + 2t$.

Eigenvectors are again in the form of (A.1)

$$\mid k >= A \sum_{n=1}^{N} \exp(i \frac{2\pi j}{N} n) \mid n >$$

The factor A is easily calculated from the normalization condition $< \Psi_j \mid \Psi_j >= 1$ as in the case of hardwall boundary conditions when $N \to \infty$

$$< \Psi_j \mid \Psi_j >= A^2 \int_0^N 1 dn = A^2 N = 1 \Rightarrow A = \sqrt{\frac{1}{N}}$$

So the resulting eigenvectors are

$$\mid k >= \sqrt{\frac{1}{N}} \sum \exp(i \frac{2\pi j}{N} n) \mid x > \tag{A.11}$$

Another interesting case is the interaction of this system with a magnetic field. Consider the closed 1d chain enclosing a magnetic flux as shown in Fig. A.6 We know from the Aharonov-Bohm effect that a full turn around this enclosed magnetic flux will change the phase of the wavefunction by a factor $2\pi \frac{\Phi}{\Phi_0}$ with $\Phi_0 = \frac{hc}{e}$. For our system this implies that the wavefunction at site one should be equal to the wavefunction at site $N + 1$ multiplied by a factor $\exp(i 2\pi \frac{\Phi}{\Phi_0})$ which gives us the

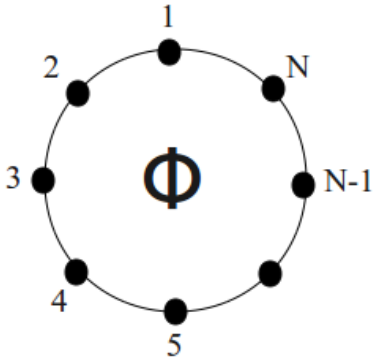

Figure A.6: A finite periodic linear chain consisted on N sites enclosing a magnetic flux Φ.

condition

$$\Psi(1) = \exp(i2\pi\frac{\Phi}{\Phi_0})\Psi(N{+}1) \Rightarrow 1 = \exp[i(kN{+}2\pi\frac{\Phi}{\Phi_0})] \Rightarrow k = \frac{2\pi(j-\frac{\Phi}{\Phi_0})}{N}, j \in [1,2,..,N] \tag{A.12}$$

so the dispersion relation in this case becomes

$$E(j) = V - 2t\cos\left(\frac{2\pi(j-\frac{\Phi}{\Phi_0})}{N}\right) \tag{A.13}$$

with the corresponding wavevectors

$$\mid \Psi_j >= \sqrt{\frac{1}{N}}\sum \exp(i\frac{2\pi(j-\frac{\Phi}{\Phi_0})}{N}n) \mid n > \tag{A.14}$$

A.3 2d tight-binding lattices

We will now study some two-dimensional tight-binding models . Those are used for the modeling various layer structures in condensed matter physics like graphene that have attracted a lot of attention lately in the concept also of nanoeletronics.

A.3.1 Square Lattice

The simplest example of a two-dimensional crystal is the square lattice, shown in Fig. A.7

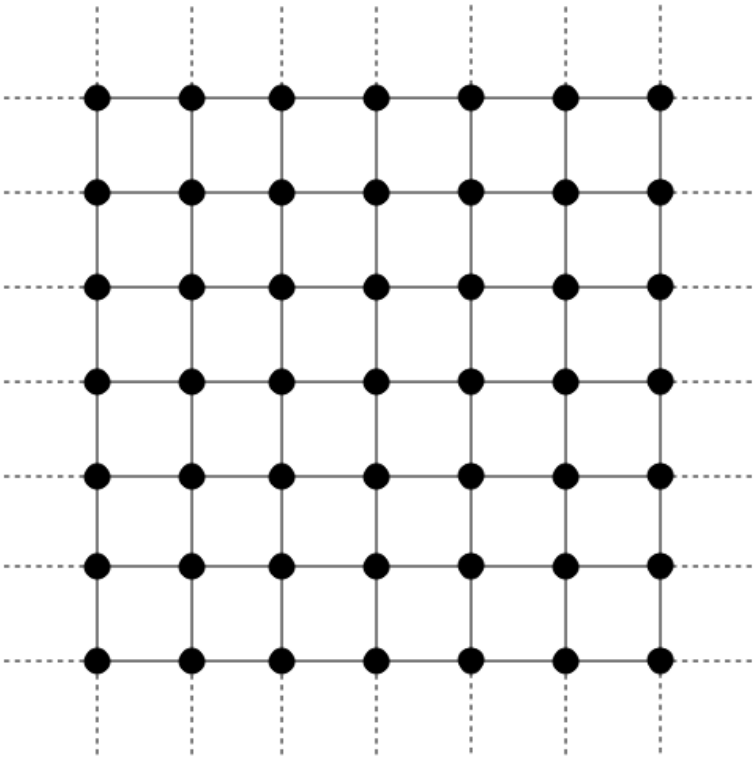

Figure A.7: Square lattice structure

As we see every site has connections with it's four nearest neighbours via hoppings $-t$. In analogy with the linear chain , the Schrodinger equation now becomes(see Fig. A.8)

$$-t\left[\Psi_{x,y+1}+\Psi_{x,y-1}+\Psi_{x+1,y}+\Psi_{x-1,y}\right]+V\Psi_{x,y}=E\Psi_{x,y}$$

where we have included the two extra hoppings in the y direction. We can solve it easily by assuming a solution of the simple form $\Psi_{x,y}=\exp(ik_x x)\exp(ik_y y)$ where $k_x$and k_y are the projections of wavevector $\overrightarrow{k}$ in x and y axis respectively. Dispersion

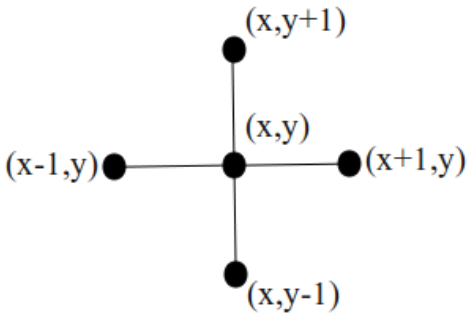

Figure A.8: One atomic site of the square lattice connected with it's four nearest neighbours

relation becomes in this case

$$-t\left[\exp(ik_y)+\exp(-ik_y)+\exp(ik_x)+\exp(-ik_x)\right]+V=E\Rightarrow$$

$$E(k_{x,}k_y)=V-2t\cos(k_x)-2t\cos(k_y) \tag{A.15}$$

This gives continuous energy values in the interval $[V-4t, V+4t]$. It also depends on two parameters, so we need a 3d plot in order to visualize it, it is shown in Fig. A.9. $E(k_{x,}k_y)$ for $t=1$ and $V=0$ as a function of $k_x, k_y \in [-\pi, \pi]$ which define the first brillouin zone

As we see in the first brillouin zone has the form of a square. The lines in Fig. A.10 characterize points that have the same energy giving infinite degeneracy for all energies apart from the minimum and maximum values $E_{max}=4, E_{min}=-4$. Clearly the first brillouin zone crosses the zero energy plane through four lines that form a square. For those lines

$$E(k_{x,}k_y)=0\Rightarrow\cos(k_x)=-\cos(k_y)\Rightarrow k_x=\pi-k_y$$

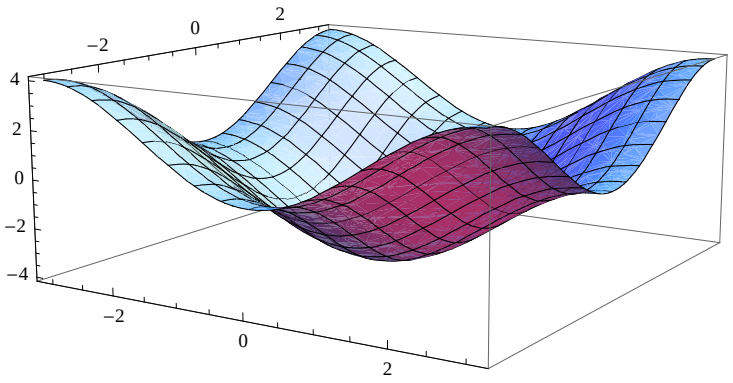

Figure A.9: Energy dispersion of a square lattice.

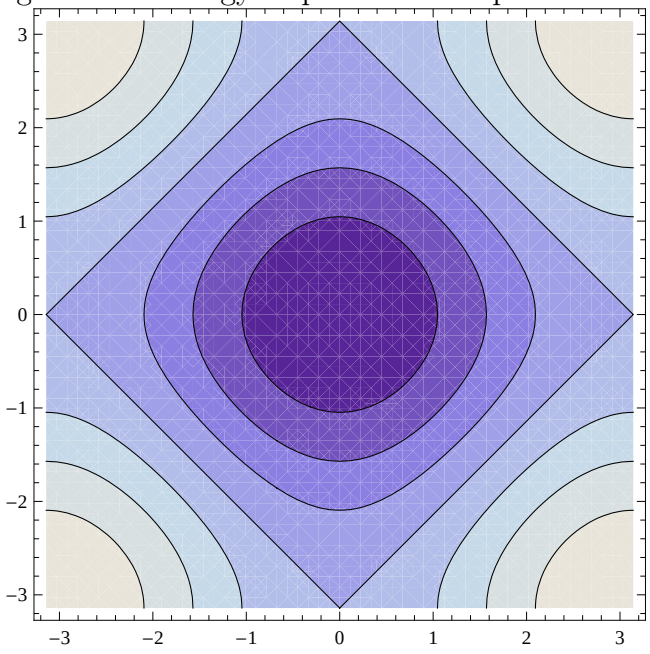

Figure A.10: Contour plot of the energy dispersion of a square lattice.

The part of the zone that lies inside this square corresponds to negative energies with one pair of $k_x, k_y = 0$ giving the minimum value $E_{min} = E(0,0) = -4$. The remaining points of the zone that lie outside this square correspond to positive energies. For this region there are four degenerate states for different pairs of k_x, k_y having all the maximum energy value $E_{max} = E(\pi,\pi) = E(-\pi,\pi) = E(-\pi,-\pi) = E(\pi,-\pi) = 4$.

We can find the density of states of this system from (1.4) by calculating the integral in analogy with the infinite 1d-chain

$$\frac{1}{2\pi^2}\int_{-\pi}^{\pi} dk_y \int_{-\pi}^{\pi} dk_x \delta(E - E(k_x,k_y)) = \frac{1}{2\pi^2}\int_{-\pi}^{\pi} dk_y \int_{-\pi}^{\pi} dk_x \delta((E+2t\cos(k_x)) - (-2t\cos(k_y)) =$$

$$= \frac{1}{2\pi^2}\int_{-\pi}^{\pi} dk_y \int_{-\pi}^{\pi} dx \frac{1}{-2t\sqrt{1-\frac{(x-E)^2}{4t^2}}} \delta(x - (-2t\cos(k_y)) =$$

$$= \frac{1}{2\pi^2}\int_{-\pi}^{\pi} dk_y \frac{1}{\sqrt{4t^2 - (E+2t\cos(k_y))^2}} = \frac{1}{2(\pi t)^2}\int_0^{\pi} dk_y \frac{1}{\sqrt{1-(\frac{E}{2t}+\cos(k_y))^2}}$$

For energies $E \neq 0$ it can be proven that this has the form of a complete elliptic integral of the first kind $K(x) = \int_0^{\frac{\pi}{2}} d\theta \frac{1}{\sqrt{1-x^2\sin^2(\theta)}}$ where $x = \sqrt{1-\frac{E^2}{16t^2}}$. At $E = 0$ the density of states is singular and decays with a logarithmic law $\log(\frac{16}{|E|})$. It is plotted in Fig. A.11.

The next thing we can do is apply hardwall boundary conditions in both spatial directions $x$and y in analogy with the 1d chain. Consider a finite square lattice with a total number of NxM sites. An example with $N = 4$ and $M = 4$ is shown in Fig. A.12. The wavefunction must be zero on the sites where the lattice is terminated. So it must be of the form of a standing wave as in the 1d case $\Psi(x,y) = A\sin(k_x x)\sin(k_y y)$.

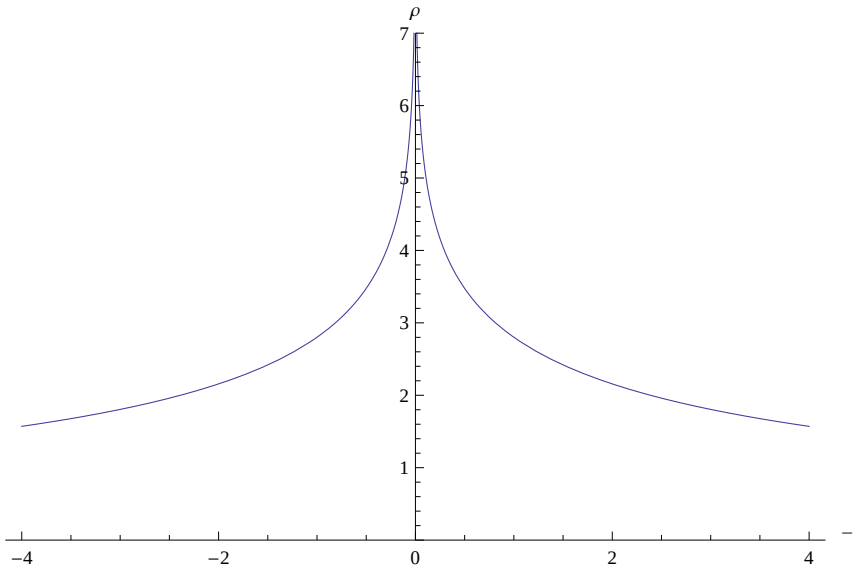

Figure A.11: The density of states $\rho(E)$ of a square lattice for hopping $t = 1$.

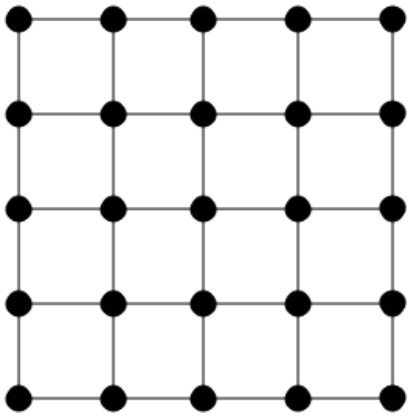

Figure A.12: Square lattice with hardwall boundary conditions.

This form fulfills the conditions $\Psi(0,y) = \Psi(x,0) = 0$ while we must have also

$$\Psi_{N+1,y} = A\sin(k_x(N+1))\sin(k_y y) \Rightarrow k_x = \frac{j\pi}{N+1}, j = 1,2,...,N$$

$$\Psi_{M+1} = A\sin(k_x x)\sin(k_y(M+1)) \Rightarrow k_x = \frac{j\pi}{M+1}, j = 1,2,...,M$$

Both $k_x$and k_y take discrete values between zero and π. Dispersion relation (A.5) becomes

$$E(l,j) = -2t\cos(\frac{j\pi}{N+1}) - 2t\cos(\frac{l\pi}{M+1}) \tag{A.16}$$

As we increase the number of sites in both directions $N\rightarrow\infty$ and $M\rightarrow\infty$ this set of energies becomes denser reproducing the positive part $k_x \in [0,\pi]$ and $k_y \in [0,\pi]$ of the first brillouin zone of the infinite system.

The corresponding eigenvectors are found easily by using the wavefunction of a finite chain

$$\mid \Psi >= \frac{2}{N+1}\sum_{x=1}^{N}\sum_{y=1}^{M}\sin(k_x x)\sin(k_y y) \mid x,y > \tag{A.17}$$

Another interesting case is applying hardwall boundary conditions only in one spatial direction y for example. In this case we can form a infinitely long strip of square lattice as shown in Fig. A.13. This strip commonly referred to as wire or ribbon is a useful structure for modelling various transport problems. It's dispersion relation is of course

$$E(k_x,l) = -2t\cos(k_x) - 2t\cos(\frac{l\pi}{M+1}) \tag{A.18}$$

For every value of l we can plot E as a function of k_x. In this way we form the band structure of this semi-infinite system which is plotted in Fig. A.14. We can see that

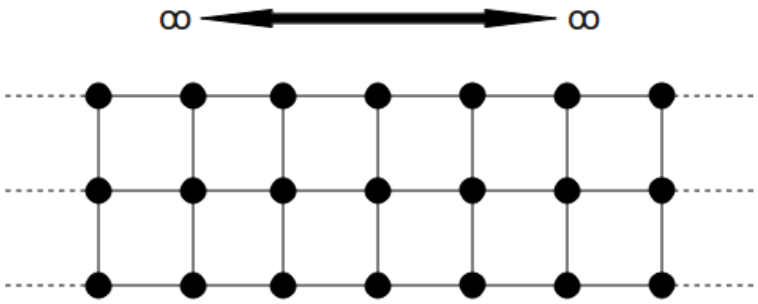

Figure A.13: Square lattice ribbon.

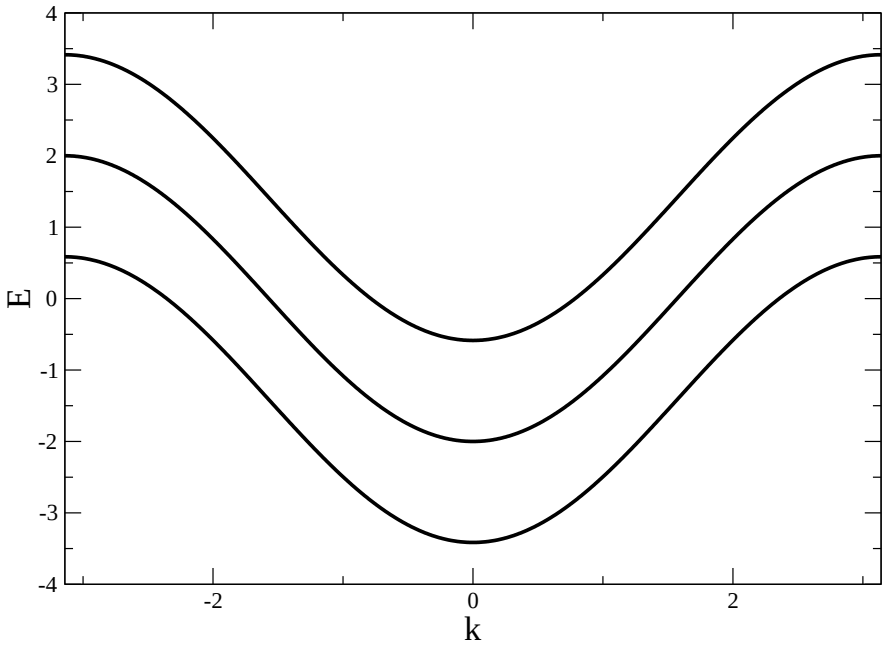

Figure A.14: The band structure a an infinite wire.

all the curves resemble the band structure of the 1d-infinite chain. This is because this system is actually constructed of N infinite chains connected with each other via a constant hopping t. This is obvious also from Eq. (1.19) since for a definite value of l this is just the dispersion relation Eq. (1.7) with $k = k_y$ and $V = -2t\cos(\frac{l\pi}{M+1})$. Those bands are also knows as channels in transport theory.

A.4 Bloch's theorem in tight binding

A very fundamental theorem in solid state physics is the Bloch's theorem. It allows us to calculate the wavefunction of an electron inside a periodic structure, like the lattices already discussed. Consider a continuous system with a periodic potential $V(\overrightarrow{r})$. Bloch's theorem states that the wavefunction $\Psi(\overrightarrow{r})$ of an electron inside this system can be simply written as

$$\Psi(\overrightarrow{r}) = u(\overrightarrow{r})\exp(i\,\overrightarrow{k}\,\overrightarrow{r})$$

where $u(\overrightarrow{r})$ is a periodic function with the periodicity of the potential $V(\overrightarrow{r})$ and $\exp(i\,\overrightarrow{k}\,\overrightarrow{r})$ the wavefunction of a free electron. So the wavefunction of an electron inside a periodic system is just the wavefunction of a free electron modified by the system's periodicity. We can easily apply this result on a simple tight binding lattice with zero on-site potential. Function $u(\overrightarrow{r})$ in this case simply discretizes the free electron wavefunction $\exp(i\,\overrightarrow{k}\,\overrightarrow{r})$, a result we have already used in the previous chapters. Bloch's theorem may not look very useful in this trivial case however it is very important for calculating more complex periodic structures.

Consider for example an 1d infinite chain with a unit cell consisting of two atoms

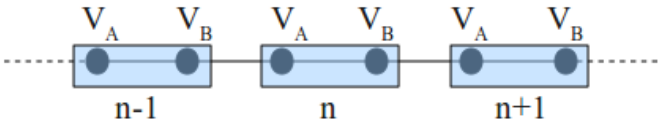

Figure A.15: A linear chain with a unit cell consisting of two atoms.

A and B with different potentials V_A and V_B on each, shown in Fig. A.15. The Schrodinger difference equations for the nth unit cell are

$$(E - V_A)\Psi_A^n = t(\Psi_B^n + \Psi_B^{n-1})$$

$$(E - V_B)\Psi_B^n = t(\Psi_A^n + \Psi_A^{n+1})$$

we can use the Bloch's theorem by taking account the periodicity of the lattice which is two times the lattice spacing $a = 1$ and write amplitudes Ψ_A^n and Ψ_B^n as

$$\Psi_A^n = \Psi_A \exp(ikn)$$

$$\Psi_B^n = \Psi_B \exp(ikn)$$

substituting on the difference equations we get

$$(E - V_A)\Psi_A = t\Psi_B(1 + \exp(-ik))$$

$$(E - V_B)\Psi_B = t\Psi_B(1 + \exp(ik))$$

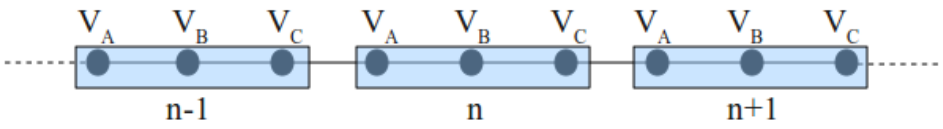

Figure A.16: A linear chain with a unit cell consisting of three atoms.

now we can solve this system of equations in order to get it's eigenvalues

$$\begin{vmatrix} E - V_A & -t(1+\exp(-ik)) \\ -t(1+\exp(ik)) & E - V_B \end{vmatrix} = 0 \Rightarrow E^2 - E(V_A+V_B) + V_A V_B - 2(1+\cos(k)) \Rightarrow$$

$$\Rightarrow E_{\pm} = \frac{(V_A+V_B) \pm \sqrt{(V_A-V_B)^2 + 8(1+\cos(k))}}{2}$$

So the band structure of this periodic system is consisted of two energy bands. Their number is equal to the number of atoms inside the unit cell which is a general rule for those kind of systems.

We can easily extend this method on a system with more than two atoms inside it's unit cell. For example in the case of three atoms which is shown in Fig. A.16. in analogy with the previous system we would have to solve the following system of equations

$$(E - V_A)\Psi_A = t(\Psi_B + \Psi_C \exp(-ik))$$

$$(E - V_B)\Psi_B = t(\Psi_A + \Psi_C)$$

$$(E - V_C)\Psi_C = t(\Psi_B + \Psi_A \exp(ik))$$

the $3x3$ matrix whose determinant will give us the eigenvalues of the system is

$$\begin{vmatrix} E - V_A & t & \exp(-ik) \\ t & E - V_B & t \\ \exp(ik) & t & E - V_C \end{vmatrix}$$

This is actually the Hamiltonian of an 1d closed chain enclosing a magnetic flux. The original periodic system is formed by infinitely repeating it's unit cell. This is equivalent to connecting it's edge sites A and C and then applying a magnetic field through it which introduces a phase factor in the wavefunction according to the Aharonov-Bohm effect.

Σύνοψη

Ένα από τα πιο ενδιαφέροντα θέματα στη σύγχρονη φυσική είναι οι νανοεπιστήμες, οι οποίες χτίζουν το υπόβαθρο για την κατανόηση των θεμελιωδών αρχών της νανοηλεκτρονικής. Το γραφένιο από την παραγωγή του το 2004 έχει γίνει ένα από τα κύρια αντικείμενα της έρευνας στον τομέα των νανοεπιστημών. Είναι το πρώτο δισδιάστατο μέταλλο που φτιάχθηκε ποτέ και οι ηλεκτρονικές ιδιότητες του, προσφέρουν ένα ευρύ πεδίο για εφαρμογές και για θεμελιώδη θεωρητική έρευνα. Στην παρούσα διατριβή μελετάμε τις ηλεκτρονικές ιδιότητες των γραφενίου παρουσία αταξίας, η οποία αποτελεί εναν αναπόφευκτο παράγοντα σε κάθε μεσοσκοπικό σύστημα. Η μελέτη των σχετικών φαινομένων γίνεται μέσω καθιερωμένων μεθόδων της μεσοσκοπικής φυσικής, όπως η μορφοκλασματική γεωμετρία και το κβαντικό χάος. Αυτό μας επιτρέπει να μελετήσουμε την αλληλεπίδραση της γνωστής ηλεκτρονικης συμπεριφοράς του καθαρού γραφενίου, με τα φαινόμενα διάχυσης και εντοπισμού που εισάγει η αταξία.

Το γραφένιο, το πρώτο δισδιάστατο μέταλλο που φτιάχθηκε ποτέ, είναι ένα ενιαίο στρώμα ατόμων άνθρακα πυκνά πακεταρισμένα σε μια δομή πλέγματος κερήθρας. Το γραφένιο παράχθηκε για πρώτη φορά το 2004, στο Manchester από την ομάδα του A. Geim και K. Novoselov[1,2], μέσω μηχανικής απολέπισης από γραφίτη. Τους απονεμήθηκε το βραβείο Νόμπελ Φυσικής το 2010. Το γραφένιο έχει εξαιρετικές ιδιότητες οι οποίες δεν συναντιόνται σε συμβατικά υλικά, όπως, μεγάλη ευελιξία, υψηλή κινητικότητα ηλεκτρονίων με ταχύτητες κοντά στην ενέργεια Fermi που πλησιάζουν την ταχύτητα του φωτός c, πολύ υψηλότερη από οποιονδήποτε συμβατικό ημιαγωγό. Μπορεί να κοπεί σε μακρόστενες ταινίες γνωστές ως νανοταινίες γραφενίου (GNR) [3], ή σε περιορισμένες δομές γνωστές ως νιφάδες [4], καθιστώντας το εναν εξαιρετικό υποψήφιο για

την αντικατάσταση του πυριτίου στα μελλοντικά νανοηλεκτρονικά. Πολλές άλλες τεχνικές παραγωγής του γραφενίου έχουν αναπτύχθεί επίσης, όπως η επιταξιακή ανάπτυξη σε καρβίδιο του πυριτίου [5], πάνω σε μεταλλικό υπόστρωμα [6] ή με την κοπή νανοσωλήνων άνθρακα [7,8].

Η θεωρητική μελέτη του γραφενίου, μέσα από γνωστές μεθόδους της κβαντική φυσικής στερεάς κατάστασης έχει αποκαλύψει μερικές εξωπραγματικές συμπεριφορές οι οποίες ουδέποτε συναντιόνται σε συμβατικά συστήματα. Η κυψελοειδής δομή πλέγματος του γραφενίου οδηγεί σε φαινόμενα κβαντικής συμβολής προκαλώντας εντοπισμό των κυματοσυναρτήσεων στα άκρα συστημάτων από γραφένιο [10, 11]. Επιπλέον, αυτές οι καταστάσεις άκρων συνεισφέρουν ενέργειες κοντά στο επίπεδο Fermi , και εξαρτώνται σε μεγάλο βαθμό τη μορφολογία των ακρών. Είναι σαφές ότι οι ηλεκτρονικές ιδιότητες του γραφενίου είναι εξαιρετικά ευαίσθητες στην επιλογή των συνοριακών συνθηκών. Η μελέτη αυτών των τοπολογικών φαινομένων και ο ρόλος τους στις ηλεκτρονικές ιδιοτήτες του γραφενίου είναι πολύ σημαντική για τη συμπερίληψη του γραφενίου στον τομέα της νανοηλεκτρονικής. Η θεωρητική μελέτη έχει αποκαλύψει επίσης τη σχετικιστική φύση των ηλεκτρονίων κοντά στην ενέργεια Fermi , ανοίγοντας έτσι το διεπιστημονικό πεδίο της σχετικιστικής Φυσικής Στερεάς Κατάστασης [1,11]. Η σχετικιστική φύση των ηλεκτρονίων για περισσότερο από μισό αιώνα ήταν γνωστή για τον γραφίτη ο οποίος αποτελείται από πολλά στρώματα γραφενίου στοιβαγμένα μαζί [11]. Στο επίπεδο Fermi τα ηλεκτρόνια στο γραφένιο συμπεριφέρονται ως ελεύθερα σχετικιστικά άμαζα σωματίδια τα οποία περιγράφονται από την εξίσωση Dirac . Αυτό ονομάζεται σημείο Dirac . Από αυτήν την άποψη το γραφένιο μπορεί να χρησιμοποιηθεί ως ένα αποτελεσματικό μοντέλο για τη μελέτη της κβαντικής ηλεκτροδυναμικής, με προφανή πλεονεκτήματα για την διεξαγωγή σχετικιστικών πειραμάτων κβαντικής όπως οι μικρές διαστάτεις του χώρου που απαιτείται.

Τα μορφοκλασματικά αντικείμενα και το χάος από την άλλη πλευρά είναι καλά εδραιωμένα φαινόμενα στον τομέα των μη γραμμικών δυναμικών συστημάτων. Η ύπαρξή τους στον κβαντικό κόσμο έχει μελετηθεί εκτενώς κατά τις τελευταίες δεκαετίες, κυρίως σε χαμηλής διάστασης άτακτα συστημάτα γνωστά ως μεσοσκοπικά. Αυτά βρίσκονται μεταξύ της μικροσκοπικής και της μακροσκοπικής κλίμακας [12]. Η φύση του Κβαντικού Χάους δεν έχει να κάνει με δυναμική εξέλιξη, αλλά με τις στατιστικές ιδιότητες του ενεργειακού φάσματος. Τα άτακτα κβαντικά συστήματα έχουν αποδειχθεί ότι υπακούουν τους ίδιους νόμους με τους συμπαντικούς νόμους του Κβαντικού Χάους. Οι νόμοι αυτοί περιγράφονται από μια μαθηματική θεωρία των πλήρως τυχαίων μητρών, η οποία κατέστη γνωστή ως Random Matrix Theory (RMT) [12,13,14].

Από την άλλη πλευρά, ενδείξεις της μορφοκλασματικής γεωμετρίας έχουν αποδειχθεί ότι υπάρχουν στον κόσμο της κβαντικής μηχανικής, π.χ. στις κυματοσυναρτήσεις των ηλεκτρονίων άτακτων δισδιάστατων μεσοσκοπικών συστημάτων [15,16,17,18]. Η μορφοκλασματική φύση των κυματοσυναρτήσεων κοντά στη μετάβαση μετάλλου-μονωτή (MIT) είναι γνωστή [19,20]. Ακριβώς στο σημείο μετάβασης οι κυματοσυναρτήσεις χαρακτηρίζονται από μη τετριμένη κρίσιμη συμπεριφορά κλιμάκωσης, είναι πολύπλοκα αντικείμενα γνωστά ως πολυμορφοκλασματικά και περιγράφονται από ένα ολόκληρο φάσμα μορφοκλασματικών διαστάσεων. Οι κυματοσυναρτήσεις κάτω από το (MIT) δείχνουν μια συμπεριφορά διάχυσης, με τα αντίστοιχα επίπεδα της ενέργειας να υπακούουν τους συμπαντικούς νόμους της RMT όπως και το Κβαντικό Χάος. Για αρκετά μεγάλο βαθμό αταξίας, πάνω από το σημείο μετάβασης, καταστροφικά φαινόμενα κβαντικής συμβολής οδηγούν σε εντοπισμό Anderson [21].

Το γραφένιο ως το πρώτο πραγματικό δισδιάστατο μέταλλο που έγινε ποτέ, προσφέρει μια μοναδική ευκαιρία για τη δοκιμή των καθιερωμένων φαινομένων του κβαντικού χάους και της μορφοκλασματικής γεωμετρίας, τα οποία συνήθως μελετώνται μέσω δισ-

διάστατων συστημάτων, γνωστά ως 2d Electron Gas (2DEG) [22]. Επιπλέον, λόγω του περιορισμένου χαρακτήρα των πειραματικά παραγώμενων συστημάτων γραφενίου όπως οι νιφάδες, με την τοπολογία να παίζει καθοριστικό ρόλο στις ηλεκτρονικές τους ιδιότητες, τίθονται σημαντικά ερωτήματα σχετικά με το ρόλο της τοπολογίας στη φύση του κβαντικού χάους και στην πολυμορφοκλασματικής φύσης των κυματοσυναρτήσεων. Το κβαντικό χάος κοντά στο σημείο Dirac αναμένεται επίσης να θέσει σχετικιστικά θέματα. Έχει μελετηθεί πειραματικά από τον Ponomarenko και τους συνεργάτες του [23] ανακαλύπτωντας μια χαοτική φύση περιγράφόμενη από την εξίσωση Dirac . Αυτά τα συστήματα είναι κοινώς γνωστά ως μπιλιάρδα Dirac , τα οποία εχουν προταθεί από τους Berry και Mondragon [24]. Θεωρητικοί υπολογισμοί από τους L. Huang [25] σε μπιλιάρδα γραφενίου προβλέπουν μια διαφορετική κβαντική χαοτική συμπεριφορά σε σύγκριση με την πειραματική, ενώ άλλοι θεωρητικοί υπολογισμοί σε γραφήνη με μικρή αταξία με περιοδικές οριακές συνθήκες [26] έχουν δείξει σχετικιστική χαοτική φύση ανεξάρτητη από το μέγεθος του δείγματος. Για ισχυρή αταξία ο εντοπισμός Anderson [21], πάντα επικρατεί.

Στην παρούσα διατριβή μελετάμε τη μορφοκλασματική φύση των κυματοσυναρτήσεων και την χαοτική συμπεριφορά του ενέργειακού φάσματος σε άτακτα συστήματα γραφενίου κοντά στο σημείο Dirac. Σε πρώτη φάση, ελέγχουμε την ύπαρξη των μορφοκλασματικών κυματοσηναρτήσεων στο επίπεδο Fermi, παρουσία αταξίας. Η μελέτη διεξάγεται σε συνδυασμό με τη γνωστή συμπεριφορά άλλων συμβατικών άτακτων υλικών. Στη συνέχεια, απευθύνουμε το εξής ερώτημα, πώς η αντισυμβατική τοπολογία του γραφενίου επηρεάζει τον μορφοκλασματικό χαρακτήρα για περιορισμένες δομές, οι καταστάσεις ακρών επιβιώνουν παρουσία αταξίας και πώς μπορεί αυτο να συνδυαστεί με τη μορφοκλασματική φύση των κυματοσυναρτήσεων; Μελετάμε, επίσης, τον ρόλο των καταστάσεων άκρων στην κβαντική χαοτική συμπεριφορά των γραφενίου κοντά στο

σημείο Dirac, μέσω των στατιστικών ιδιοτήτων του ενεργειακού φάσματος.

Στο δεύτερο κεφάλαιο δίνουμε μια σύντομη εισαγωγή του γραφενίου, αναλύοντας λεπτομερώς τις αντισυμβατικές ηλεκτρονικές ιδιότητες του, μέσω ενός απλού μοντέλου ισχυρής δέσμευσης το οποίο εισάγεται στο προσάρτημα. Το μοντέλο αυτό μας δίνει τη δυνατότητα να μελετήσουμε την σχετικιστική φύση της διασποράς ενέργειας και τις ηλεκτρονικές ιδιότητες οι οποίες εξαρτώνται σε μεγάλο βαθμο από την τοπολογία, όπως οι καταστάσεις άκρης.

Στο τρίτο κεφάλαιο, μετά από μια σύντομη εισαγωγή στη μορφοκλασματική γεωμετρία, μελετάμε λεπτομερώς τις μορφοκλασματικές ιδιότητες των κυματοσυναρτήσεων σε δομές γραφενίου με αταξία, σε συνδυασμό με άλλα συστήματα όπως το τετράγωνο πλέγμα και την γραμμική αλυσίδα. Παρουσιάζουμε επίσης σημαντικές ιδιότητες συμμετρίας για το γραφένιο με αταξία όπως η κατοπτρική συμμετρία.

Στο τέταρτο κεφάλαιο, μετά από μια σύντομη εισαγωγή στο κβαντικό χάος, συγκρίνουμε την κβαντική χαοτική φύση άτακτων δομών γραφενίου με ένα τετράγωνο πλέγμα με αταξία μικρής εμβέλειας.

Στο πέμπτο κεφάλαιο παρουσιάζουμε τα συμπεράσματά της μελέτης. Στο προσάρτημα συζητάμε το μοντέλο ισχυρής δέσμευσης, για διάφορους τύπους πλεγμάτων, ετσι ώστε να καθορισουμε τις ηλεκτρονικές ιδιότητες τους.

Η κυψελωτή δομή πλέγματος του γραφενίου έχει σημαντικές ιδιότητες όπως κατοπτρική συμμετρία και χωρική ανισοτροπία. Αυτές είναι υπεύθυνές για τις υποδεικνυόμενες εξαρτώμενες από την τοπολογία ηλεκτρονικές ιδιότητες. Το γραφένιο χαρακτηρίζεται επίσης από ακραία ευαισθησία στις συνοριακές συνθήκες. Ο μηχανισμός κβαντικής συμβολής διαδραματίζει καθοριστικό ρόλο. Η ύπαρξή του οφείλεται στο γεγονός ότι το πλέγμα κερήθρας έχει κάθε άτομο συνδεμένο με τους τρεις κοντινότερους γείτονές του. Για πεπερασμένα συστήματα, ο μηχανισμός αυτός οδηγεί σε κυματοσυναρτήσεις

εντοπίσμένες στα όρια. Αυτές είναι γνωστές ως καταστάσεις άκρης. Η ύπαρξη τους εξαρτάται από τη μορφολογία των ορίων. Η λεγόμενος τύπος άκρων zigzag συνισφέρει ενέργειες κοντά στο επίπεδοFermiγια οποιοδήποτε περιορισμένο σύστημα γραφενίου. Ο άλλος πιθανός τύπος άκρης,armchair , δεν συνισφέρει καταστάσεις στο επίπεδο Fermi. Δείχνουμε τις καταστάσεις άκρης σε διάφορα συστήματα, ημι-άπειρα φύλλα γραφενίου, νανοταινίες και νιφάδες σε τετράγωνους και κυκλικούς σχηματισμούς όταν υπάρχει ανάμειξη ακμών zigzag και armchair.

Δείχνουμε επίσης ότι οι ευαίσθητες στις συνοριακές συνθήκες ηλεκτρονικές ιδιότητες του γραφενίου διαδραματίζουν σημαντικό ρόλο στην μορφοκλασματική φύση των κυματοσυναρτήσεων στο σημείο Dirac. Παρουσία αταξίας εκτός της διαγωνίου η οποία διατηρεί την κατοπτρική συμμετρία των δύο υποπλεγμάτων του πλέγματος κερύθρας του γραφενίου, ο μηχανισμός που οδηγεί στις καταστάσεις άκρης επιβιώνει. Οι κυματοσυναρτήσεις βρίσκονται στα όρια των πεπερασμένων συστημάτων και μοιάζουν με τις μορφοκλασματικές κυματοσυναρτήσεις για αλυσίδες μικρού μήκους με αταξία εκτός της διαγωνίου. Αυτό υποδηλώνεται σαφώς από τη διάσταση κλιμάκωσης D_2 η οποία λαμβάνει τιμές από το ένα στο μηδέν, αντί από το δύο στο μηδέν καθώς αυξάνεται ο βαθμός της αταξίας. Αυτό συμβαίνει και για τις μορφοκλασματικές κυματοσυναρτήσεις στο κέντρο του ενεργειακού φάσματος για ένα τετράγωνο πλέγμα με αταξία εκτός της διαγωνίου. Μηδενική τιμή του D_2 υποδηλώνει εντοπισμό Anderson, $D_2 \approx 1$ σημαίνει καταστάσεις άκρης και $D_2 \approx 2$ πλήρως χαοτικές, διάχυτες ή βαλλιστικές κυματοσυναρτήσεις.

Ο μηχανισμός καταστρεπτικής συμβολής διαδραματίζει επίσης σημαντικό ρόλο στην κβαντική χαοτική συμπεριφορά του γραφενίου με αταξία. Τα επίπεδα της ενέργειας, στο σημείο Dirac για τετράγωνα δείγματα με αταξία επί της διαγωνίου εμφανίζουν μια στατιστική συμπεριφορά η οποία δεν απαντάνται σε συμβατικά δισδιάστατα συστήματα, όπως το τετράγωνο πλέγμα. Η κατανομής διαστημάτων μεταξύ διαδοχικών επίπεδων

ενέργειας $P(S)$ έχει μία ενδιάμεση μορφή κοντά στην κατανομή Semi-Poisson, υποδεικνύοντας μία ασθενώς χαοτική συμπεριφορά. Αυτή η συμπεριφορά παραμένει για πολλά διαδοχικά επίπεδα ενέργειας κοντά στο σημείο όπου οι καταστάσεις άκρης υπάρχουν για καθαρό γραφένιο. Υποστηρίζουμε ότι αυτή η συμπεριφορά οφείλεται στον μηχανισμό καταστάσεων άκρης ο οποίος επιβιώνει ακόμα και με την παρουσία ατάξίας επί της διαγωνίου. Αυτό υποδηλώνεται σαφώς από τη σύγκριση με την στατιστική συμπεριφορά για τά επίπεδα ενέργειας στο κέντρο του ενεργειακού φάσματος σε ένα τετράγωνο πλέγμα με αταξία επί της διαγωνίου, για το οποίο οι καταστάσεις άκρης απουσιάζουν. Για την τελευταία περίπτωση, η γνωστή χαοτική συμπεριφορά χαρακτηριζόμενη από την μορφή Wigner για το $P(S)$ αναδύεται.

Ως εκ τούτου, και στις δύο περιπτώσεις αταξίας, εκτός και επί της διαγωνίου, ο κβαντικός μηχανισμός καταστρεπτικής συμβολής του πλέγματος κερύθρας του γραφενίου επιβιώνει δίνοντας καταστάσεις άκρης στο επίπεδο Fermi, επηρεάζοντας σημαντικά τη μορφοκλασματική φύση των κυματοσυναρτήσεων και την χαοτική συμπεριφορά των επιπέδων ενέργειας για το γραφένιο με αταξία. Ο μηχανισμός αυτός είναι εξαιρετικής σημασίας για την κατασκευή νανοηλεκτρονικών βασισμένων στο γραφένιο. Η ασθενώς χαοτική συμπεριφορά στο σημείο Dirac, συνεπάγεται μία ημι-μεταλλική συμπεριφορά ενδιάμεση μεταξύ μετάλλων και μονωτών.

Βιβλιογραφία

[1]Geim, A. K. and Novoselov, K. S, Nature Materials 6, 183-191 (2007)

[2]K.S.Novoselov et al., Science 306, 666 (2004)

[3]Michael S. Fuhrer Nature Materials, 9, 611-612 (2010)

[4]L. A. Ponomarenko et al., Science 320, 356 (2008)

[5]Sutter, P., Nature Materials 8 (3) (2009)

[6]Geim, A. K. MacDonald, A. H., Physics Today 60: 35-41 (2007)

[7]Brumfiel, G., Nature, doi:10.1038/news.2009.367 (2009)

[8]Kosynkin, D. V. et al., Nature 458 (7240) (2009)

[9]K. Nakada, M. Fujita, G. Dresselhaus, M.S. Dresselhaus, Phys. Rev. B54, 17954 (1996)

[10]A. H. Castro Neto, F. Guinea, N. M. R. Peres, K. S. Novoselov and A. K. Geim, RevModPhys. 81. 109 (2009)

[11]P. R. Wallace,PhysRev. 71. 622 (1947)

[12]Y. Alhassid Rev. Mod. Phys. 72, 895 (2000)

[13]A. V. Andreev, O. Agam, B. D. Simons, and B. L. Altshuler, Phys. Rev. Lett. 76, 3947 (1996)

[14]F. Haake, Quantum Signatures of Chaos, 2nd Edition, Springer (2000)

[15]Hideo Aoki Phys. Rev. B 33, 7310 (1986)

[16]V.I. Falko and K.B. Efetov, Europhys. Lett. 32, 627 (1995); Phys. Rev. B 52, 17413 (1995)

[17]Michael Schreiber and Heiko Grussbach, Phys. Rev. Lett. 67, 607 (1991)

[18]S. N. Evangelou, J. Phys. A: Math. Gen. 23 L317 (1990)

[19]Masatoshi Imada, Atsushi Fujimori, and Yoshinori Tokura, Rev. Mod. Phys. 70, 1039 (1998)

[20]Evangelou, S. N., Katsanos, D. E. Journal of Statistical Physics, Volume 85, Issue 5-6, pp. 525-550 (1996)

[21]P. W. Anderson, Phys. Rev. 109, 1492 (1958)

[22]C. Weisbuch, B. Vinter, Academic Press, London (1991)

[23]L. A. Ponomarenko et al., Science 320, 356 (2008)

[24]M. V. Berry, R. J. Mondragon, Proc. R. Soc. London A 412, 53 (1987)

[25]Liang Huang, Ying-Cheng Lai, and Celso Grebogi, Phys. Rev. E 81, 055203(R) (2010)

[26]I. Amanatidis and S. N. Evangelou, Phys.Rev.B 79, 205420 (2009)